Morphological Studies of Crystallization in Thin Films of PEO/PMMA Blends

by

Brian C. Okerberg

Dissertation submitted to the faculty of the
Virginia Polytechnic Institute and State University
in partial fulfillment of the requirements for the degree of

Doctor of Philosophy
In
Materials Science & Engineering

Dr. Hervé Marand, Chairman
Dr. Bill Reynolds Dr. Sean Corcoran
Dr. Alan Esker Dr. Garth Wilkes

September 16, 2005
Blacksburg, Virginia

Keywords: Crystallization, Morphology, Polymers, Polymer Blends, PEO, Dendrites, Spherulites, Confinement, Thin Films

Morphological Studies of Crystallization in Thin Films of PEO/PMMA Blends

Brian C Okerberg

ABSTRACT

Morphological development during crystallization of thin films of poly(ethylene oxide) (PEO) / poly(methyl methacrylate) (PMMA) blends has been reported. Studies have focused on the effects of the blend composition, PMMA molecular weight, film thickness, and crystallization temperature on the observed crystal morphology. As the blend composition was varied from 90 to 30 wt% PEO, the crystal morphology varied from spherulites to needles and dendrites. Variation of the crystallization temperature and PMMA molecular weight resulted in similar changes in morphology. A morphological map demonstrating the roles of the experimental controls on the observed crystal morphology has been developed. This map was used as a tool for more detailed studies of the observed morphologies and morphological transitions. The dendritic region of the map (~ 30 – 40 wt% PEO) was studied in detail. Changes in the diffusion length were achieved through variation of the PMMA molecular weight, and were shown to influence the secondary sidebranch spacing. Sidebranch spacing measurements revealed that coarsening of the dendritic microstructure occurred well after the competition between diffusion fields of neighboring dendrite arms vanished, indicating the existence of another coarsening mechanism. These studies of dendritic sidebranching indicate that polymer dendrites develop by mechanisms similar to those in small molecules and metals. A number of in-situ observations of morphological transitions have also been reported, including a dense-branched morphology (DBM)/dendrite transition, a DBM/stacked-needle/needle transition, and a transition from dendrites with 90^{o} sidebranching to dendrites with 45^{o} branching or a dense-branched morphology, both of which grow at 45^{o} to the original dendrite trunk. The DBM/dendrite transition occurred over a range of crystallization temperatures, indicating that the transition is not sharp. Crystal growth rate measurements verified this result. The DBM/stacked-needle/needle transitions demonstrated distinct jumps in the crystal growth rate,

indicating a change in the growth mechanism or direction. For the transition involving a change in the growth direction, the effective level of noise (fluctuation) was found to be important in morphological selection. The results of this work have helped to define new directions for the study of crystal morphologies, especially in the areas of spherulite formation and dendritic growth.

Acknowledgements

I would like to thank the following people for their help and support during my work on this dissertation:

- My advisor, Dr. Hervé Marand, for his encouragement, guidance, and mutual patience over the last five years
- Dr. Sean Corcoran, Dr. Bill Reynolds, Dr. Alan Esker, and Dr. Garth Wilkes for serving on my committee and helping with many aspects of this work
- Chris Fratini, Julie Uan-Zo-li, and Zhenyu Huang for many helpful discussions in the lab
- Steve McCartney for help with AFM
- David Berry for frequent help with laboratory equipment
- Dr. Jack Douglas and Dr. Vincente Ferreiro for helpful discussions involving PEO/PMMA blends

I would especially like to thank my parents for their love and support.

Special thanks to Todd and Dave for their friendship and many helpful and interesting discussions over the years.

Most importantly, thanks to my wife, Laura, for her love and patience throughout our life together.

Table of Contents

List of Figures

List of Tables

Chapter 1. Introduction

Crystallization morphologies, kinetics, and growth mechanisms have been studied extensively many years. Requirements for stronger, tougher, and lighter materials have driven the need for a more detailed understanding of solidification and crystallization processes in particular. Despite recent advances in material characterization, many aspects of the crystallization process are still not well understood.

Early studies of crystallization focused on crystal morphologies in metals and small molecules [1]. The rapid development of polymeric materials in the 1950's introduced a host of new issues to the field of crystallization. The long-chain nature of these molecules led to a variety of problems with general crystallization theories because of their unique crystallization mechanisms. These problems resulted in a separation of polymer crystallization researchers from those in other areas of the crystallization field. Although polymer crystallization theories were developed from modifications of theories developed for metals, the differences between polymers and other materials have often been considered to be too great for any general theories to apply. Recently, however, researchers have attempted to reconcile the differences between work in the area of polymer crystallization and that in other areas of the crystallization field [2].

The spherulitic morphology, shown in Figure 1.1, is very common in polymer crystallization. However, examples of this morphology are evident in many other materials, raising the question of whether spherulites should be considered a general growth morphology or one specific to certain material classes and growth conditions. The discovery of dense-branched morphology (DBM), or seaweed, has led some researchers to argue that DBM and spherulites are the same morphology [2]. Such statements are certainly speculative given the current (lack of) consensus on the mechanisms of spherulitic growth in polymers [3,4,5].

Recent studies of confined crystallization of polymers have also led to renewed interest in crystallization morphologies [6,7]. Many of the morphologies observed in these studies are found in diffusion-limited crystal growth and have not been previously

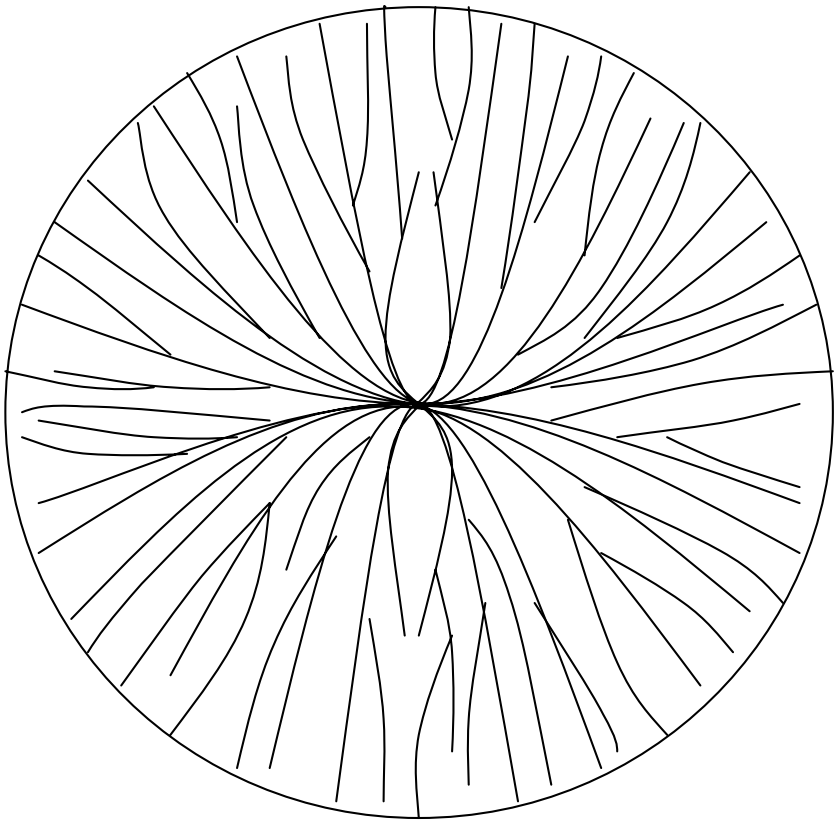

Figure 1.1 Schematic of a typical polymer spherulite.

observed in polymeric systems. The observation of dendritic morphologies in polymer thin films [6,7,8] has opened new avenues for detailed studies of dendritic growth, due to the slow growth rates and the fact that only simple experimental setups are required. In addition to probing dendritic crystallization, these recent observations have helped to formulate new questions about the origins of spherulitic growth. Detailed studies of morphological development and selection in polymeric systems may lead to a better understanding of crystallization and help to reconcile differences between polymer crystallization and crystallization of small molecules and metals.

This work focuses on the development of crystal morphologies in thin-film polymer blend systems because a number of morphologies have been observed in blend systems [6,7] and they offer unique opportunities to "tune" a number of parameters involved in the crystal growth process. A number of fundamental areas must be addressed in such a study, including polymer crystallization/spherulitic growth, polymer blends, the glass transition temperature, diffusion, crystallization morphologies, and thin-film crystallization. For obvious reasons, these topics are not addressed in detail. However, a number of references are provided in each section to provide the reader with resources for further study. The goal of this work is to provide new avenues for studying pattern-formation, and to investigate similarities between polymeric crystallization and that of other materials. Following this introduction, three papers (in preparation for publication) are presented, demonstrating several new areas of research in the area of pattern formation during crystallization. Following these papers, several directions for further work in this area are described.

Chapter 1.1 Crystallization Processes

In this section, some of the basic aspects of crystal growth and diffusion are discussed. A more detailed discussion of limitations to crystal growth is found later in this text. To maintain notation and terminology consistent with polymer literature, this section is outlined in a manner similar to that of the work of Schultz on polymer microstructure [9].

The Driving Force for Crystallization

The driving force for crystallization is related to the "undercooling" or "supercooling," which refer to the difference between the thermodynamic melting point and the temperature of the melt far from the melt/crystal interface, $\Delta T = T_m^{eq} - T_x$. At the melting point, the driving force is zero and increases with decreasing temperature (increasing undercooling). The rate of crystal growth depends on the undercooling:

$$V_n = V_n(\Delta T) \qquad \text{Eq (1.1)}$$

where V_n is the natural (or "preferred") growth velocity. The exact form of the dependence of the growth velocity on the undercooling is not always known, but can be assumed linear over small variations in temperature. The important point is that the growth velocity is low at small undercooling and increases with increasing driving force in the absence of other restrictions.

During crystal growth, two important processes occur at the crystal/melt interface. First, the interface moves forward, releasing heat of crystallization, L. The amount of heat liberated per unit area per second is LV, where V is the actual crystal growth velocity. Second, the heat of fusion must be driven from the interface by some conduction mechanism (i.e. diffusion or convection). As the rate of crystal growth increases, the amount of heat evolved per unit time increases and thus must be removed more and more efficiently.

In the case of alloy or blend, solute must also be removed from the growth front. In polymer systems, the solute is often a non-crystallizable species (in a blend), stereo-irregular species (frequently encountered in homopolymers), and/or species of a different molecular weight (blends or homopolymers). If the concentration of non-crystalline species initially present in the system is c_o and the concentration that may enter the crystalline solid is c_s, then the amount of solute rejected per unit area per second is $(c_o - c_s)V$. This solute species, as in the case of latent heat, must be removed by a convective or diffusive mechanism.

Diffusion Considerations

The transport of heat or solute away from the crystal can limit the rate at which the crystal growth front can move forward. Here, the rate of crystal growth of a planar interface is considered. In addition, only diffusive mechanisms are discussed because convective transfer is very limited in high molecular weight polymers where the viscosity is extremely large. The diffusion-limited growth velocity (defined by the rate at which the heat or solute can be removed from the growth front), V_D, is assumed by the crystal in the case that V_D is much smaller than the natural growth velocity (growth velocity in the absence of limitations), V_n. This scenario is described below.

At small undercooling (small driving force), V_n is very small. If $V_n << V_D$, the heat and solute have plenty of time to diffuse away and the interface moves at its natural velocity, V_n. As the undercooling is increased, V_n quickly becomes much larger than V_D because the rate of diffusion (in alloy or blends) slows with increasing undercooling while the natural growth velocity rapidly increases. In this regime, the actual (observed) velocity is controlled by the rate of diffusion. As previously mentioned, as the growth rate become increasingly fast, more efficient removal of the heat or solute becomes necessary. Usually, this increase in efficiency is achieved by a breakdown of the interface into dendritic or rod-like protuberances that increase the dimensionality of the removal process. These processes are referred to as pattern-formation during crystallization and will be discussed at some length later in this text.

The diffusion-limited growth kinetics will now be addressed in further detail. For simplicity, this discussion will be restricted to one-dimensional heat flow in a pure material. The situation will further be limited to a slightly undercooled melt where all of the latent heat is transported into the melt and the growth front is planar. The growth front moves at a rate V_D and the heat released per unit time per unit area is LV_D. The flux of heat, LV_D, must be proportional to the thermal gradient, $(dT/dx)_o$ at the surface:

$$LV_D/c_p = -D_T (\partial T/\partial x)_o \qquad \text{Eq (1.2)}$$

where c_p is the specific heat of the non-crystalline phase, D_T is the thermal diffusion coefficient and x is the distance ahead of the interface. The temperature, T, at each location, x, is given by Fourier's law:

$$\partial T/\partial t = - D_T (\partial^2 T/\partial x^2) \qquad \text{Eq (1.3)}$$

Using the boundary conditions ($T \rightarrow T_o$ as $x \rightarrow \infty$ and $T \rightarrow T_m$ at $x = 0$) and assuming local equilibrium at the interface, we arrive at the solution:

$$V_D = \lambda(D_T/t)^{1/2} \qquad \text{Eq (1.4)}$$

where λ is given by the error function:

$$\lambda^2 \exp(\lambda^2)\mathrm{erfc}(\lambda) = (T_m - T_o)\, c_p / \pi^{1/2} L \qquad \text{Eq (1.5)}$$

where c_p is the specific heat of the non-crystalline phase.

This problem is now modified for solute rejection. The amount of solute rejected per unit area per second is given by $V_D[c_n(\mathrm{int}) - c_s]$, where c_s is the solute concentration in the solid and $c_n(\mathrm{int})$ is the solute concentration of the melt at the interface. The flux equation is:

$$V[c_n(\mathrm{int}) - c_s] = -D_s(\partial c_n/\partial x) \qquad \text{Eq (1.6)}$$

Using the boundary conditions $c_n \rightarrow c_o$ as $x \rightarrow \infty$, and Fick's second law:

$$\partial c_n/\partial t = -D_s (\partial^2 c_n/\partial x^2) \qquad \text{Eq (1.7)}$$

the diffusion-limited growth rate is:

$$V_D = \lambda(D_s/t)^{1/2} \qquad \text{Eq (1.8)}$$

where λ is given by the error function:

$$\lambda^2 \exp(\lambda^2)\mathrm{erfc}(\lambda) = \{[c_n(\mathrm{int}) - c_o]/[c_n(\mathrm{int})-c_s]\}/ \pi^{1/2} \qquad \text{Eq (1.9)}$$

The Diffusion Length

The diffusion length is a very important parameter in pattern-forming systems, and relates in a general way to important length scales of these patterns. The diffusion length is the distance that a field (composition or temperature) decays to 1/e of its value at the interface. Heat or solute is rejected from the crystal at a rate of $V_D L \rho_m$ (ρ_m is the density of the non-crystalline phase) or $V_D (c_o - c_s)$. With the assumptions that the flux is

constant and the interface is stationary, the following sets of equations describe the interface:

$$LV_D/c_p = -D_T(\partial T/\partial x)_{x=0} \qquad \text{Eq (1.10)}$$

$$V_D(\partial T/\partial x) = -D_T(\partial^2 T/\partial x^2) \qquad \text{Eq (1.11)}$$

for the case of heat flow, and:

$$(c_o - c_s)V_D = -D_s(\partial c_n/\partial x)_{x=0} \qquad \text{Eq (1.12)}$$

$$V_D(\partial c_n/\partial x) = -D_s(\partial^2 c_n/\partial x^2) \qquad \text{Eq (1.13)}$$

for the case of solute flow. Solving these equations gives the following results (for heat and solute, respectively):

$$[T(x)-T_o]/[T(0) - T_o] = \exp(-V_D x/D_T) \qquad \text{Eq (1.14)}$$

$$[c_n(x)-c_o]/[c_o-c_s] = \exp(-V_D x/D_s) \qquad \text{Eq (1.15)}$$

The left hand side of these equations represents the fractional decrease in temperature or solute concentration from that at the interface to the value far from the interface. When this value is 1/e of the initial value, the diffusion length, δ, is given as:

$$\delta = D / V_D \qquad \text{Eq (1.16)}$$

where D is either the thermal or solutal diffusion coefficient. For polymeric systems, δ(thermal) >> δ(solutal), so thermal diffusion is generally irrelevant to the crystallization process (for quiescent melts). This point will be addressed in more detail later in this text.

Chapter 1.2 Polymer Crystallization

In this section, some of the basic aspects of crystallization of polymers, such as nucleation, two- and three- dimensional growth shapes, and the kinetics of crystal growth are described.

Primary Nucleation

Primary nucleation in polymeric systems can be treated similarly to that of other materials, with the exception that the critical nucleus involves a number of chain stems

rather than a collection of atoms. Turnbull and Fisher developed a general theory for the rate of nucleation [10]. In general, the rate of nucleation is given by an Arrhenius type relationship.

In polymer systems, the formation of a critical nucleus is highly improbable due to the large size of the critical nucleus and the large surface energy of the fold surface. For this reason, nucleation in these materials is believed to occur heterogeneously (exclusively) on impurities, such as dust or leftover catalyst. In most cases, these impurities can not be sufficiently removed from the system to prevent heterogeneous nucleation from occurring. Nucleation is also possible via mechanical deformation. In thin films, for example, a sharp probe can be used to scratch the film to induce nucleation (strain-induced crystallization).

Single Crystals (2D crystal-growth)

Early observations of single crystals grown from solution were reported by Till [11] and Keller [12]. A number of reviews of studied single crystals (and other crystal morphologies) are available, including texts by Geil [13], Khoury et al. [14], and Bassett [15]. Polymer single crystals, shown schematically in Figure 1.2, are comprised of a number of folded polymer chains. Growth of single crystals is only observed under very specific conditions, such as crystallization from very dilute solutions or at small undercooling from the melt. These single crystals generally have regular shapes and reflect the symmetry of the unit cell (as is generally true of most crystallization morphologies). These crystals are highly faceted, for reasons to be discussed later. In addition, single crystals are often sectorized. Sectors represent different directions of chain-folding and are normally defined by the diagonals of the crystal [12].

Polymer single crystals are very unusual for a number of reasons. For example, they are very thin in one dimension (tens of nanometers) while relatively large in the other two (microns). In addition, these crystals inherently contain some non-crystalline material due to the disordered nature of the fold loops on the crystal surface.

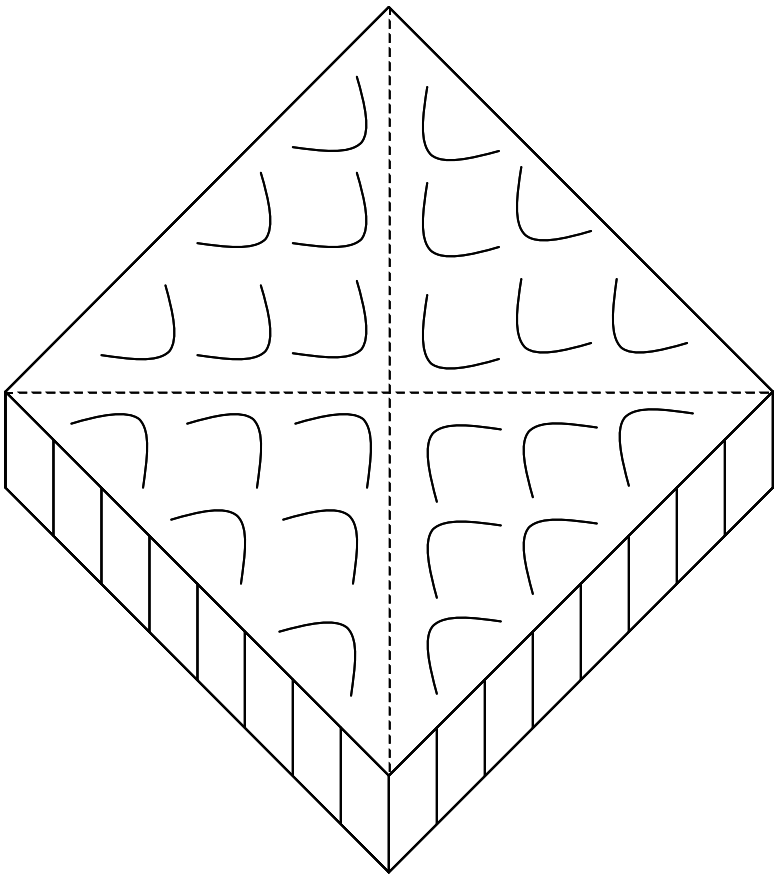

Figure 1.2 Sectorized polymer single crystal (lamella).

Growth of single crystals occurs along specific crystallographic planes, which are determined by the surface energy of the planes. These crystals often have a plate-like or ribbon-like geometry. Plate-like single crystals are normally observed in polymers with high symmetry unit cells (e.g. hexagonal, tetragonal, etc.), while ribbon-like crystals are normally observed for lower symmetry unit cells [5]. The geometry of these crystals may have important consequences in morphological development as will be shown later.

Single crystals are normally only observed very near the melting point and in solution growth where growth rates are very slow. Growth at higher velocities results in a higher density of defects and ultimately leads to the formation of multiple crystalline layers through some branching mechanism [16,17]. The result of branching is a stacked lamellar structure. Hence, polymer single crystals are often referred to simply as lamellae (regardless of whether they are in a stacked form or in a single layer).

Three-dimensional Growth Morphologies (Axialites and Spherulites)

Early studies of crystallization in polymer melts revealed that spherulites are the predominant macroscopic morphology in crystallizable macromolecules [18]. This observation was quite surprising, given the rarity of spherulitic structures in other systems.

Very near the melting point, the single crystals tend to be more perfect (few defects are introduced into crystal). However, during the growth of these single-crystal lamellae, new layers develop by some branching mechanism(s). The nature of the branching mechanism is still highly debated, although screw dislocations are believed to be the dominant mechanism [14,15]. These screw dislocations may form due to a buildup of mechanical stress at the interface. Nucleation of new layers by an epitaxial mechanism (heteronucleation) has been observed in isotactic poly(propylene) (iPP), but this is considered to be a special case and is not generally applicable [19,20].

Both of these mechanisms (screw dislocations and heteronucleation) occur out of the plane of crystal growth. Mechanisms for branching in the plane of growth are not frequently discussed in polymer literature, but recent studies have shown that these

mechanisms may be important, especially in thin film geometries [21]. More discussion of this point is found in the Chapter 1.8 on crystallization of polymer thin films.

As new layers develop on the crystal, they begin to splay apart. The details of this splaying process are not well understood. Bassett et al. conjectured that splaying is the result of cilia pressure or stress on the fold surface [3]. On the other hand, Schultz proposed that splaying occurs as a result of diffusion, where the lamellae splay in order to be exposed to the largest amount of material [9].

Collections of slightly splayed lamellae are often referred to as hedrites for high symmetry crystals (or axialites for highly elongated crystals). Hedrites are often considered to be the precursors to spherulite formation, although hedrites may not always develop into well-defined spherically symmetric spherulites. At larger undercooling, growth of new layers in conjunction with splaying results in the well-known spherulitic morphology, as shown in Figure 1.1.

Another important issue is whether spherulites are polycrystalline structures. If the branching process occurs exclusively through the formation of screw-dislocations, then spherulites should be single crystals. X-ray diffraction studies of spherulites reveal polycrystalline textures, but these patterns do not necessarily indicate that spherulites are polycrystalline because lamellae have the ability to bend and twist, resulting in a relatively disordered array of crystal axes. However, if multiple independent primary lamellae are nucleated from a single nucleation site, the resulting spherulitic morphology is indeed polycrystalline. Spherulites are generally considered to be polycrystalline despite the fact that this classification may be purely artificial.

Crystal Growth Kinetics

Crystal growth in polymeric materials is normally considered to be a nucleation-controlled process, meaning that the rate of crystal growth is governed by the rate of secondary nucleation at the growth front. Secondary nucleation (not to be confused with secondary crystallization) is the rate-limiting process during which a stable nucleus forms on the growth front by the addition of new stems. Once a stable chain-folded nucleus is

formed, further chain-folding proceeds parallel to the growth face, leading to a new crystalline layer at the crystal growth front.

In polymers, diffusion of heat from a growing crystal is usually not a rate-limiting process as is typical of solidification of metals. At very large undercooling where crystal growth rates are large, diffusion of heat could potentially limit the rate of crystal growth. The onset of the glass-transition temperature in these materials often prevents access to this diffusion-limited regime in standard crystallization experiments.

Hoffman has developed a kinetic theory for the rate of crystal growth in polymeric materials [22]. While detailed discussions of this are beyond the scope of this introduction, some important points of crystal growth kinetics are discussed below.

Very near the melting point, growth of the lamellae is very slow because the formation of a stable secondary nucleus is associated with a large free energy of activation. In addition, in polymeric materials, the initial thickness of the crystal increases with decreasing undercooling [23]. As a result of the large crystal thickness, the energy penalty for the addition of new stems is very large. At larger undercooling, the crystals become thinner and the rate of secondary nucleation becomes larger, resulting in faster growth.

At very large undercooling (near the glass-transition temperature), the crystal growth process is slowed by the limited mobility of the polymer chains. The competing effects of the secondary nucleation and chain mobility are shown in Figure 1.3.

When growth rate measurements are made, the position of growth "envelope" is often measured, which represents an average growth front for a collection of lamellar crystals. The rate of growth measured via the envelope is an acceptable measure of the individual crystal growth rate because the lamellae have a radial orientation. One would expect that the lamellae would compete for the material available for crystallization, and thus the growth rate of a spherulite would be less than that of individual lamellae. However, since crystallization in polymers is generally a nucleation-controlled process, the limiting factor in crystal growth is the attachment of a polymer segment to the lamellar crystal and not the availability of crystallizable components. This issue will be readdressed later when discussing other modes of crystallization such as dendritic growth.

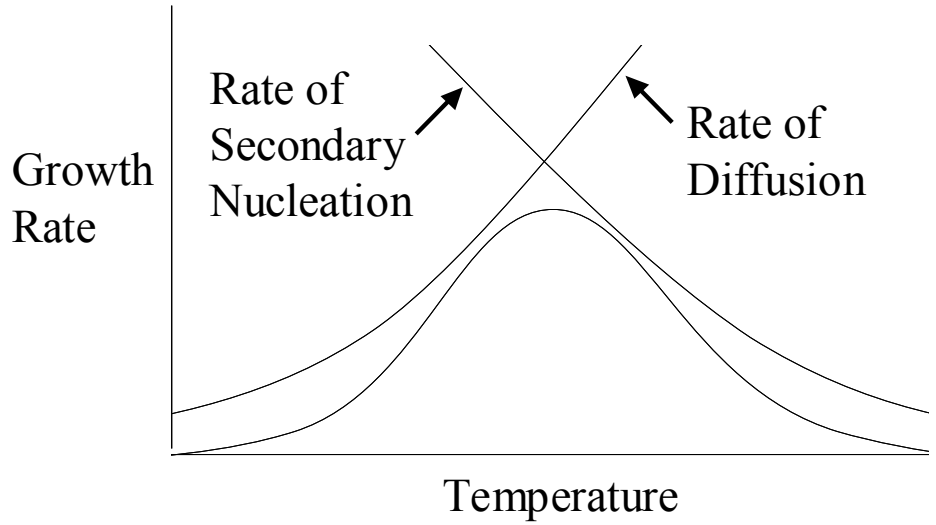

Figure 1.3 Competition between the rates of secondary nucleation and diffusion results in a bell-shaped growth rate curve.

Chapter 1.3 Polymer Blends and Phase Separation

Metallurgists have used alloying processes for many years in efforts to increase the performance of metallic systems. Similarly, polymer blends have been the subject of great interest due to their unique materials properties [24,25]. These systems generally have improved properties (electrical, optical, etc) over that of the individual components. However, the mechanical properties of polymers are not generally derived from the same mechanisms as metals and their mechanical properties generally lie somewhere between the properties of the individual components [26].

Thermodynamics of Polymer Miscibility

Most polymer systems are not miscible. A quick review of the thermodynamics involved gives the somewhat unexpected result that the entropy of mixing (ΔS_{MIX}) is usually very small, so there is little drive for mixing to occur. If the heat of mixing is only slightly positive, the polymers are generally not miscible and phase separation occurs. Specific interactions between polymers, such as hydrogen bonding, can result in a slightly negative heat of mixing, making the polymers miscible.

The kinetics of phase separation can vary quite widely and can be a function of chain flexibility, branching, and side-group interactions [26]. The size-scale and morphology of phase separation is also affected by a number of factors, including molecular details and kinetics. More detailed reviews of the thermodynamics involved can be found in texts by Olabisi et al. [26] and Paul et al. [27].

Phase Separation in Confined Geometries

Phase separation in thin film geometries is known to differ quite dramatically from that in the bulk. Confinement of the polymer chains in two dimensions usually limits the ability of the blend to phase separate in the plane of the film, although some

phase separation may occur through the film thickness due to interactions with the air or substrate interfaces [28,29]. The mechanisms that hinder phase separation in confined geometries are not well understood, but may be related to the reduced mobility (glass-transition temperature and/or diffusion coefficient) in thin-film geometries.

The presence of impurities may also play a role in phase separation processes. Impurities added to thin film samples have also been observed to affect the phase separation process. Fullerenes, for example, have been observed to stop phase separation in polystyrene and polybutadiene from occurring at all [30]. The mechanisms are also not well understood in this case.

Phase separation during crystallization

Another type of phase separation occurs in polymer blends when only one of the components is crystallizable. In polymeric systems, co-crystallization is an extremely rare phenomenon. Hence, the non-crystallizable components are generally completely rejected from the crystal. As crystallization progresses, the non-crystallizing component may be rejected ahead of the crystal into the melt. If rejection occurs in this manner, the melt is enriched in the non-crystallizing component resulting in a different value for the glass-transition temperature of the melt (may be raised or lowered) and often a lower melting temperature.

The details of rejection of the non-crystallizing components are not well understood [9,31]. For blends where the crystal melting point is not affected by blending (small χ values), the growth rate is often constant with time, meaning that the melt ahead of the crystal is not enriched in the non-crystallizing component. In this case, the rejection may occur either between the lamellae or in the plane of the lamellae. However, if the melt ahead of the interface were enriched in the non-crystalline component, the growth rate often decreases with time (depending on a variety of factors such as the glass-transition temperature of the second component). Despite the large number of studies focusing on this issue, an understanding of this process at the molecular level is still incomplete. For further discussion, the reader is directed to papers by Kit and Schultz [32,33], Keith [34], and Keith and Padden [35].

In addition to affecting the crystal growth rate, phase separation can play a dramatic role in crystallization morphologies. Phase separation can affect the crystalline domain size and the observed morphology because of the role of the T_g (determined by the blend composition) in the diffusion coefficient and the crystal growth rate. These issues will be touched upon in more detail later in this text.

Chapter 1.4 The Glass Transition Temperature

Glass transition in bulk homopolymers

The glass transition temperature (T_g) is generally considered to be the temperature below which no long-range coordinated motion occurs in the amorphous state. The experimental glass transition is believed to be a purely kinetic phenomenon, and its location depends highly on the cooling rate.

T_g determinations are very common in polymeric materials because of the ease of measurement and the important role of the mechanical properties and crystal growth rate. Since crystallization is relatively slow and incomplete in most polymers, the observation of the glass-transition temperature is possible. This is not the case in many metallic systems because the material crystallizes completely before the T_g can be reached.

One of the most common experimental methods of determining T_g is by differential scanning calorimetry (DSC). However, the measured value of T_g is highly dependent on the scan rate and the sample's thermal history.

Glass transition in polymer blends

Determination of the glass transition temperature of a polymer blend can be much more complicated. If the blend is immiscible, the polymers will phase separate, and the T_g's of the individual components will be observed. For a completely miscible blend, the T_g is a function of the composition and can often be described by the Fox equation [36]:

$$1/T_g = x_A/T_{g,A} + x_B/T_{g,B} \qquad \text{Eq (1.17)}$$

where x_A is the weight fraction of component A, x_B is the weight fraction of component B, $T_{g,A}$ is the glass-transition temperature of component A, $T_{g,B}$ is the glass-transition temperature of component B, and T_g is the glass-transition temperature of the blend. The T_g is also dependent on the molecular weight since the chain ends typically exhibit larger segmental mobility than repeat units in the middle of the chain. Fox and Flory developed a basic theory based on studies of the molecular weight dependence of T_g in polystyrene [37].

Recent studies have called into question the meaning of the T_g in miscible blends. For example, relaxation studies of miscible PEO/PMMA blends have shown very large differences in the relaxation time between the PEO and PMMA components [38,39,40]. These results indicate that PMMA is largely immobile on the time scale of motion of the PEO chains, meaning that the bulk T_g does not reflect the mobility of the individual components.

Glass transition in thin film / confined geometries

Recent studies in thin polymer films have revealed that the T_g can be dependent on the sample thickness [41,42,43,44,45]. Some researchers initially believed that T_g would be lower in thin films due to an increase in mobility at the polymer-air interface, while the confining effects of the thin film geometry were thought to increase the T_g. Experiments later showed that the T_g is highly dependent on the relative surface energies of the polymer and the substrate surface [45]. Attraction between the polymer and the surface can result in a much higher T_g, while no interaction or repulsion may result in a much lower T_g.

Although the nature of the interactions between the polymer and substrate may play the largest role in the magnitude of the observed T_g, a number of other factors may also play a role (such as plasticization of the polymer by air may also affect the T_g near the air surface). In addition, the role of the polymer/substrate interface may not extend through the film thickness. The combination of these effects may result in a highly different T_g at the film surface.

Ellison and coworkers recently studied confinement effects on the T_g of polystyrene films [46]. These studies stressed the importance of the dynamics of cooperative motion. Adam and Gibbs originally introduced this idea in their discussion of the cooperatively rearranging region (CRR) for glass-forming materials [47]. Since the dynamics vary widely with the position in the film thickness for reasons discussed above, there may be a significant gradient in the magnitude of the T_g through the film thickness. Such a gradient may affect other processes such as crystal nucleation and growth.

Chapter 1.5 Diffusion of Polymer Chains

Diffusion of polymer chains is important in many processes, including crystallization and phase separation. The rate of diffusion can be affected by several factors including the chain length, blend composition, glass transition temperature, absolute temperature, and other details of the chain structure. Reviews of diffusion in polymers have been given by Kausch et al. [48], Klein [49], Graessley [50], and Pearson [51]. This section is outlined in a manner similar to that of Kausch et al. [48].

Background and Definitions

Diffusion in polymeric materials is a highly complex process. Two factors control this process, one is thermodynamic and the other is a dynamic effect. The thermodynamic effect relates simply to the interactions between dissimilar molecules (typical of all materials). The dynamic effect takes into account the fact that polymers are long chains and contain entanglements. The large size of polymer molecules means that the entanglements of segments between different molecules whose centers of mass are highly separated must be considered. This dynamic effect is what differentiates polymer diffusion from diffusion of metals and small molecules.

Several terms must be defined to specify what type of diffusion is occurring. *Self-diffusion* refers to the case where a molecule is surrounded by identical neighbors. The self-diffusion coefficient is defined by the evolution of the position of the center of mass, r_{CM}, of the molecule in the limit of long times:

$$D_s = < [r_{CM}(t+t_o) - r_{CM}(t_o)]^2 > / 6t \qquad \text{Eq (1.18)}$$

Tracer-diffusion (D^*) is the same as self-diffusion with the exception that the background need not be composed of identical molecules. The molecule is assumed to be in thermal and chemical equilibrium with the background. This tracer-diffusion coefficient is often dependent on the composition due to different amounts of friction experienced by the molecule. Both self- and tracer-diffusion coefficients are driven by entropy, which pushes the system towards randomization.

Mutual-diffusion (or interdiffusion), D_M, is a much more complicated process. In this case, D_M is given by Fick's Law, which relates the flux of a species i, J(i), to the gradient in concentration, ∇c_i, given in moles of molecules per unit volume:

$$- J_i = D_M \nabla c_i \qquad \text{Eq (1.19)}$$

Here, the flux J_i is defined with respect to a coordinate system with a fixed center of volume and is related to the fluxes, J_i^m, defined in the center of mass frame of reference as $J_i = \rho V_i^m J_i^m$ (where ρ is the mass density and V_i^m is the partial specific volume). D_M is dependent on thermodynamic interactions (attractive or repulsive) and thus can be considerably larger or smaller than the self-diffusion coefficients.

Chain Length Dependence of Diffusion

The chain length dependence of the diffusion coefficient is now discussed in further detail. In order to do so, the random-coil model of a molecule is used due to its simplicity.

The Rouse model is commonly used for discussions of the dynamics of random coil chains [52]. This model involves a linear series of beads connected by springs. These springs have some friction with the surrounding medium and a corresponding friction coefficient, ξ. The result for the diffusion coefficient is:

$$D_{ROUSE} = kT/N\xi \approx M^{-1} \qquad \text{Eq (1.20)}$$

Since the diffusion coefficient is inversely proportional to the molecular weight, each bead feels the same amount of friction and the whole molecule feels the sum of the friction acting on each bead.

This model does not describe the effects of entanglement however. Thus, D_{ROUSE} is used to describe the self- or tracer-diffusion coefficients for molecules with lengths below the entanglement point.

To account for these entanglement effects, de Gennes proposed the reptation model [53]. Reptation requires snake-like motion of a chain through a series of entanglements for diffusion to occur. Doi and Edwards defined a tube through which this motion occurs [54]. The diffusion coefficient in this case is related to the time necessary for the chain to escape the tube and the rate of motion of the center of mass of the chain. In this reptation regime:

$$D_{REPTATION} \approx M^{-2} \qquad \text{Eq (1.21)}$$

Lodge has collected experimental data from a large number of polymers and shown that the correct scaling law is $D \sim M^{-2.2}$ [55]. The reasons for this discrepancy are not well understood but are likely related to the simplicity of the reptation model in accounting for entanglement effects (such as neglecting constraint-release or tube renewal processes).

Diffusion in Polymer Blends

Kramer [56], Silescu [57], and Brochard [58] later developed theories for the mutual diffusion in polymer blends. The theories of Kramer and Silescu are generally referred to as "fast theory" meaning that the component with the larger diffusion coefficient is largely responsible for the mutual diffusion coefficient, while Brochard's theory is referred to as "slow theory" for the opposite reason.

Since experiments have generally shown that the fast theory applies [59,60], this theory will be discussed in more detail. The composition dependence of the mutual diffusion coefficient is given as [61]:

$$D_M = k_B T[\{(1-\phi_2)(B_1 N_{e1}/N_1) + (\phi_2)(B_2 N_{e2}/N_2)\}*$$
$$\{(1-\phi_2)/N_1 + \phi_2/N_2 + 2\phi_2(1-\phi_2)|\chi|\}] \qquad \text{Eq (1.22)}$$

where k_B is the Boltzmann constant, T is the absolute temperature, ϕ_2 is the volume fraction of component 2, $(N_e)_i$ is the entanglement molecular weight of component i with segmental mobility B_i, N_i is the number of repeat units, and χ is the Flory-Huggins interaction parameter. The self-diffusion coefficients are given by:

$$D = k_B T B_1(T) N_{e1}/N_1^2 = D_1 \qquad \text{Eq (1.23)}$$
$$D = k_B T B_2(T) N_{e2}/N_2^2 = D_2 \qquad \text{Eq (1.24)}$$

The segmental mobilities are a function of temperature, so the temperature dependence of the diffusion coefficient comes from the T and B_i terms.

Theories for polymer blends become particularly complicated when trying to account for the temperature dependence of D_M in the temperature range encompassing the blend component T_g's. An Arrhenius type relationship is often used at high temperatures, while a Williams-Landel-Ferry (WLF) relationship can be used near the glass-transition temperature; however, the temperature dependence of D_M is often not reported in experimental studies of blends (especially ones where the homopolymers have very different glass-transition temperatures) very near the T_g so the applicability of the WLF theory is certainly speculative.

Another problem with diffusion coefficients in blends systems is that in some systems where the blend components have widely different T_g's, the chain dynamics can vary by several orders of magnitude [62]. In these situations, it is not clear that the mutual diffusion coefficient determined by "fast" or "slow" theory has any physical meaning.

Chapter 1.6 Crystallization Morphologies

Background on Crystallization Morphology

The study of crystalline morphologies has had a long history, dating back to studies of snowflake morphologies [63]. Nakaya published one of the most complete

studies of snowflake morphology in the 1950's [64]. Metallurgists began much of the academic research on crystalline morphologies because the morphology is known to have a dramatic effect on mechanical properties [65]. Both academic and industrial researchers have developed interest in controlling the morphology and understanding the mechanisms of morphological development.

The term "morphology" refers to the shape of the crystallization pattern. There are several morphologies that are commonly found in crystallization of materials, including *single crystals*, *dendrites*, *seaweed*, and *spherulites*. Many of these names refer to the growth shape of single crystals. Some important limitations to crystal growth will be addressed followed by a more detailed discussion of each of these morphologies.

Crystal/melt Interfaces and Limitations on Crystal Growth

Two classes of interfaces are common in crystal growth: faceted (or smooth) and non-faceted (or rough). An interface may exist in an intermediate state, but this type of growth will not be addressed here. A faceted interface is one that is smooth at the atomic level, while a non-faceted interface is one that is atomically rough. The nature of the interface type has direct consequences on the process of atom attachment to the growing crystal. When the interface is rough, there are a large number of favorable atomic attachment sites. The result is that growth proceeds in a manner that is relatively independent of crystallographic orientation, which is often the case experimentally. If the interface is smooth, there are few favorable sites for atom attachment during crystal growth. Thus, after the formation of a stable nucleus on the flat interface (termed "secondary nucleation"), growth occurs by a lateral spreading process. This "secondary nucleation" mechanism is believed to be dominant in polymer crystal growth.

Jackson has proposed a parameter to describe whether an interface will take on a smooth or rough interface [66]. This parameter is referred to as the "Jackson alpha parameter" and is given as:

$$\alpha = \Delta S_f / R \qquad \text{Eq (1.25)}$$

where ΔS_f is the entropy of fusion and R is the gas constant. In metallic systems, the entropy of fusion is relatively small (little change in entropy between the liquid and solid states) so the alpha factor is also small (~1). In polymeric systems, the ordering of the chains upon crystallization results in a relatively large change in entropy, resulting in a much larger value of alpha (~100). However, metals can grow with smooth interfaces from a vapor phase (in this case, alpha has a value near 10 due to the relatively large change in entropy between the vapor and solid phases).

As previously discussed, the driving force for crystallization is related to the undercooling ($\Delta T=T_m^o - T_x$), where T_m^o is the equilibrium melting temperature and T_x is the crystallization temperature. The undercooling can be partitioned into several quantities based on the portion of the free energy consumed during each of the processes involved in crystal growth [67,68]:

$$\Delta T = \Delta T_S + \Delta T_E + \Delta T_K + \Delta T_H \qquad \text{Eq (1.26)}$$

where ΔT_S drives solute transport, ΔT_E drives production of a non-equilibrium (curved) solid, ΔT_K drives interface attachment, and ΔT_H drives heat dissipation. These terms are defined as:

$$\Delta T_S = T_L(C_\infty) - T_L(C_i) \qquad \text{Eq (1.27)}$$

$$\Delta T_E = T_L(C_i) - T_E(C_i) \qquad \text{Eq (1.28)}$$

$$\Delta T_K = T_E(C_i) - T_i \qquad \text{Eq (1.29)}$$

$$\Delta T_H = T_i - T_x \qquad \text{Eq (1.30)}$$

where $T_L(C_\infty)$ is the melting temperature of the pure material (frequently denoted T_m^o in polymer literature), $T_L(C_i)$ is the interface temperature at composition C_i, $T_E(C_i)$ is the equilibrium interface temperature (considering Gibbs-Thompson effects), T_i is the actual interface temperature, and T_x is the bath temperature (temperature far from the interface). Each of these terms may play an important role in determining the overall undercooling of the system, depending on the system. In most systems, the bulk of the driving force comes from the ΔT_H or ΔT_S term, which are related to diffusion. In polymers, growth is normally limited by molecular attachment (secondary nucleation) so ΔT is primarily controlled by the ΔT_K term.

There are several limitations to growth of an interface, including the kinetics of atom attachment, capillarity (or surface tension), and diffusion of heat or mass. The interplay of these limitations determines the growth morphology and length scales of the resulting crystallization pattern.

Capillarity is related to change in melting point due to the pressure drop across a curved interface. The capillary term is referred to as the Gibbs-Thomson relation and is given as [65]:

$$\Delta T = \Gamma K \qquad \text{Eq (1.31)}$$

where K is the radius of curvature and Γ is the Gibbs-Thomson coefficient given by:

$$\Gamma = \sigma / \Delta S_f \qquad \text{Eq (1.32)}$$

where σ is the interfacial energy (which is anisotropic and thus also a function of the curvature) and Δs_f is the entropy of fusion. Thus, capillarity tends to be a stabilizing force for an interface, resulting in flat interfaces. However, capillary forces are only active at extremely small length scales, given by the capillary length:

$$d_o = \gamma T_m c_p / L^2 \qquad \text{thermal mode} \qquad \text{Eq (1.33)}$$

$$d_o = \gamma/(\Delta C)^2(\partial\mu/\partial C) \qquad \text{chemical mode} \qquad \text{Eq (1.34)}$$

where γ is the liquid/solid surface tension, T_m is the melting point, c_p is the heat capacity of the solid, L is the latent heat, C is the concentration of solute, and μ is the chemical potential of the solute.

As in nucleation, any protrusion developing on a planar interface will have a high surface to volume ratio, meaning the surface will have a large surface energy. As a result, any protrusion that develops will be unstable and tend to melt back into the liquid. Similarly, any part of the liquid lagging the crystallization front tends to crystallize rapidly.

Since the surface energy is dependent on the crystal face, the surface energy term can be highly anisotropic. Close-packed planes (low index type) are often low energy, while the high index planes are rough and high energy. Thus, growth occurs quickly along the high index planes and growth quickly becomes limited by the slower growing close-packed planes. This anisotropy in attachment kinetics results in the development of faceted crystal faces.

In polymers, where growth is limited by nucleation, growth typically occurs along low index planes and the crystals are highly faceted. Slight differences in the surface tension along different planes can result in ribbon-shaped lamellar crystals.

Diffusion, generally considered a destabilizing force, acts to counter the stabilizing action of capillarity and anisotropic attachment kinetics. Diffusion of heat or mass from an interface acts to make protrusions stable because these protrusions are more exposed to the undercooled melt. As previously discussed, a common measure of the effect of diffusion in a crystallizing system is the "diffusion length". The diffusion length is defined as:

$$\delta = D / V_D \qquad \text{Eq (1.35)}$$

where D is the diffusion coefficient and V_D is the growth velocity. The diffusion length can be considered an upper-bound for the length scale of the crystallizing solid.

Single Crystals

Now that the limitations to crystal growth (which often determine the observed morphology) have been discussed, frequently encountered crystal growth morphologies are discussed, starting with single crystals.

In the case of metals and other materials with small entropies of fusion, continuous crystals with no grain boundaries are often referred to as single crystals. These single crystals do not take on any particular shape in the absence of external constraints (such as the container holding the sample). However, in discussions of pattern-formation, the term "single crystal" takes on a different meaning. Here, single crystals are described in a similar manner to those already described, with the additional constraint that the crystals have geometric (polyhedral) shapes that are determined by the low-index (smooth) planes. Polymer lamellae crystallized from solution represent one such example.

Dendritic Growth

Dendrites are often encountered in the casting of metals and in nature in the form of snowflakes. The mechanisms involved in dendrite formation vary with the type of system, but in all cases, dendritic growth is a diffusion-limited growth process. In pure melts, thermal dendrites may form, while compositional dendrites may form in multi-component systems. A more detailed description of the dendritic growth process is found later in this text. Here, only a basic summary of dendritic growth is given.

Thermal dendrites are generated by small fluctuations in temperature at the solid/liquid interface. If a temperature fluctuation causes a small protrusion to develop in the interface, heat can more easily be removed from the interface, as illustrated in Figure 1.4. In addition to the increased ability of a protrusion to remove heat, the heat leaving the sides of the protrusion prevents growth of surrounding interface. This type of instability is generally referred to as a Mullins-Sekerka instability [69,70].

As the protrusion grows, sidebranches form along the length of the trunk. These "secondary" sidebranches grow and eventually develop sidebranches of their own ("tertiary" sidebranches). This tree-like crystal is called a dendrite (Figure 1.5).

Compositional, or solutal, dendrites are formed in multi-component melts where crystal growth is limited by the rejection of one component back into the melt. In this case, solute can be preferentially rejected at a protrusion, causing a build-up of the solute surrounding the protrusion. New protrusions are developed along the length of the first one, resulting in a similar structure to a thermal dendrite.

Dendrite sidebranches normally form at crystallographic angles to the dendrite trunk and reflect the symmetry of the crystal structure for the given material [65]. Some anisotropy in the surface energy of the crystal or atomic attachment kinetics is required to drive the sidebranches to form in such a manner. A detailed discussion of dendritic growth is found later in this text.

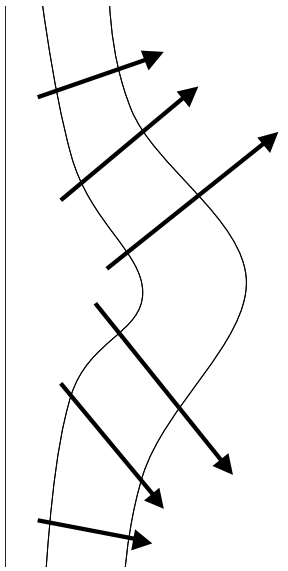

Figure 1.4 Formation of a Mullins-Sekerka instability from an initially planar interface. The arrows show the directions heat or solute is rejected from the protrusion.

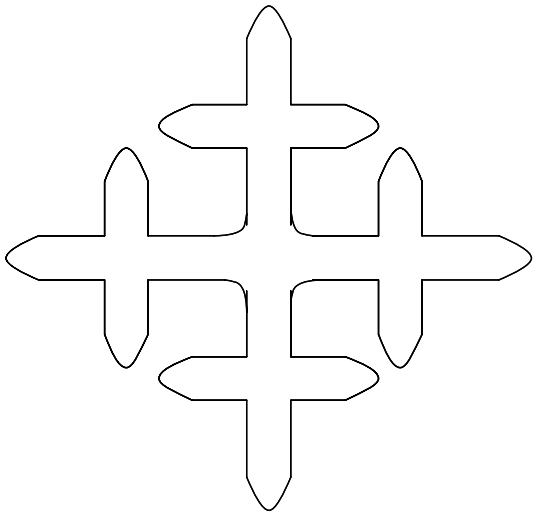

Figure 1.5 A schematic of a dendrite with 90^{o} secondary sidebranches.

Dense-Branched Morphology (or Seaweed)

The dense-branched morphology (DBM), also called seaweed, is characterized by frequent branching of the growth front. This morphology is often controversial in literature over its classification at a true morphology [71]. Dense-branched morphologies are often single crystals (crystallographically) but lack orientational order [21]. In other reports, the seaweed morphology is polycrystalline and geometrically disordered [72].

The dense-branched morphology is expected when there is weak anisotropy in the surface energy. Anisotropic systems can be driven to DBM by increasing the undercooling (where crystallization becomes equally probable on all planes) [73]. Noise (defined as small fluctuations due to Brownian motion, thermal or compositional variations, etc.) may also play a role in formation of this morphology [71]. In systems with a high noise level, dendrites are often unstable and degenerate into DBM.

Spherulitic Growth

Spherulites have already been described in some detail. The spherulitic growth morphology is very common in polymer crystallization experiments, but is certainly not well understood. This morphology is different from the other morphologies presented here in that it is normally considered to describe a polycrystalline aggregate (often of a number of large single crystalline lamellae), despite the fact that there is no evidence for distinct grain boundaries.

Lamellar eutectics are not very different in appearance from polymer spherulites. These spherical growth forms are comprised of alternating layers of (two) different phases. This is similar to polymers where the crystalline lamellae are separated by amorphous layers. However, the formation of screw dislocations in lamellar eutectic growth is not considered necessary for the formation of these "spherulites" and small angle branching is also not reported.

Spherulitic morphologies are also reported in small molecules crystallized in gels or other viscous environments [16,74,75]. The relationships between these spherulitic morphologies and polymer spherulites are certainly not well understood. Ben-Jacob [72]

and Goldenfeld [2] have suggested that spherulites are simply a three dimensional representation of the dense-branched morphology. However, such a conclusion is not supported by the current understanding of the mechanisms of spherulitic growth in polymers. Certainly further studies in this area are important in order to understand the relationships between different types of spherical morphologies.

Morphological Transitions

Morphological transitions involve a change in the observed morphology during crystal growth. These transitions may be the result of some change in the growth mechanism, such as a change from nucleation control to diffusion control. Other mechanisms may include instabilities in the growth tip (causing tip-bifurcation), changes in the noise level, and changes in the anisotropy (kinetic anisotropy or anisotropy of the surface energy).

There have been some attempts to compare morphological transitions to thermodynamic transitions [76]. In this regard, first and second order transitions have been reported. In first-order transitions, the growth velocity is discontinuous with temperature through the transition. In second order transitions, the growth velocity is continuous while its derivative is not. Although this comparison seems natural, problems may arise in the case of transient growth modes or large energy barriers between growth morphologies. The result of these transient modes is that multiple growth morphologies can coexist at a given temperature, and may depend on previous growth conditions as well as current ones [77,78].

Morphological transitions are more often reported in theoretical studies of crystal growth [79,80,81,82], although there are some experimental examples [83,84,85]. In experimental systems, the conditions can often not be varied sufficiently to promote multiple transitions. In metallic systems, for example, the rates of nucleation and crystal growth increase rapidly with the supercooling, preventing access to the kinetic regime. Small molecules suffer from similar problems in solution. Studies of melt growth in polymers have demonstrated a wide variety of morphologies, especially in thin film

geometries [6,7,21]. Polymeric systems are particularly interesting because of the large range of possible supercooling and the abilities to tune diffusion coefficients and crystal growth rates. These issues are addressed in more detail in the section on crystallization of polymer thin films.

Chapter 1.7 Dendrite Theory

Background on Dendritic Growth

Dendritic growth is a highly complex non-equilibrium growth process. Some important issues related to dendritic growth include the formation of sidebranches, the size or width of the dendrite arms, the spacing between the arms, and mechanisms for selection of dendrites over other morphologies. These issues are not only academically interesting, but are also highly important in industry because mechanical properties can depend highly on the microstructure that develops [65]. In addition, recent interest in non-equilibrium pattern-formation has renewed interest in dendritic growth because of their prevalence in solidification processes and the relatively simple mechanisms of growth.

The formation of a dendrite involves two main processes, the propagation of the dendrite tip and the formation of sidebranches [86]. The dendrite tip is normally considered to have a paraboloidal shape [87]. The sidebranches develop at some distance behind the tip, usually on the order of several times the radius of the tip curvature, and grow at a specific angle from the dendrite trunk, reflecting the symmetry of the crystal lattice (90^{o} for cubic materials).

Detailed mathematical descriptions of dendritic growth have been worked on for a number of years. Ivanstov is credited with the the first model for the growth of needle crystals [87]. Ivanstov's theory models the steady state-state growth of the dendrite as a paraboloid of revolution. This analysis is applicable only near the tip region where the dendrite is indeed parabolic. The time-dependent aspects of dendritic growth, such as sidebranch formation were ignored in this treatment. Capillarity effects were also

ignored, so the interface was considered to be isothermal. The major result of this theory is the prediction of a relationship between the dendrite growth velocity, V, and the tip radius, R as a function of the undercooling or supersaturation. In this scenario, the tip radius and growth velocity are related by:

$$VR = \text{constant} \qquad \text{Eq (1.36)}$$

and unique values of the V and R are not known. Thus, a family of solutions for V and R are predicted. Obviously, one would like to predict unique values of V and R for a given set of growth conditions. In order to do so, the kinetics of molecular attachment and the effect of local curvature (capillarity) must be considered in the problem.

Temkin later made these important modifications to dendrite growth theory [88]. As previously mentioned, the curvature of the interface implies that the equilibrium melting temperature must vary with position on the interface. Thus, the driving force for crystallization also varies with position. Temkin then applied the "maximum velocity principle" which suggests that the selected growth velocity is the fastest one possible. For a number of years, this assumption was assumed to be correct. Nash and Glicksman later worked on this problem and eventually concluded that the maximum velocity principle was incorrect and led to inaccurate estimates of the crystal growth rate [89].

Müller-Krumbhaar and Langer later proposed the marginal stability hypothesis (MSH) [90,91,92,93]. The idea of this theory has that stability mechanisms were very important in selection of the dendrite radius and growth velocity. A number of other theories have been developed since this time, including the microscopic solvability condition (MSC) [94,95,96,97], and interfacial wave theory (IFW) [98]. Although these theories represent progress toward a deeper understanding of dendritic growth, there is still much disagreement in this area.

Another major problem in the area of dendritic growth has been the lack of detailed experimental studies. Often, morphological studies have focused on growth shapes without paying attention to other details such as the crystal growth rate. In polymeric systems, one major obstacle for experimental studies is often the lack of fundamental information about the materials, such as the anisotropy of the surface tension and diffusion coefficients. However, by using ideas developed from the field of dendritic crystallization, some of this information may be extracted.

Sidebranch Formation

The formation of sidebranches in dendritic growth has been studied for a number of years [99,100]. Two mechanisms for sidebranch formation have been proposed. The first mechanism involves the role of noise [101,102,103] and the second involves the existence of a limit-cycle during crystal growth [104,105,106].

Noise is generally considered an integral part of crystallization because of its importance in nucleation of undercooled melts [107]. Noise during dendritic growth may cause fluctuations (protrusions) of the interface. If the fluctuation is large enough to stabilize the protrusion against capillary action, the protrusion is stable and growth of the new sidebranch continues. For noise-induced sidebranches, the sidebranches are not correlated along the length of the dendrite trunk. Indeed, such a situation is often observed experimentally [108]. Williams and coworkers have also attempted to stabilize a system against noise by pulsing a laser at the tip of a dendrite to heat it slightly [109]. In these experiments, the normally dendrite has uncorrelated sidebranches, while the one heated one has perfectly correlated sidebranches.

Other studies have demonstrated perfect correlation of the sidebranches in normal growth experiments [104]. A limit-cycle is believed to be the cause of sidebranch formation in these systems. In a limit-cycle, the rate of growth is not constant but is periodic. This periodic growth is the result of changes in the tip radius with time. As the tip grows, it becomes fatter and ultimately flattens out. This flattening process releases two sidebranches that grow in unison. A new dendrite tip develops at the growth front and eventually flattens to release a new set of sidebranches. This type of growth mechanism is less commonly observed for reasons not well understood.

Huang and Glicksman have reported detailed studies of the time dependent aspect of sidebranch growth [99]. Some of the important features of the growth of sidebranches are the coarsening process and the shape of the growth envelope (the shape of the crystal if the tips of the leading dendrite arms are connected).

When the dendrite arms are formed, they compete in a diffusion field with other nearby arms. Some of the branches slow down and are cut-off by neighboring sidebranches. This processes is known is kinetic coarsening. As the “winning” branches

escape the overlapping diffusion fields, they begin to grow faster until they reach the steady-state velocity of the dendrite trunk.

Another coarsening process is that of isothermal coarsening. This mechanism involves a reduction in the overall surface energy of the system as it tries to return to equilibrium (after the non-equilibrium growth process). Here, the growth arms are eliminated completely as the solid fills in behind the growth front. This isothermal coarsening process is much slower than kinetic coarsening. As discussed in Chapter 3, isothermal coarsening may be eliminated altogether in polymeric systems.

The envelope surrounding the crystal has been studied for a number of reasons. Huang and Glicksman have used the envelope to determine the time scale over which competition between sidebranches occurs [99]. Shochet and coworkers have attempted to use the envelope as a means of describing the morphology (seaweed versus dendrites) [110]. A significant amount of information is contained in this envelope, including the diffusion length and competition effects, and is very important for the analysis of pattern formation during crystallization.

Chapter 1.8 Thin Film Crystallization of Polymers

Crystallization of thin polymer films has recently become a topic of great interest due to the industrial need for high performance thin films. Many studies of thin films have focused on the thickness range of one to a few hundred nanometers because of changes in the glass transition temperature [41,42,43,44,45,46] and crystal growth rates [111,112,113]. Changes in the crystal orientation and morphology have been noted in this in thin film samples [8,114,115,116,117].

The crystal growth rate in the thin film geometry is often lower than that of the bulk state. Despotopoulou and coworkers reported reduced growth rates in thin films of poly(di-n-hexylsilane) [111]. They reported that the growth rate slowed when the film thickness was of the same order as the crystallite size. As discussed previously, the glass-transition temperature in the thin film geometry may be substantially different from the bulk state, and may have an influence on the observed growth rate. In addition, the

lower dimensionality of the thin film geometry means that fewer chains are available at the growth front for crystallization, making diffusion of the chains a much more important process than in the bulk state. Any chains that are available at the interface may also have difficulty arranging themselves in a position that is favorable for crystallization given the large size of the secondary nucleus in polymeric materials.

Diffusion of material to and away from the interface becomes very important in the thin film geometry. In polydisperse or blend systems, the non-crystallizing species must diffuse away from the interface for growth to proceed. Since diffusion is largely two-dimensional in thin films, these impurities must be rejected in the plane of growth. As in the dendritic growth processes described above, the rejection of these impurities results in an unstable interface and is subject to destabilization by Mullins-Sekerka type mechanisms.

In addition to diffusive destabilization, changes in density upon crystallization can result in a depletion zone surrounding the crystal and further destabilization of normally faceted crystals [21].

The lamellar thickness is another important issue in thin-film growth. Mareau and coworkers have reported that the lamellar thickness is independent of the film thickness [115]. However, the thickness of the lamellae is still dependent on the crystallization temperature. At small undercooling, the crystals are relatively thick and a larger depletion zone may be expected in front of the crystal. As the undercooling increases, the thickness decreases, as does the depletion zone. In addition, growth becomes increasingly three-dimensional with increasing undercooling because of the larger amount of space available for crystallization. The increased dimensionality may take the form of layered growth through the formation of screw dislocations, increased bending and twisting of lamellae, or a number of other alternatives.

The typical morphologies in bulk polymeric systems are single crystals at very high temperatures and spherulites at lower temperatures. However, as studies have moved into the thin film regime, new morphologies (to polymer crystallization) have been observed, including the dense-branched morphology [115,116,117,118,120], dendrites [6,7,8], and fractals [6,7]. These morphologies can depend strongly on film thickness, crystallization temperature, and a variety of other factors.

Taguchi et al. [21] and Beers et al. [118] recently studied crystallization of thin films of isotactic polystyrene (iPS). At high temperatures (low undercooling), faceted single crystals were observed. As the crystallization temperature was lowered, the single crystal became unstable, leading to dendritic, seaweed, and spherulitic morphologies. The observation of dendritic and seaweed morphologies was highly surprising since these morphologies had not been previously observed in polymeric systems. These findings pose new questions for crystal growth in polymers, especially in regards to the mechanisms of spherulite formation.

Studies of thin film crystallization have also given insight into the mechanisms of crystal growth in polymers. For example, atomic-force microscopy studies of PS thin-films have confirmed the development of screw dislocations, which are believed to be one of the underlying mechanisms for spherulite formation [119].

PEO thin films have been studied by a number of researchers. The effects of film thickness on the growth rate and morphology have been reported [114,120,121,122]. As the film thickness approaches about 10 nm, the observed morphology is similar to that seen in diffusion-limited aggregates. Thicker samples produce spherulitic and single crystal morphologies. The crystal growth rate in these samples increases as a function of increasing thickness (up to several hundred nanometers), above which, growth is considered to be similar to that of "bulk" samples [113]. The increased growth rate with thickness may be related to the increased amount of material available for crystallization and increase in the diffusion coefficient.

Chapter 1.9 PEO/PMMA Blends

Poly(ethylene oxide) (PEO) has been studied for a number of years because of its relatively simple chain structure and the fact that it readily crystallizes in a spherulitic morphology. The equilibrium melting point is near 70^{o}C and the glass transition temperature is near –67^{o}C (for high molecular weight samples). Poly(methyl methacrylate) (PMMA) is normally an amorphous polymer used in a number of industrial applications. For high molecular weight atactic PMMA, the Tg is often near 130^{o}C.

A large number of studies of poly(ethylene oxide) (PEO) / poly(methyl methacrylate) (PMMA) blends have been reported. This system is particularly interesting because the components are available commercially in a large range of molecular weights with narrow distributions. Many studies have focused on the miscibility of this system [123,124,125,126]. These studies have shown that PEO and PMMA are miscible over the whole range of composition for atactic PMMA. At high PEO content, crystallization is frequently observed, complicating these studies.

Other researchers have focused on chain dynamics in the blend state [127,128,129,130,131]. These results have been contradictory, partly due to the influences of PMMA tacticity and crystallization on the blend behavior. The dynamics of the PEO chains are much faster than those of the PMMA chains despite that fact that the blend is miscible. Lutz and coworkers have shown that the segmental dynamics of PEO are 12 orders of magnitude fasters than the PMMA dynamics at the blend T_g [127]. In addition, the dynamics of the PEO chains were nearly independent of composition for PEO concentrations of 0.5-30%.

The observation of widely spaced chain dynamics indicates that the PMMA acts glassy on the time scale for motion of the PEO chains. The implications of these highly different dynamics may be very important in crystallization processes. The relatively slow motion of the PMMA chains may hinder the PEO from reaching a growing crystal and affect the observed morphology.

A number of bulk crystallization studies of this blend have also been reported [61,132,133,134,135]. Many of these studies have focused on bulk crystallization behavior of blends with PEO contents above 50%. Experimental variables such as the molecular weight, crystallization temperature, and PMMA tacticity have been studied. The rate of crystallization was shown to decrease with increasing PMMA content [61]. Russell and coworkers also showed the PMMA is rejected between the lamellae in this system [135]. This point will become very important as we limit the film thickness to small dimensions and force the PMMA to be rejected in the plane of crystal growth.

Recent studies of thin film samples by Ferreiro et al. have revealed a wide variety of morphologies, including single crystals, dendrites, compact seaweed, fractal seaweed, and spherulites [6,7,136]. Further study of this system is warranted to open new avenues

to develop a better understanding of complex crystallization morphologies, such as spherulites and dendrites.

Chapter 1.10 References

[1] See B Chalmers. In *Growth and Perfection of Crystals, p. 291*, Wiley-Interscience: New York (1958) and references therein.

[2] N Goldenfeld. Journal of Crystal Growth 84, 601 (1987).

[3] DC Bassett. Journal of Macromolecular Science, Part B – Physics B42(2), 227 (2003).

[4] JH Magill. Journal of Materials Science 36, 3143 (2001).

[5] HD Keith and FJ Padden Jr. Polymer 27, 1463 (1986).

[6] V Ferreiro, JF Douglas, JA Warren, and A Karim. Physical Review E 65, 042802-1 (2002).

[7] V Ferreiro, JF Douglas, J Warren, and A Karim. Physical Review E 65, 051606-1 (2002).

[8] F Zhang, J Liu, H Huang, B Du, and T He. European Physical Journal E8, 289 (2002).

[9] JM Schultz. Polymer 32(18), 3268 (1991).

[10] D Turnbull and JC Fisher. Journal of Chemical Physics 20, 817 (1949).

[11] PH Till. Journal of Polymer Science 24, 301 (1957).

[12] A Keller. Philosophical Magazine 2, 1171 (1957).

[13] PH Geil. *Polymer Single Crystals*, Interscience Publishers: New York (1963).

[14] F Khoury and E Passaglia. In *Treatise on Solid State Chemistry, Volume 3, Chapter 6*. Plenum: New York (1976).

[15] DC Bassett. *Principles of Polymer Morphology*. Cambridge University Press: New York (1981).

[16] HD Keith and FJ Padden Jr. Journal of Applied Physics 34(8), 2409 (1963).

[17] MI Abo el Maaty, IL Hosier, and DC Bassett. Macromolecules 31(1), 153 (1998).

[18] A Keller. In *Growth and Perfection of Crystals p. 499*, Wiley-Interscience: New York (1958).

[19] F Khoury. Journal of Research of the National Bureau of Standards 70A, 29 (1966).

[20] B Lotz and JC Wittmann. Journal of Polymer Science B: Polymer Physics 24, 1541 (1986).

[21] K Taguchi, H Miyaji, K Izumi, A Hoshino, Y Miyamoto, and R Kokawa. Polymer 42, 7443 (2001).

[22] JD Hoffman and RL Miller. Polymer 38, 3151 (1997).

[23] PJ Barham, RA Chivers, A Keller, J Martinez-Salazar, SJ Organ. Journal of Materials Science 20(5), 1625 (1985).

[24] J Huang, A Prasad, and H Marand. Polymer 35(9), 1896 (1994).

[25] J Huang and H Marand. Macromolecules 30(4), 1069 (1997).

[26] O Olabisi, LM Robeson, and MT Shaw. *Polymer-Polymer Miscibility*. Harcourt Brace Jovanovich: New York (1979).

[27] DR Paul and S Newman, eds. *Polymer Blends*. Academic Press: New York (1979).

[28] L Sung, A Karim, JF Douglas, and CC Han. Physical Review Letters 76(23), 4368 (1996).

[29] BD Ermi, A Karim, and JF Douglas. Journal of Polymer Science: Part B: Polymer Physics 36, 191 (1998).

[30] KA Barnes, A Karim, JF Douglas, AI Nakatani, H Gruell, and EJ Amis. Macromolecules 33, 4177 (2000).

[31] HD Keith and FJ Padden Jr. Journal of Polymer Science B: Polymer Physics 25, 2371 (1987).

[32] KM Kit and JM Schultz. Macromolecules 35, 9819 (2002).

[33] KM Kit and JM Schultz. Journal of Polymer Science Part B: Polymer Physics 36, 873 (1998).

[34] HD Keith. Journal of Polymer Science Part A 2, 4339 (1964).

[35] HD Keith and FJ Padden Jr. Journal of Applied Physics 35(4), 1270 (1964).

[36] TG Fox. Bulletin of the American Physical Society 1, 123 (1956).

[37] TG Fox and PJ Flory. Journal of Applied Physics 21, 581 (1950).

[38] JA Zawada, CM Ylitalo, GG Fuller, RH Colby, and TE Long. Macromolecules 25, 2896 (1992).

[39] M Dionisio, AC Fernandes, JF Mano, NT Correia, and RC Sousa. Macromolecules 33, 1002 (2000).

[40] TR Lutz, Y He, MD Ediger, H Cao, G Lin, and AA Jones. Macromolecules 36, 1724 (2003).

[41] JH Kim, J Jang, D Lee, and W Zin. Macromolecules 35, 311 (2002).

]42] JL Keddie, RAL Jones, and RA Cory. Faraday Discussions 98, 219 (1994).

[43] OKC Tsui, TP Russell, and CJ Hawker. Macromolecules 34, 5535 (2001).

[44] JH van Zanten, WE Walace, and W Wu. Physical Review E 53(3), R2053 (1996).

[45] DS Fryer, RD Peters, EJ Kim, JE Tomaszewski, JJ de Pablo, PF Nealey, CC White, and W Wu. Macromolecules 34, 5627 (2001).

[46] CJ Ellison, MK Mundra, and JM Torkelson. Macromolecules 38(5), 1767 (2005).

[47] G Adam and JH Gibbs. Journal of Chemical Physics 43, 139 (1965).

[48] HH Kausch and M Tirrell. Annual Review of Materials Science 19, 341 (1989).

[49] J Klein. In Encyclopedia of Polymer Science & Engineering, Wiley, New York (1987).

[50] WW Graessley. Advances in Polymer Science 47, 67 (1982).

[51] DS Pearson. Rubber Chemistry and Technology 60, 439 (1987).

[52] PE Rouse. Journal of Chemical Physics 21, 1272 (1953).

[53] De Gennes, PG. Journal of Chemical Physics 55, 572 (1971).

[54] M Doi and SF Edwards. Journal of the Chemical Society Faraday Transactions 2 74, 1789 (1978).

[55] Lodge, TP. Physical Review Letters 83, 3218 (1999).

[56] EJ Kramer, P Green, and CJ Palmstrom. Polymer 25, 473 (1984).

[57] H Silescu. Makromolecular Chemistry, Rapid Communications 5, 519 (1984).

[58] F Brochard, J Jouffroy, and P Levinson. Macromolecules 16, 1638 (1983).

[59] RJ Composto, EJ Kramer, and DM White. Nature 328, 234 (1987).

[60] E Kim, EJ Kramer, WC Wu, and PD Garrett. Polymer 35, 5707 (1994).

[61] GC Alfonso and TP Russell. Macromolecules 19, 1143 (1986).

[62] See, for example, H Cao, G Lin, and AA Jones. Journal of Polymer Science B: Polymer Physics 42, 1053 (2004).

[63] See KG Libbrecht. Reports on Progress in Physics 68, 855 (2005) for a review of the history of studies of snowflake morphologies.

[64] U Nakaya. *Snow Crystals*. Cambridge: Harvard University, 1954.

[65] W Kurz and DJ Fisher. *Fundamentals of Solidification*. Switzerland: Trans Tech Publications, 1984.

[66] KA Jackson. Liquid Metals and Solidification ASM. Cleveland, Ohio, 174 (1958).

[67] GF Bolling and WA Tiller. Journal of Applied Physics 32, 2587 (1961).

[68] WA Tiller. *The Science of Crystallization*. New York: Cambridge University Press, 1991.

[69] WW Mullins and RF Sekerka. Journal of Applied Physics 34(2), 323 (1963).

[70] WW Mullins and RF Sekerka. Journal of Applied Physics 35(2), 444 (1964).

[71] T Ihle and H Müller-Krumbhaar. Physical Review E 49(4), 2972 (1994).

[72] E Ben-Jacob, G Deutscher, P Garik, ND Goldenfeld, and Y Lareah. Physical Review Letters 57(15), 1903 (1986).

[73] H Xu, R Matkar, and T Kyu. Physical Review E 72, 011804-1 (2005).

[74] SM Carr and KN Subramanian. Journal of Crystal Growth 60, 307 (1982).

[75] T Matsuno and M Koishi. Journal of Crystal Growth 94, 798 (1989).

[76] JL Hutter and J Bechhoefer. Physical Review E 59(4), 4342 (1999).

[77] B Billia and R Trivedi (ed. DTJ Hurle). In *Handbook of Crystal Growth 1, Fundamentals Part B: Transport and Stability, Chapter 14*. New York: Elsevier Science, B.V., 1993.

[78] O Shochet and E Ben-Jacob. Physical Review E 48(6), R4168 (1993).

[79] E Brener, H Müller-Krumbhaar, and D Temkin. Physical Review E 54(3), 2714 (1996).

[80] E Brener, H Müller-Krumbhaar, D Temkin, and T Abel. Physica A 249, 73 (1998).

[81] O Shochet, K Kassner, E Ben-Jacob, SG Lipson, and H Müller-Krumbhaar. Physica A 187, 87 (1992).

[82] VA Bogoyavlenksiy and NA Chernova. Physical Review E 61(2), 1629 (2000).

[83] JL Hutter and J Bechhoefer. Physical Review E 59(4), 4342 (1999).

[84] FJ Lamelas, S Seader, M Zunic, CV Sloane, and M Xiong. Physical Review B 67, 045414-1 (2003).

[85] AA Shibkov, YI Golovin, MA Zheltov, AA Korolev, and AA Leonov. Physica A 319, 65 (2003).

[86] ME Glicksman and AO Lupulescu, Journal of Crystal Growth 264, 541 (2004).

[87] GP Ivanstov. Doklady Akademii Nauk SSSR 58, 567 (1947).

[88] DE Temkin. Doklady Adakemii Nauk SSSR 132, 1307 (1960).

[89] GE Nash and ME Glicksman. Acta Metallurgica 22, 1283 (1974).

[90] JS Langer and H Müller-Krumbhaar. Journal of Crystal Growth 42, 11 (1977).

[91] JS Langer and H Müller-Krumbhaar. Acta Metallurgica 26, 1681 (1978).

[92] JS Langer and H Müller-Krumbhaar. Acta Metallurgica 26, 1689 (1978).

[93] JS Langer and H Müller-Krumbhaar. Acta Metallurgica 26, 1697 (1978).

[94] D Kessler, J Koplik, and H Levine. Physical Review A 34, 4980 (1986).

[95] P Pelcé. *Dynamics of Curved Fronts*. Academic Press: New York (1988).

[96] JP Gollub. In *Nonlinear Phenomena Related to Growth and Form*. eds M Ben Amar, P Pelcé, and P Tabeling. Plenum Press: New York (1991).

[97] W Kurz and R Trivedi. Acta Metallurgica et Materialia 38, 1 (1990).

[98] J Xu. *Interfacial Wave Theory of Pattern Formation*. Springer: New York (1998).

[99] SC Huang and ME Glicksman, Acta Metallurgica 29, 717 (1981).

[100] O Martin and N Goldenfeld. Physical Review A 35(3), 1382 (1987).

[101] R Pieters and JS Langer. Physical Review Letters 56(18), 1948 (1986).

[102] DA Kessler and H Levine. Europhysics Letters 4(2), 215 (1987).

[103] PH Bouissou, A Chiffaudel, B Perrin, and P Tabeling. Europhysics Letters 13(1), 89 (1990).

[104] LR Morris and WC Winegard. Journal of Crystal Growth 1, 245 (1967).

[105] Y Sawada, B Perrin, P Tabeling, and P Bouissou. Physical Review 43(10), 5537 (1991).

[106] H Honjo, S Ohta, Y Sawada. Physical Review Letters 55(8), 841 (1985).

[107] M Castro. Physical Review B 67, 035412 (2003).

[108] E Hürlimann and JH Bilgram. In *Growth and Form*, eds Ben Amar et al., p79, Plenum Press: New York (1991).

[109] LM Williams, M Muschol, X Qian, W Losert, and HZ Cummins. Physical Review E 48(1), 489 (1993).

[110] O Shochet, K Kassner, E Ben-Jacob, SG Lipson, and H Müller-Krumbhaar. Physica A 187, 87 (1992).

[111] MM Despotopoulou, CW Frank, RD Miller, and JF Rabolt. Macromolecules 29(18), 5797 (1996).

[112] VH Mareau and RE Prud'homme. Macromolecules 36(3), 675 (2003).

[113] K Dalnoki-Veress, JA Forrest, MV Massa, A Pratt, and A Williams. Journal of Polymer Science B: Polymer Physics 39, 2615 (2001).

[114] H Schönherr and CW Frank. Macromolecules 36(4), 1188 (2003).

[115] VH Mareau and RE Prud'homme. Macromolecules 38(2), 398 (2005).

[116] Y Sakai, M Imai, K Kaji, M Tsuji. Journal of Crystal Growth 203, 244 (1999).

[117] Y Sakai, M Imai, K Kaji, and M Tsuji. Macromolecules 29(27), 8830 (1996).

[118] KL Beers, JF Douglas, EJ Amis, A Karim. Langmuir 19, 3935 (2003).

[119] SJ Sutton, K Izumi, H Miyaji, Y Miyamoto, and S Miyashita. Journal of Materials Science 32, 5621 (1997).

[120] G Reiter and J Sommer. Journal of Chemical Physics 112(9), 4376 (2000).

[121] G Reiter and J Sommer. Physical Review Letters 80(17), 3771 (1998).

[122] MV Massa, K Dalnoki-Veress, and JA Forrest. European Physical Journal E 11, 191 (2003).

[123] N Parizel, F Lauprêtre, and L Monnerie. Polymer 38(15), 3719 (1997).

[124] SA Liberman, ADS Gomes, and EM Macchi. Journal of Polymer Science: Polymer Chemistry Ed. 22, 2809 (1984).

[125] S Cimmino, E Martuscelli, and C Silvestre. Polymer 30, 393 (1989).

[126] C Silvestre, S Cimmino, E Martuscelli, FE Karasz, and WJ MacKnight. Polymer 28, 1190 (1987).

[127] TR Lutz, Y He, MD Ediger, H Cao, G Lin, and AA Jones. Macromolecules 36(5), 1724 (2003).

[128] C Brosseau, A Guillermo, and JP Cohen-Addad. Macromolecules 25(18), 4535 (1992).

[129] S Schantz. Macromolecules 30(5), 1419 (1997).

[130] JA Zawada, CM Ylitalo, GG Fuller, RH Colby, and TE Long. Macromolecules 25(11), 2896 (1992).

[131] M Dionisio, AC Fernandes, JF Mano, NT Correia, RC Sousa. Macromolecules 33(3), 1002 (2000).

[132] E Martuscelli, M Pracella, and WP Yue. Polymer 25, 1097 (1984).

[133] J Baldrian, M Horky, A Sikora, M Steinhart, P Vlcek, H Amenitsch, and S Bernstorff. Polymer 40, 439 (1999).

[134] WB Liau and CF Chang. Journal of Applied Polymer Science 76, 1627 (2000).

[135] TP Russell, H Ito, and GD Wignall. Macromolecules 21(6), 1703 (1988).

[136] V Ferreiro, JF Douglas, EJ Amis, and A Karim. Macromolecular Symposia 167, 73 (2001).

Chapter 2. Crystal Morphologies in Thin Films of PEO/PMMA Blends

Chapter 2.1 Introduction

Pattern formation during crystallization has been studied for a number of years. Many studies have focused on dendritic crystallization of metals and small molecules because these dendritic microstructures are known to play a large role in the resulting mechanical properties [1]. Pattern formation in facet forming materials, such as polymers, has been studied in less detail, although early studies have shown that the presence of facets does not necessarily preclude pattern formation [2,3,4]. One of the outstanding problems in pattern formation is an understanding of the processes by which substances forming faceted crystals can be driven to form non-equilibrium diffusion-limited morphologies.

In general, faceted crystals involve atomically smooth interfaces and grow through a layer-by-layer mechanism such as secondary surface nucleation (nucleation-limited growth). Non-faceted crystal morphologies involve rough interfaces characterized by many favorable sites for atom attachment. In this case, crystal growth is controlled by diffusion of heat or mass away from the melt-crystal interface (diffusion-limited growth). Jackson suggested that the nature of the interface (faceted vs. non-faceted) correlates with the magnitude of the entropy of fusion [5]. Smooth interfaces are observed in materials exhibiting large entropies of fusion (polymeric materials), while rough interfaces are typically found in metals and other materials with small entropy of fusion.

Metals typically solidify from the melt in a dendritic manner. Dendrites result from a thermal or solutal diffusion field surrounding the crystal and their symmetry reflects the crystallography of the unit cell (for cubic materials, sidebranches typically form at 90^{o} to the dendrite trunk). Some small anisotropy in the surface energy is required for the formation of the dendritic pattern [6]. One of the important length scales in dendritic growth is the diffusion length, $\delta = D/V$ (where D is the heat or mass diffusion coefficient and V is the crystal growth velocity). This length represents the characteristic distance over which impurities (or heat) are rejected from the growing crystal.

Metallic dendrites are often difficult to study experimentally because they are not transparent and crystal growth rates are extremely large. These experimental difficulties have been overcome in studies of substances such as succinonitrile [7,8], pivalic acid [9], ammonium chloride [10], and ammonium bromide [11] crystallized from solution. These model systems have allowed for measurements of the sidebranching spacing, tip radius, and growth velocity, which have subsequently been used to test existing theories of dendritic growth [7]. For detailed discussions of the fundamental aspects of dendrite formation, the reader is referred to papers by Langer [12], Billia et al. [13], and Glicksman et al. [14].

As discussed previously, polymeric materials usually crystallize in a faceted manner. These faceted crystals take the form of lamellae, which are single crystals with ribbon or plate-like shapes, resulting from highly anisotropic atom attachment kinetics. Lamellae are usually organized in a spherulitic fashion when crystallization takes place from the pure melt or from a concentrated solution [15]. In contrast, crystallization from dilute solution leads to isolated single crystal lamellae at small undercooling and to dendritic patterns at larger undercooling [16,17,18]. Recent studies of crystallization in thin films have confirmed the ability of polymeric materials to crystallize in a variety of non-spherulitic morphologies [19,20,21,22,23,24,25,26,27,28].

In addition to faceted single crystals, spherulites and dendrites, other morphologies, such as the dense-branched morphology (DBM) [29,30] have been encountered in crystal growth experiments. The dense-branched morphology (DBM) is usually observed in low anisotropy conditions and is characterized by frequent splitting of the growth tip and a lack of pronounced morphological (orientational) order [31,32]. This morphology is rarely reported experimentally and has generated some controversy over its classification as a true morphology [33]. Another problem with use of the term "DBM" is that some of these morphologies are single crystals while others are polycrystalline. This is an important distinction because in the former case, diffraction patterns show pronounced crystallographic order (despite the lack of morphological order), while in the latter case, the diffraction pattern reveals polycrystalline textures. Reports of DBM in polymeric materials are almost exclusively single crystals [19,23,25].

The spherulitic growth morphology has also generated significant confusion in literature. In some cases, such as selenium [34], lead glasses [35], sulfites in gels [36], and lamellar eutectics [37], the term spherulite is used to describe a polycrystalline pattern with a spherical envelope consisting of a lamellar microstructure. In polymeric materials, the term spherulite generally refers to an aggregate of lamellar crystals which originates from a single primary nucleus and achieves spherical symmetry through repeated low angle branching and splaying [38,39]. Branching at the lamellar level is usually associated with the occurrence of screw dislocations [40].

Goldenfeld proposed that spherulites are three-dimensional representations of the dense-branched morphology [32]. Although this statement may be generally true, the situation is more complicated for polymers than for small organic or inorganic molecules. In polymeric materials, there are two types of instabilities. Instability at the growth tip of a thin polymer lamellae, often resulting from mechanical stress, leads to the generation of a screw dislocation and eventually to the formation of a lamellar stack. Following the reasoning of Keith [41], Keith and Padden [42] and Schultz [43], single lamellae are too thin to lead to a Mullins-Sekerka growth instability. In contrast, once lamellar stacks (fibers) reach lateral dimensions commensurate with the diffusion length, a growth instability leads to non-crystallographic branching (splitting of the growth envelope into separate fibers). In thin film geometries where lamellar crystals grow parallel to the substrate, rejection of impurities (resulting in tip-splitting) can only occur in the crystal plane [42]. Such tip-splitting has indeed been observed recently in thin film geometries for a number of polymers [19,20,22,23,25,26,27].

A number of theoretical studies of transitions between morphologies have been reported [44,45]. These morphological transitions have been observed upon changes in some control parameter such as the effective anisotropy or the undercoooling. Experimentally, these transitions are commonly reported in Hele-Shaw experiments [29] but have been more elusive in studies of phase transitions [46,47,48]. Often, only a single morphology is observed, suggesting that transitions between morphologies may require large changes in a control parameter. These large changes in experimental conditions are often not possible in standard experiments due to a variety of factors such as rapid nucleation at large undercooling and large crystal growth rates. We anticipate

here that polymeric materials may provide some insight into these transitions because of their relatively small rates of nucleation and crystal growth, large crystallization window, and variable diffusion coefficients.

Ferreiro and coworkers have recently reported morphological transitions in thin film blends of poly(ethylene oxide) (PEO) and poly(methyl methacrylate) (PMMA) upon changes in the blend composition [27,28]. In this system, the PEO crystallizes and the non-crystallizable PMMA chains are rejected from the growth front. The crystal morphologies were compared to those observed in a phase field model where the effective anisotropy was varied. Changes in anisotropy resulted in similar morphologies to those observed in the PEO/PMMA samples. Montmorillonite clay was used as a nucleating agent in these experiments and the amount of clay in the system was shown to have a dramatic effect on the observed morphology.

In the present study, we report further studies of morphological development in thin films of PEO/PMMA blends. The PEO content is varied between 50 and 30 wt% since a number of morphological transitions were reported over this composition range [27,28]. Clay was not used in our study to minimize the number of experimental variables. The focus of this paper is twofold: first, to identify the different morphologies in PEO/PMMA blends as well as their location in parameter space (morphological maps), and second, to provide directions for further study of morphological development and pattern formation in polymeric systems. The effects of the control parameters (blend composition, PMMA molecular weight, crystallization temperature) on morphological development will be discussed.

Chapter 2.2 Experimental

Poly(ethylene oxide) and poly(methyl methacrylate) were obtained either from Scientific Polymer Products or Polymer Laboratories and used as received. The molecular weights and polydispersities are reported in Table 2.1. In this study, crystallized blend samples are referred to by the PMMA molecular weight (names shown

in Table 2.1). The tacticity of the PMMA chains is approximately 16.5% isotactic, 80% syndiotactic, and 3.5% atactic, as reported by the manufacturer.

The PEO and PMMA were dissolved in HPLC-grade 1,2-dichloroethane and stirred overnight. The polymer concentration was approximately 1.25 wt% and the composition of the blend was varied from 50 to 30 wt% PEO. Silicon wafers (100) were cleaned with a hot solution of 70 vol% sulfuric acid and 30 vol% hydrogen peroxide for 2 hours to create a hydrophilic surface. After cleaning, the wafers were rinsed with deionized water and blown dry with nitrogen.

Before spin-coating, the wafers were rinsed with HPLC-grade 1,2-dichloroethane and spun dry. The polymer solutions were then spin-coated onto the silicon wafer at approximately 1000 RPM. The resulting film thickness was approximately 120 nm, as determined using a JA Woollam spectroscopic ellipsometer. The film thickness is not affected dramatically by the PMMA molecular weight, but is highly sensitive to the concentration of polymer in solution. Blend composition was also shown to have a moderate influence on film thickness (110 nm for (30/70) and 130 nm for (50/50) PEO/PMMA blends). Studies carried out with blend films of a specific composition but slightly different thickness (± 30 nm) showed no significant change in morphology. Spin-coated samples were then dried under vacuum at 60^{o}C for 2 hours and then heated to 80^{o}C for 1 minute (to melt any nuclei formed during drying). The samples were then crystallized under nitrogen in a Linkam hotstage. Initially, the undercooling was varied after nucleation to determine which morphologies were possible and to observe transitions between these morphologies. In some cases, transient periods were noted during these non-isothermal experiments but these transients are not reported here. Each of the reported transitions can be observed during in-situ experiments and are reversible with temperature. Isothermal experiments were subsequently carried out near the transition points to avoid any artifacts associated with previous crystallization history. In this latter case, crystal growth was initiated by scratching the film (nucleation in this manner was not found to significantly affect the observed crystal morphology).

An Olympus BH-2 reflected light microscope equipped with a Cohu CCD camera was used to observe the crystal growth morphology. The image contrast was digitally enhanced to show the morphologies more clearly.

Table 2.1 Weight-Average Molecular Weights and Polydispersities of Polymers Used in this Study.

Material	Mw (g/mol)	Mw/Mn
PEO	101,200	1.04
PMMA5	4, 900	1.10
PMMA7	6,880	1.07
PMMA12	12,000	1.08
PMMA13	12,500	1.03
PMMA17	16,700	1.06
PMMA18	17,900	1.10
PMMA30	30,490	1.02
PMMA53	52,700	1.08
PMMA68	68,200	1.13
PMMA101	101,000	1.09

Chapter 2.3 Results

(50/50) PEO-PMMA Blends

A wide range of morphologies were observed in studies of the 50/50 blends. These morphologies are highly dependent on the PMMA molecular weight and crystallization temperature. At small undercooling and low PMMA molecular weight (near PMMA12), dendritic (D90) morphologies are observed, as shown in Figure 2.1a. These dendrites have sidebranches at 90^{o} to the dendrite trunk. Increasing the undercooling results in the formation of the dense-branched morphology (DBM), as shown in Figure 2.1b. A more detailed study of this transition is reported in Chapter 4. The dendrite and dense-branched morphology continuously decrease in size (branch width) with increasing undercooling. Increasing the undercooling from the DBM regime results in the formation of a stacked-needle (SN) morphology (concomitant with a jump decrease in the crystal growth velocity). The stacked-needle morphology is shown in Figure 2.1c. Further increases in the undercooling results in a needle (N) morphology, as

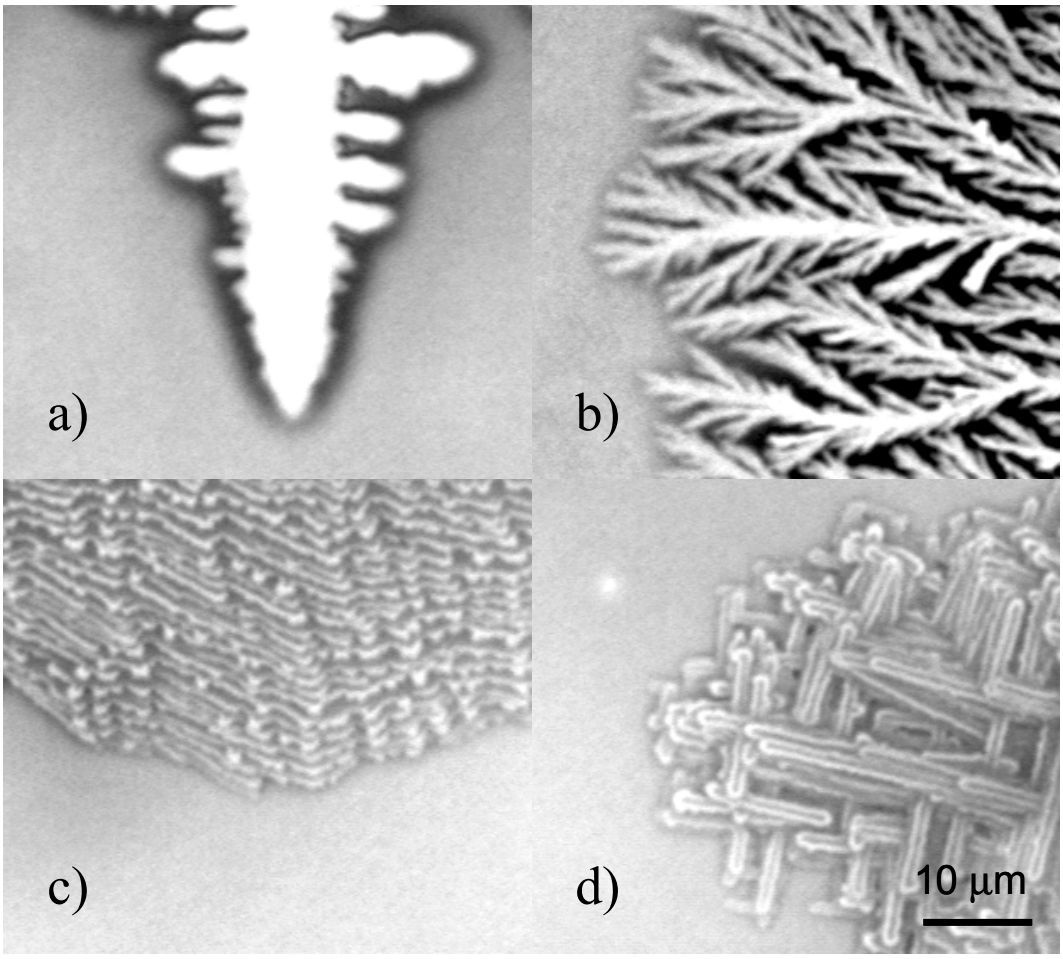

Figure 2.1 Morphologies observed in a 50/50 samples: a) Dendrite (D90) - PMMA16, Tx = 58°C, b) Dense-Branched Morphology (DBM) - PMMA101, Tx = 50°C, c) Stacked Needles (SN) - PMMA101, Tx = 42°C, d) Needles (N) - PMM101, Tx = 40°C.

shown in Figure 2.1d. The DBM/SN/N transition is also discussed in more detail in Chapter 4. The needle morphology has a relatively small number of sidebranches at 90^{o} to their trunk. Increased sidebranching and bending of these needles is observed at larger undercooling. Eventually, these needles become very dense with a circular envelope. At very low molecular weight and large undercooling, these dense-needled morphologies appear very similar to spherulites commonly observed in polymeric systems.

Increasing the PMMA molecular weight results in similar transitions to those observed for changes in the undercooling, especially for low PMMA molecular weight.

(40/60) PEO-PMMA Blends

A number of morphologies are also observed in 40/60 blends. In many cases, the observed morphologies observed for this blend composition appear to be intermediates between two different morphologies (i.e. dendrites and spherulites) and are difficult to categorize.

At large undercooling and high PMMA molecular weight, dendrites with 90^{o} sidebranching (D90) are observed. At smaller undercooling, a dense-branched morphology is observed. As discussed in Chapter 4, the transition between the D90 and DBM morphologies results in a change in the growth direction of approximately 45^{o}C. At large undercooling and low PMMA molecular weight, the observed morphologies include needles, stacked needles, and DBM (or spherulites). Occasionally, a morphology that resembles a dendrite with a spherulitic microstructure is observed under these conditions. Each of these morphologies exists over a limited range of conditions.

(35/65) PEO-PMMA Blends

For 35/65 blends, the morphologies are deeply in the dendritic (D90) regime. At large undercooling, the D90 morphology is observed across the range of PMMA molecular weights studied. At smaller undercooling, the DBM morphology is still

occasionally observed at low PMMA molecular weight. However, dendrites with 45° sidebranching (D45) generally dominate this region, especially for larger PMMA molecular weight. Sidebranches are still occasionally observed at 90° depending on the temperature relative to the transition temperature and the PMMA molecular weight. An example of the D90/D45 transition is shown in Figure 2.2.

The density of well-developed (independent) sidebranches decreases with increasing PMMA molecular weight but appears to be relatively independent of the crystallization temperature over the relatively small range of temperature used in this study. This observation becomes clearer in the 30/70 blends discussed below.

(30/70) PEO-PMMA Blends

The observed morphologies in 30/70 blends are entirely dendritic. However, because of the relatively slow crystal growth rates (less than 10^{-4} μm/s) at small undercooling, the region above the observed dendritic region has not been extensively studied. The D45 morphology has been observed at small undercooling in low PMMA molecular weight samples. As in 35/65 blends, the density of developed sidebranches decreases significantly with increasing PMMA molecular weight, as shown in Figure 2.3. These dendrites are discussed below and in more detail in Chapter 3.

Morphological Maps

Morphological maps for blend compositions of 50/50, 40/60, 35/65, and 30/70 as a function of crystallization temperature and PMMA molecular weight are reported in Figures 2.4-2.7, respectively. As discussed above, in some cases the growth rates become prohibitively slow and data are not reported. It is interesting to note that the morphology boundaries (especially in Figure 2.5) mirror the evolution of the PMMA (and PEO/PMMA) glass transition temperature as a function of increasing PMMA molecular weight (see Appendix 1). This observation may also be relevant for

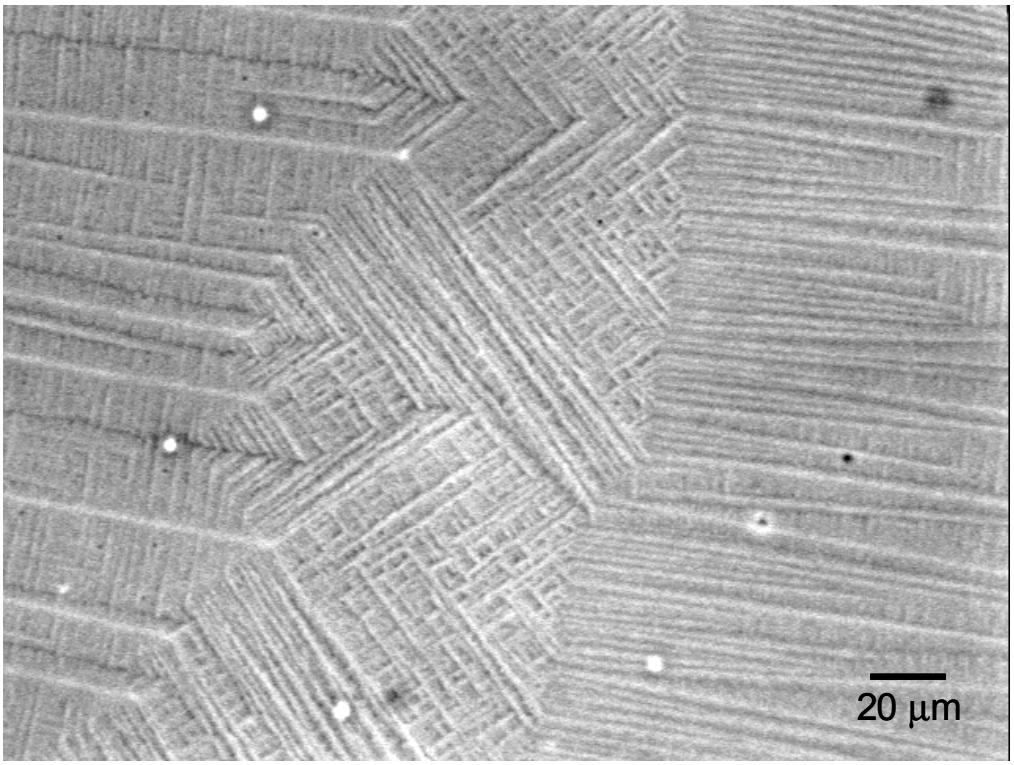

Figure 2.2 A 35/65 PMMA7 sample crystallized at various temperatures. The dendrites grew from left to right. The left hand portion of the micrograph corresponds to Tx = 33°C, the center to Tx = 41°C, and the right to Tx = 25°C.

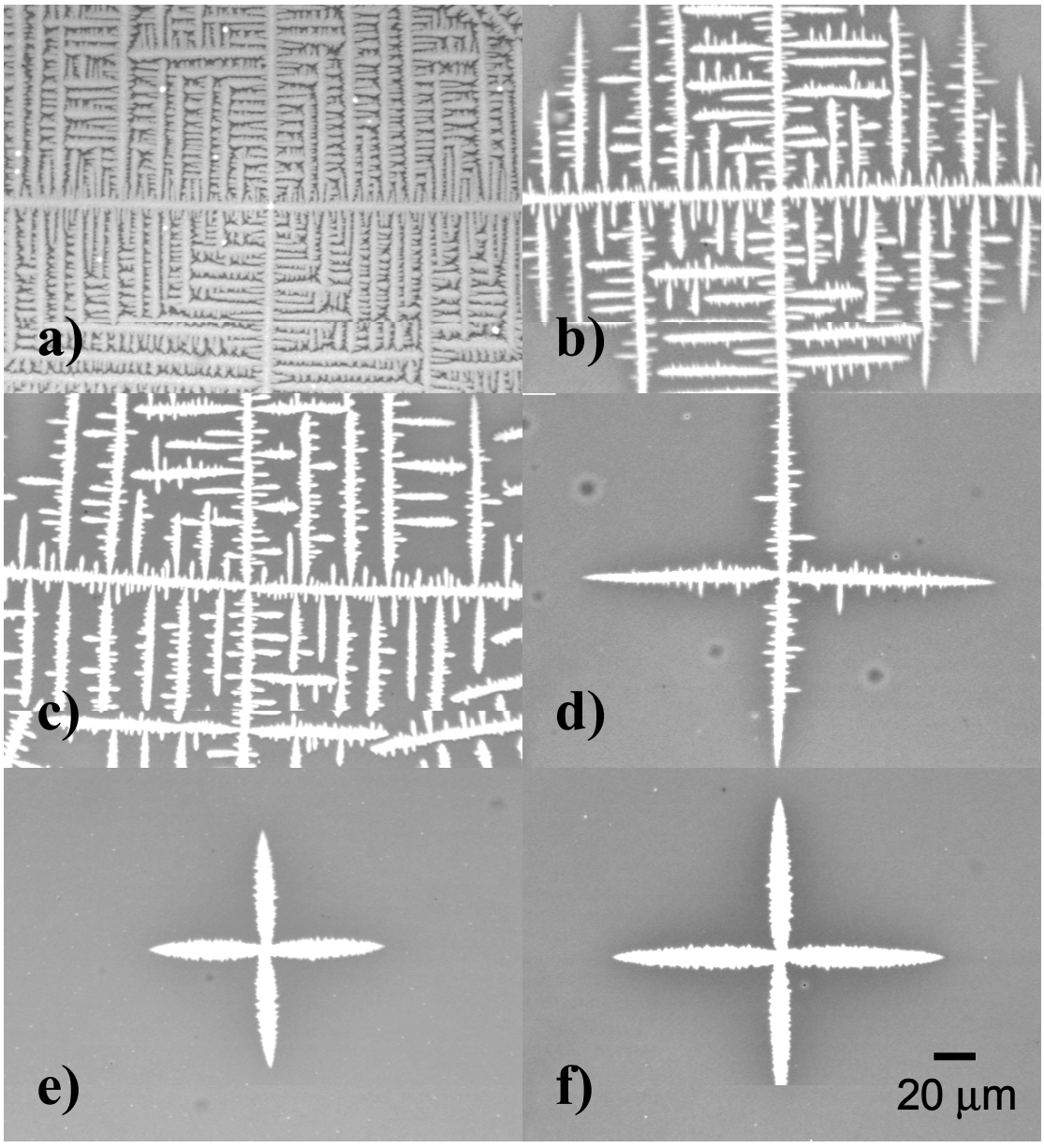

Figure 2.3 Dendritic morphologies in 30/70 samples crystallized at 37°C: a) PMMA7, b) PMMA12, c) PMMA18, d) PMMA53, e) PMMA68, and f) PMMA101.

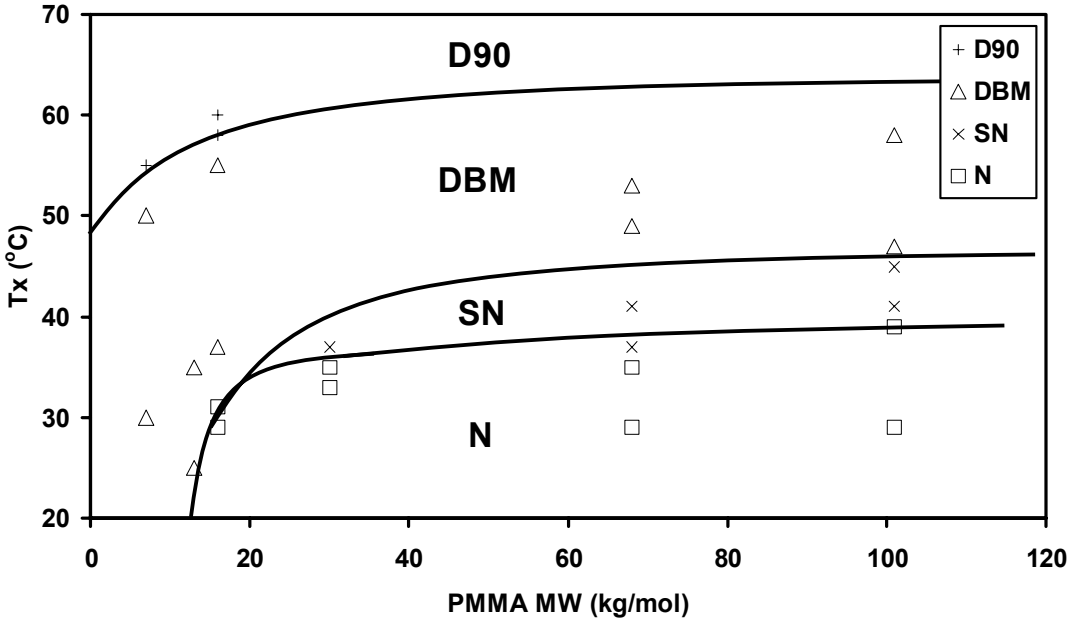

Figure 2.4 Morphological map for 50/50 blends as a function of PMMA molecular weight and crystallization temperature.

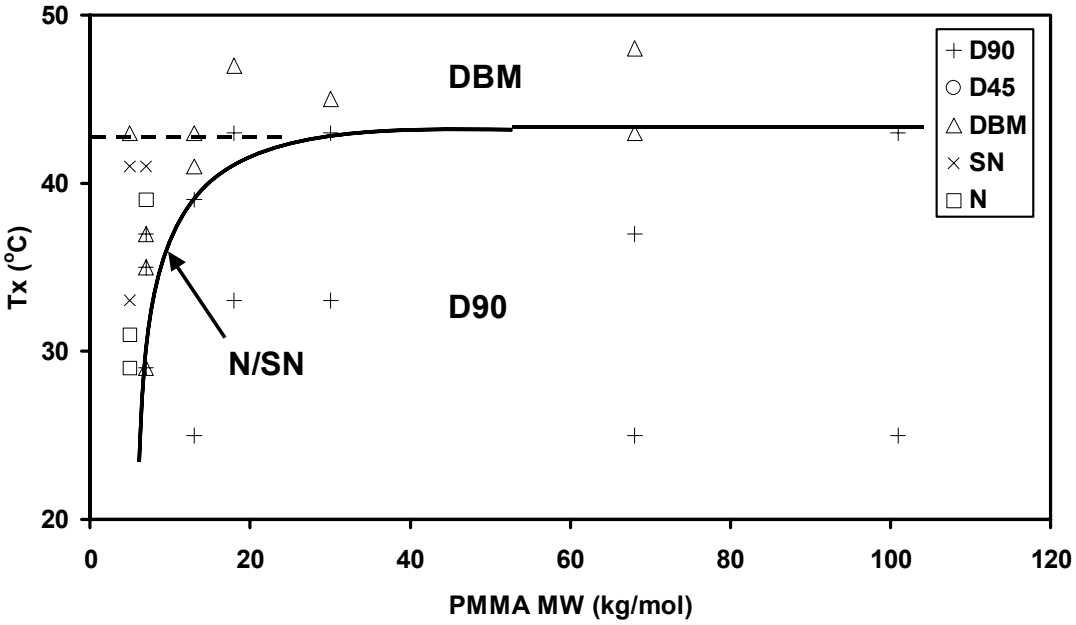

Figure 2.5 Morphological map for 40/60 blends as a function of PMMA molecular weight and crystallization temperature.

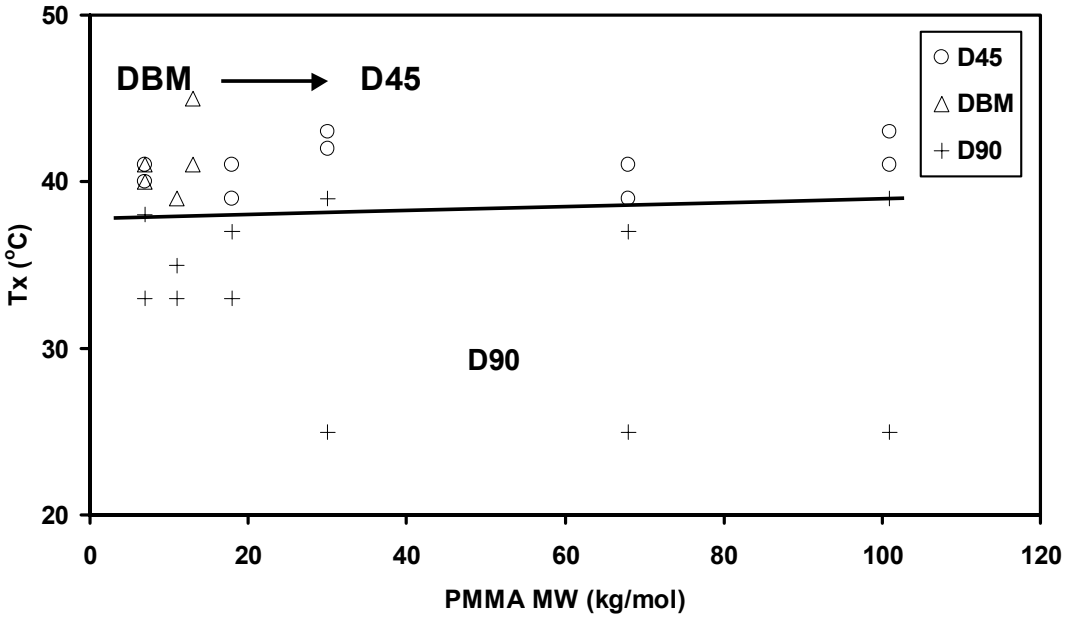

Figure 2.6 Morphological map for 35/65 blends as a function of PMMA molecular weight and crystallization temperature.

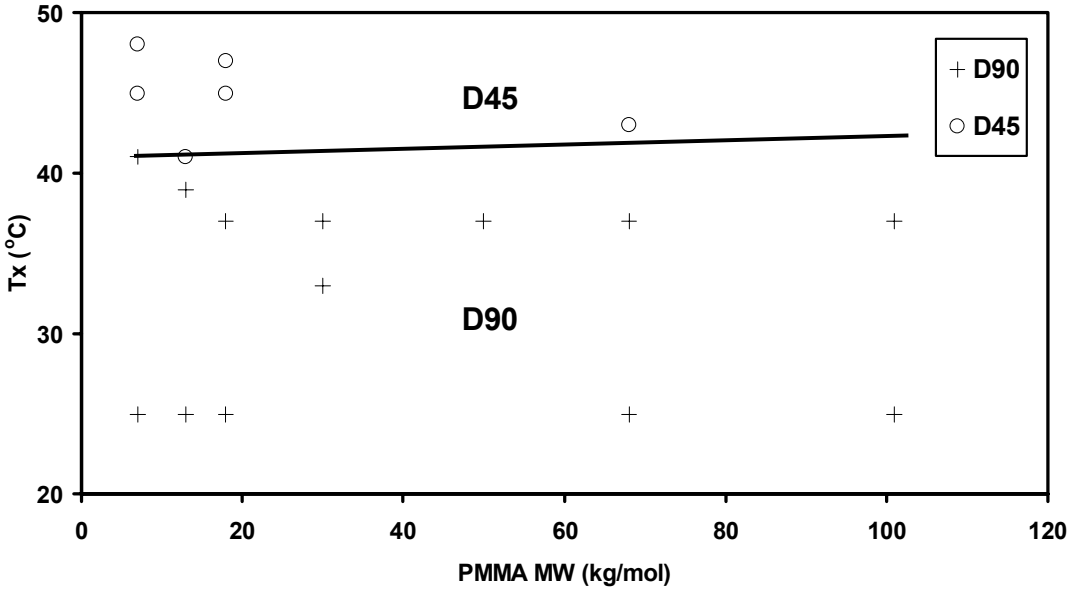

Figure 2.7 Morphological map for 30/70 blends as a function of PMMA molecular weight and crystallization temperature.

the discussion of the mutual diffusion coefficient (discussed in more detail later in this chapter and also in Chapter 3).

In addition, there is some fluctuation in film thickness in individual samples and between samples. Similarly, there is some variation in the blend composition and polymer concentration that occurs while making the solutions for spin-coating. These variations result in slightly different transition temperatures for different samples. Different morphologies are sometimes observed for low PMMA molecular weights (particularly in 40/60 blends) for different samples under the same crystallization conditions. Despite the difficulty in determining exact transition temperatures, the same trend in morphologies is always observed in different samples, and the reported maps can be used as a general guide for determining where the different morphologies are observed.

Chapter 2.4 Discussion

Morphological Development in Polymers

Several important points about pattern formation in polymeric systems (versus small molecules or metals) must be addressed before any detailed discussion of the observed morphologies. Polymer crystals involve folded polymer chains and the crystal thickness decreases with increasing undercooling [49]. At small undercooling, the crystal growth rates are very slow but a large amount of crystallizable material is needed due to the large crystal thickness. In addition, the crystalline phase is denser than the amorphous phase, resulting in some depletion zone near the growth front [23]. The combined effects of crystal thickness requirements and density change during crystallization may play an important role in pattern formation in these systems. Convection effects are negligible because of the large melt viscosity of polymeric materials. Another interesting feature of polymeric dendrites is that isothermal coarsening does not occur to any significant degree due to limited surface diffusion and the inability of new crystallizable material to reach the crystal (diffusion is slow and the

PEO crystal is essentially enclosed in a glassy PMMA-rich phase). These features are discussed in more detail in Chapter 3.

As previously discussed, morphological development in homopolymers is normally thought to be a result of a limited amount of crystallizable material at the growth front due to the thin film geometry and the change in density upon crystallization. The situation in thin films of polymer blends is much less clear. In many bulk systems, rejection of non-crystalline components occurs between the crystalline lamellae as evidenced by linear growth kinetics and an increased long spacing [50]. This situation is shown in Figure 2.8a. This rejection process may differ in thin film geometries. In this case, the crystals may grow near the film surface due to enhanced diffusion [51]. Farther from the surface, the glass transition temperature may be much larger (in systems with attractive polymer/substrate interactions such as PEO/PMMA). In this situation, it is likely that the non-crystalline PMMA component is rejected in the plane of crystal growth (Figure 2.8b). The result of these constraints (low dimensionality and rejection of PMMA) is that the normal lamellar faceted crystals may not be able to grow in an unperturbed manner. Instead, the growth front breaks down in a variety of growth morphologies that depend on the effective anisotropy and noise levels.

Spherulites

Spherulites are common to crystallization of polymeric materials. For samples with PEO contents greater that 50wt%, spherulitic textures have been exclusively reported in bulk samples [52,53]. In our study, the low PMMA molecular weight and low PMMA content (50/50 blends) samples at high undercooling, the observed morphologies are not clearly spherulitic, although they appear very similar. These conditions represent cases where growth is relatively unconstrained (where typical spherulitic growth is expected). Increasing the PEO content further (at moderate undercooling) would likely result in the formation of spherulites due to a number of factors, including the decrease in the glass-transition temperature and an increase in

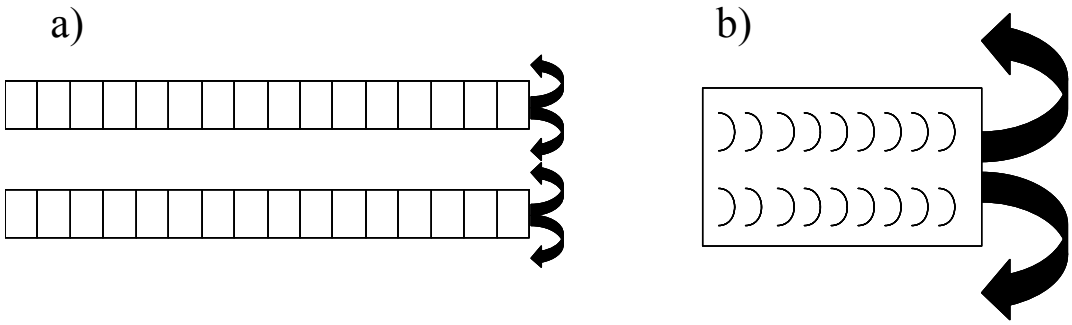

Figure 2.8 a) Lamellar stack viewed edge-on with rejection occurring between lamellae. b) Flat-on lamellae with rejection occurring in the plane of growth.

crystallizable fraction (with a concomitant decrease in non-crystallizable component that must be rejected).

Needles (N)

The term "needle" is often used to describe a dendritic crystal with no sidebranching. The needles observed in this study resemble dendrites because of the 90^{o} sidebranching (indicating a crystallographic relationship between the needle and sidebranch). This relationship also indicates that the needles are flat-on (vertical chain axis) with respect to the substrate. However, the reason that sidebranching is suppressed at high mobility (50/50 blends) is not clear, but may be related to the relatively large diffusion length. Detailed studies of the growth tip are not currently possible due to the small size and rapid growth rates of these needles.

Needle crystals morphologies have scarcely been reported in morphological studies. In polymers, needle-like morphologies have been observed in polypropylene but these are a result of epitaxial growth of crystals with different crystallographic orientations [54,55], which is not the case in the current study.

Shibkov and coworkers have reported similar morphologies in studies of supercooled ice [48]. Ice crystals are similar to polymer lamellae in that ice often grows in two-dimensions (in the basal plane) with a large anisotropy in the atom attachment kinetics. In our studies, the sidebranching and spatial density of these needles increased with increasing undercooling, as also reported by Shibkov et al. [48]. More studies of similar materials would be useful to determine if the needle morphology is common in materials with large anisotropies of attachment kinetics or if the two-dimensionality of the crystal is critical for the observation of the needle morphology.

Stacked-Needles (SN)

The stacked-needle morphology is observed at slightly higher temperatures than the needle morphology. This morphology is also not common to crystallization

experiments. Keith reported crystal aggregates in thin films of isotactic polystyrene that appear somewhat similar but no mechanism for their formation was described [41]. The fact that this morphology grows slower than the needle morphology by an order of magnitude indicates a transition in growth mechanism or growth direction. We speculate that this morphology is comprised of needles tilted toward the film surface. More evidence for this suggestion is found in Chapter 4. We hope to conduct detailed x-ray diffraction experiments in the future to resolve this issue.

Dense-branched morphology (DBM)

In our study, the dense-branched morphology is observed at high PEO content and large undercooling. In theoretical studies of DBM, this morphology is normally observed at large undercooling and/or small anisotropy of the surface energy [56]. Xu and coworkers have suggested that the observation of DBM in isotactic polystyrene is a result of the decrease in the anisotropy associated with the large undercooling [57]. Ben-Jacob has also suggested that the anisotropy of the surface energy in polymeric materials is very small, resulting in DBM rather than dendrites. Since DBM is frequently observed during crystallization of thin polymer films, such a mechanism for DBM formation is indeed plausible. However, such a suggestion relies on the existence of a mechanism that reduces anisotropy of atom attachment that normally stabilizes faceted interfaces associated with polymer crystallization. In our case, this mechanism may be related to the rejection of PMMA, as discussed in Chapter 3.

In addition to the above mechanisms, noise may play an important role for the development of DBM (and destabilization of dendritic morphologies), given that we observe DBM in situations where the noise level is expected to be large (large PEO contents and large undercooling). This suggestion has been frequently been proposed in theory and can not be ruled out [56,58].

Dendrites

Dendritic growth in polymers has also been reported in highly constrained environments [23,24,26,27,28]; however, dendrites are reported much less frequently than DBM. This observation is initially surprising given that dendrites are considered to be the normal mode of pattern formation in metallic and small molecule systems. However, for reasons already discussed, DBM is expected to be the general mode of crystallization in thin polymer films, with dendrites occurring only under the proper growth environments (low noise levels and slow crystal growth).

The transition from 45^o and 90^o sidebranching to 90^o sidebranching with increasing undercooling is not well understood in this system, but may by related to the (010)/(210) growth front transition noted by Marentette et al. [59] at much higher temperatures (this point is discussed further in Chapter 4).

Effects of the Blend Composition on Morphological Development

To more fully illustrate the effects of the blend composition on morphological development, a series of morphologies for PMMA68 samples are shown in Figure 2.9. Figure 2.9a (40/60) shows a compact dendrite characterized by very dense growth of the sidebranches. Increasing the PMMA content results in increasingly slow development of the sidebranches. In Figure 2.9c (30/70) for example, the sidebranches are highly competitive and very long times are needed for selection of "winning" sidebranches. These details are discussed in more detail in Chapter 3.

In the dendritic regime, the diffusion length, δ, is the physical parameter important in selection of the crystal length scale. As more PMMA is added to the system, the diffusion coefficient decreases significantly due to changes in the effective glass transition temperature [60]. Although the crystal growth rate also decreases, the changes in the diffusion coefficient with blend composition are much more drastic. A detailed analysis of the diffusion coefficient is not possible due to a number of theoretical and experimental limitations (see Chapter 3 for a further discussion of this point); however, a qualitative discussion of the effects of variation of the diffusion coefficient is possible.

The effects of the diffusion length are apparent in the large changes in sidebranch density observed in Figure 2.9. As the diffusion coefficient (diffusion length) is decreased, longer selection times are needed for the system to adjust the sidebranch spacing because the small diffusion length means that the crystal is surrounded by a highly immobile PMMA layer. As a result, competitive growth continues at much larger length scales resulting in an increased curvature of the crystallization envelope.

For larger changes in the blend composition, changes in the effective noise level may also become important. As previously discussed, morphological transitions (from dendrites to DBM) require some change in the noise or effective anisotropy. Since the anisotropy is only thought to be a strong function of the undercooling [57] (rather than the blend composition), the noise must be important in the observed transitions. As more PEO is added (lowering the Tg), the chain dynamics become much faster and dendritic structures become unstable. However, when growth and chain dynamics are relatively slow (as in a 30/70 blend), the dendritic regime is recovered.

Effects of PMMA Molecular Weight on Morphological Development

The PMMA molecular weight also plays an important role in the mobility of the polymer chains in terms of both the glass transition temperature and the diffusion coefficient of the blend. The diffusion coefficient is expected to decrease significantly with increasing PMMA molecular weight due to changes in both chain length (varies as $M^{-2.2}$ in homopolymers [61]) and the effective T_g. These changes are apparent in Figure 2.3, which shows how the dendritic morphology is affected by the PMMA molecular weight. These results are similar to those observed for changes in the blend composition.

Since the melting point of PEO crystals does not vary with the PMMA molecular weight, no changes in the anisotropy are expected. As a result, the PMMA molecular weight can be used directly to probe the influence of noise on the crystal morphology. Lower PMMA molecular weights are expected to impart more noise to the system through faster chain dynamics (resulting from Tg and diffusion effects). As discussed

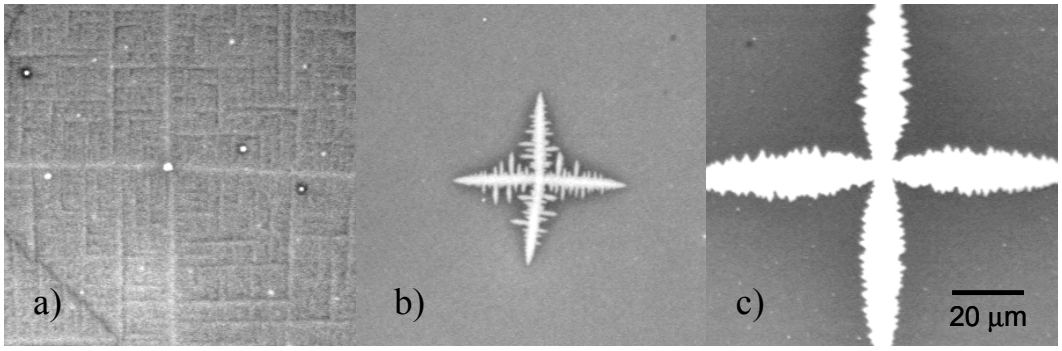

Figure 2.9 Dendritic morphologies in PMMA68 blends crystallized at 37°C: a) 40/60, b) 35/65, and c) 30/70.

above, noisy growth is expected to more quickly select winning sidebranches, as shown in Figure 2.3. This situation is confirmed in simulations by Kobayashi [62].

In general, large changes in the PMMA molecular weight results in relatively few morphological transitions (except at very low PMMA molecular weight where the glass-transition temperature and diffusion coefficient vary rapidly). However, the PMMA molecular weight does play a large role in the compactness of the morphologies. This result suggests that the PMMA molecular weight does not play a large role in the magnitude of the diffusion coefficient (consistent with "fast" theory discussed above).

Effects of Undercooling on Morphological Development

As demonstrated in Figures 2.4-2.7, the undercooling can also play a significant role in morphological transitions. The undercooling is tied to a number of important factors in this system, including the crystal thickness, the noise, and the effective anisotropy. The effects of the undercooling are thus difficult to explain on a mechanistic basis.

At small undercooling, the system is noisy but the attachment kinetics are highly anisotropic. In this case, when the growth rate is sufficiently slow, the anisotropy wins, resulting in the formation of dendritic morphologies. Increasing the undercooling results in less noise but growth become less anisotropic. The decrease in anisotropy is apparently important in this case because DBM is observed at these large undercoolings, in accord with the work by Xu [57].

Chapter 2.5 Conclusions

The effects of blend composition, PMMA molecular weight, and crystallization temperature on the observed crystal morphology have been studied in thin film blends of PEO/PMMA. A number of morphologies have been reported, including dendrites, dense-

branched morphology (DBM), needles, and stacked-needles. Morphological maps demonstrating the roles of the various control parameters (blend composition, PMMA molecular weight, and crystallization temperature) on the observed morphology have been proposed. The needle and stacked-needle morphologies have not been previously reported in polymeric systems. In addition, a transition in the direction of sidebranching for dendritic crystals has been observed. This transition is not fully understood and warrants further investigation. The blend composition and crystallization temperature play an important role in morphological selection when conditions are varied sufficiently. The PMMA molecular weight can promote morphological transitions but plays a larger role in the density (compactness) of the observed morphologies. The effective noise level is also thought to play an important role in morphological selection. The noise level varies with the blend composition and crystallization temperature, but can also systematically varied through changes in the PMMA molecular weight. In addition, the anisotropy of the surface energy may play some role in the formation of DBM at large undercooling. The results of this study provide a number of immediate directions for detailed studies of dendritic growth and morphological transitions.

Acknowledgments.

The authors would like to thank Jack Douglas and Vincent Ferreiro for helpful discussions involving the PEO/PMMA system.

Chapter 2.6 References

[1] W Kurz and DJ Fisher. *Fundamentals of Solidification*. Trans Tech Publications, Switzerland (1998).

[2] M Ben Amar and Y Pomeau. Europhysics Letters 6(7), 609 (1988).

[3] J Maurer. Europhysics Letters 8(1), 67 (1989).

[4] M Adda Bedia and M Ben Amar. In *Growth and Form*, pages 187-199, Plenum Press, New York (1991).

[5] KA Jackson. Liquid Metals and Solidification ASM. Cleveland, Ohio, 174 (1958).

[6] DA Kessler, J Koplik, and H Levine. Physical Review A 30, 2820 (1984).

[7] ME Glicksman, RJ Schaefer, and JD Ayers. Metallurgical Transactions A 7, 1747 (1976).

[8] SC Huang and ME Glicksman. Acta Metallurgica 29, 701 (1981).

[9] A Dougherty and A Gunawardana. Physical Review E 50(2), 1349 (1994).

[10] H Honjo, S Otha, and Y Sawada. Physical Review Letters 55(8), 841 (1985).

[11] H Honjo and Y Sawada. Journal of Crystal Growth 58, 297 (1982).

[12] JS Langer. Reviews of Modern Physics 52(1), 1 (1980).

[13] B Billia and R Trivedi. In *Handbook of Crystal Growth, Fundamentals: Transport and Stability,* Volume 1B, pages 899-1073, Elsevier Science Publishers B.V.: New York (1993).

[14] ME Glicksman and SP Marsh. In *Handbook of Crystal Growth, Fundamentals: Transport and Stability*, Volume 1B, pages 1075-1122, Elsevier Science Publishers B.V., New York (1993).

[15] A Keller. In *Growth and Perfection of Crystals,* p. 499-532, Wiley-Interscience: New York (1958).

[16] F Khoury and FJ Padden. Journal of Polymer Science 47, 455 (1960).

[17] PH Geil and DH Reneker. Journal of Polymer Science 51, 569 (1961).

[18] B Wunderlich and P Sullivan. Journal of Polymer Science 61, 195 (1962).

[19] VH Mareau and RE Prud'homme. Macromolecules 38(2), 398 (2005).

[20] Y Sakai, M Imai, K Kaji, and M Tsuji. Macromolecules 29 (27), 8830 (1996).

[21] G Reiter and J Sommer. Journal of Chemical Physics 112(9), 4376 (2000).

[22] M Wang, H Braun, and E Meyer. Polymer 44, 5015 (2003).

[23] K Taguchi, H Miyaji, K Izumi, A Hoshino, Y Miyamoto, and R Kokawa. Polymer 42, 7443 (2001).

[24] F Zhang, J Liu, H Huang, B Du, and T He. European Physical Journal E8, 289 (2002).

[25] AJ Lovinger and RE Cais. Macromolecules 17(10), 1939 (1984).

[26] KL Beers, JF Douglas, EJ Amis, A Karim. Langmuir 19, 3935 (2003).

[27] V Ferreiro, JF Douglas, J Warren, and A Karim. Physical Review E 65, 042802-1 (2002).

[28] V Ferreiro, JF Douglas, J Warren, and A Karim. Physical Review E 65, 051606-1 (2002).

[29] E Ben-Jacob, G Deutscher, P Garik, ND Goldenfeld, and Y Lareah. Physical Review Letters 57(15), 1903 (1986).

[30] E Ben-Jacob, R Godbey, ND Goldenfeld, J Koplik, H Levine, T Mueller, and LM Sander. Physical Review Letters 55(12), 1315 (1985).

[31] E Brener, H Müller-Krumbhaar, and D Temkin. Europhysics Letters 17(6), 535 (1992).

[32] N Goldenfeld. Journal of Crystal Growth 84, 601-608 (1987).

[33] H Müller-Krumbhaar, M Zimmer, T Ihle, and Y Saito. Physica A 224, 322 (1996).

[34] J Bisault, G Ryschenkow, and G Faivre. Journal of Crystal Growth 110, 889-909 (1991).

[35] SM Carr and KN Subramanian. Journal of Crystal Growth 60, 307-312 (1982).

[36] T Matsuno and M Koishi. Journal of Crystal Growth 94, 798-802 (1989).

[37] W Kurz and R Trivedi. Acta Metallurgica Materialia 38(1), 1 (1990).

[38] HD Keith and FJ Padden Jr. Journal of Applied Physics 34(8), 2409 (1963).

[39] HD Keith and FJ Padden Jr. Journal of Applied Physics 35(4), 1270 (1964).

[40] DC Bassett, RH Olley, and IAM al Raheil. Polymer 29, 1539 (1988).

[41] HD Keith. Journal of Polymer Science A 2, 4339 (1964).

[42] HD Keith and FJ Padden Jr. Journal of Polymer Science Part B: Polymer Physics 25, 2371 (1987).

[43] JM Schultz. *Polymer* 32(18), 3268 (1991).

[44] E Brener, H Müller-Krumbhaar, and D Temkin. Physical Review E 54(3), 2714 (1996).

[45] O Shochet, K Kassner, E Ben-Jacob, SG Lipson, and H Müller-Krumbhaar. Physica A 187, 87 (1992).

[46] JL Hutter and J Bechhoefer. Physical Review E 59(4), 4342 (1999).

[47] FJ Lamelas, S Seader, M Zunic, CV Sloane, and M Xiong. Physical Review B 67, 045414-1 (2003).

[48] AA Shibkov, YI Golovin, MA Zheltov, AA Korolev, and AA Leonov. Physica A 319, 65 (2003).

[49] PJ Barham, RA Chivers, A Keller, J Martinez-Salazar, SJ Organ. Journal of Materials Science 20(5), 1625 (1985).

[50] TP Russell, H Ito, and GD Wignall. Macromolecules 21(6), 1703 (1988).

[51] For a discussion of the variation of Tg with film thickness, see: CJ Ellison, MK Mundra, and JM Torkelson. Macromolecules 38(5), 1767 (2005).

[52] E Calahorra, M Cortazar, and GM Guzman. Polymer 23, 1322 (1982).

[53] E Martuscelli, M Pracella, and WP Yue. Polymer 25, 1097 (1984).

[54] F Khoury. Journal of Research of the National Bureau of Standards 70A, 29 (1966).

[55] B Lotz and JC Wittmann. Journal of Polymer Science Part B: Polymer Physics 24(7), 1541 (1986).

[56] E Brener, H Müller-Krumbhaar, and D Temkin. Physical Review E 54(3), 2714 (1996).

[57] H Xu, R Matkar, and T Kyu. Physical Review E 72, 011804-1 (2005).

[58] T Ihle and H Müller-Krumbhaar. Physical Review Letters 70, 3083 (1993).

[59] JM Marentette and GR Brown. Polymer 39(6-7), 1405 (1998).

[60] TG Fox. Bulletin of the American Physical Society 1, 123 (1956).

[61] TP Lodge. Physical Review Letters 83, 3218 (1999).

[62] R Kobayashi. Physica D 63, 410 (1993).

Chapter 3. The Diffusion Length, Growth Envelope, and Sidebranching in Dendritic Crystallization of PEO/PMMA Blends in Thin Films

Chapter 3.1 Introduction

Dendritic morphologies have been studied for a number of years both theoretically [1,2,3,4] and experimentally for small molecules and metals (for examples see [5,6,7]). A number of reviews of dendritic growth are available [8,9,10,11]. In these systems, the dendrite morphology results from a diffusion field (either heat or solute) surrounding the crystal. These dendrites are normally modeled as needle-crystals with a parabolic tip. Selection of the dendritic morphology requires some anisotropy to stabilize the growth tip. As the dendrite grows, sidebranches periodically develop along the length of the dendrite trunk [7,12]. Two mechanisms for sidebranch formation have been proposed. The first mechanism involves the presence of noise near the dendrite tip and results in imperfectly correlated sidebranches [13,14,15]. The second mechanism involves the existence of a limit-cycle during crystal growth where the growth tip slows and fattens before emitting two synchronized sidebranches [16,17,18]. Since both of these situations have been reported experimentally, the mechanism for their formation may not be unique [19]. In either case, the Mullins-Sekerka instability describes the conditions necessary for these sidebranches to become stable [20]. A complete understanding of sidebranch formation will require more extensive experimental studies in order to determine the important system parameters.

As mentioned above, dendrites result from a diffusion field and are thus referred to as a "diffusion-controlled" growth morphology. Diffusion-controlled growth is normally observed for materials with low entropies of fusion, where the growth front is rough. Jackson and coworkers have proposed that the entropy of fusion can be used to determine whether a rough or smooth interface will form during crystallization [21]. Crystallization of metals and small molecules, which have small entropies of fusion, is believed to occur through continuous growth at rough interfaces. On the other hand, crystals of polymeric materials generally have relatively large entropies of fusion and atomically smooth interfaces. These materials are believed to grow through a surface

nucleation mechanism ("nucleation-controlled growth"), although some debate still exists regarding this issue [22,23]. In polymers, growth on rough interfaces occurs very rapidly and the crystals quickly become limited by the low-index growth planes. However, under the proper growth conditions (i.e. polymer blends), a diffusion-limited regime may be accessed where the rate of diffusion (of impurities) away from the interface becomes the rate-limiting step.

Early studies of polymer crystallization from dilute solutions at high undercooling have demonstrated that a transition from nucleation-controlled to diffusion-controlled growth may be possible. Keller [24], Khoury et al. [25], Geil et al. [26], and Wunderlich et al. [27], for example, have reported dendrites in the crystallization of polyethylene from solution. However, these dendrites exhibit smooth facets and sharp tips (at the resolution provided by TEM), suggesting that diffusion mechanisms may not be active. Zhang and coworkers recently reported dendritic growth from the melt in thin films of polyethylene [28]. In this case, the thin film geometry was suggested to result in dendritic growth due to the lack of crystallizable chains at the growth front. Taguchi et al. reported similar results for thin films of isotactic polystyrene (iPS) [29]. More recent studies by Ferreiro et al., have demonstrated dendritic morphologies in thin films of blends of polyethylene oxide (PEO) and poly(methyl methacrylate) (PMMA) [30,31]. In this system, the non-crystallizable PMMA is rejected from the growing PEO crystal. Despite these reports, very little detailed information about dendritic growth in polymeric systems has been presented, especially in regard to dendrite growth theories developed for small molecules and metals.

Characterization of dendrite growth morphologies usually involves measurements of the crystal growth velocity, tip radius, sidebranch spacing, sidebranch amplitude, and dendrite trunk width. These measurements have frequently been used to compare experimental data with theoretical models [32]. Such measurements have not been reported in polymeric materials probably because of a lack of appreciation for dendritic growth theories in the polymer field and the limited number of experimental studies.

There has been some effort to describe the crystallization envelope of growing dendritic morphologies [33]. The envelope is composed of the leading dendrite tip and the train of sidebranches following behind. For cubic materials, this envelope takes the

shape of a square diamond or four-pointed star. Near the dendrite tip, the length of the arms is predicted to grow as $|z|^{1/2}$, where z is the distance from the dendrite tip [34]. Once the diffusion fields begin to interact, the sidebranches grow as $|z|^{3/5}$ [35]. In this region, the diffusion fields of the arms interact and growth is slow until 'winning' sidebranches are selected. At longer times, these winning arms become independent dendrites and grow as |z|. If the initial sidebranch spacing is sufficiently large, the diffusion fields of the arms do not interact and the sidebranches always grow at the same rate as the dendrite trunk, resulting in a perfectly polygonal (square) dendrite. If the initial sidebranch spacing is very small, the diffusion fields of the arms interact and neighboring sidebranches compete with each other and this competition results in a smaller growth rate than that of the dendrite trunk. This situation leads to the formation of a more needle-like dendrite with a curved envelope.

Noise may play an important role in the selection of the winning sidebranches [36]. In 'noisy' systems, the winning sidebranches are selected more quickly and a square polygonal growth envelope may be observed (even for situations where very competitive growth is expected). In systems with lower noise, selection is slower and the growth envelope becomes more needle-like.

Huang and Glicksman have studied aspects of dendritic growth related to sidebranching, such as sidebranch formation and coarsening [7]. Sidebranches normally develop at a distance of several times the tip curvature (ρ) from the growth tip. Following the development of sidebranches, two types of coarsening processes are known to occur. One of these processes is isothermal coarsening, which involves a lowering of the surface energy of the crystal by a reduction in its surface area. This is a relatively slow process where some of the small arms disappear or merge with larger arms. The second type of coarsening process is called dynamic coarsening. In this process, the secondary sidebranches continually adjust their spacing due to competition between neighboring sidebranches.

The diffusion length, $\delta = D / V$ (where D is the diffusion coefficient of the impurity and V is the growth velocity), is the characteristic length scale over which impurities are rejected from the growing crystal front. Large diffusion lengths mean that the crystal can grow relatively unperturbed since impurities diffuse from the interface

rapidly (and/or crystal growth is very slow). In small molecule systems, these length scales are typically on the order of microns to millimeters for solute diffusion. In high molecular weight bulk polymer systems, typical values of the diffusion length are in the range 10^{-4} to 1 micron(s) [37]. Confinement of a polymer chains into a thin film geometry and dilution of the crystallizable chains by a non-crystallizable component will affect these values due to changes in both the diffusion coefficient and the growth rate. In particular, the diffusion coefficient may be influenced by confinement and by changes in the glass transition temperature (due to substrate/surface interactions [38,39,40] as well as variation of the blend composition [41]).

In small molecule systems, crystallization often occurs at relatively low undercooling and significant changes in growth velocity may be observed over limited changes in crystallization temperature. Under these conditions, the diffusion coefficient is relatively independent of the growth conditions. However, changes in the diffusion coefficient are possible through the use of a different solvent. Such studies are also problematic because changing the solvent can lead to changes in the surface tension, range of crystallization temperatures, and a number of other factors. As a result of these constraints, the effect of varying the diffusion coefficient on pattern formation has not been demonstrated experimentally in small molecule systems. Akamatsu et al. have attempted to circumvent these problems in studies of liquid-expanded / liquid-condensed phase transitions in 2-D systems by varying the viscosity of the liquid sublayer, but reported problems with interpretation of the results [42].

Polymer mixtures are a natural choice for studies of the variation of the diffusion coefficient. In a polymer mixture, the diffusion coefficient can be tuned by varying the molecular weight (chain length) and the concentration of the non-crystallizable component. For entangled chains, the diffusion coefficient varies as $M^{-2.2}$ [43]. While a theoretical understanding of the relationship between the mutual diffusion coefficient for chains in the mixture and the self-diffusion coefficients of the individual chains is not complete [44,45,46,47], one expects the mutual diffusion coefficient to decrease with an increase in the concentration of the high glass transition temperature component.

We reported a morphological map for the PEO/PMMA system in Chapter 2. In the current study, we focus on the dendritic regions of this map, namely, on blend

compositions of 35/65 (wt% PEO / wt% PMMA) and 30/70 for a range of PMMA molecular weights. The effects of the PMMA molecular weight and composition on the diffusion length, growth envelope, sidebranch spacing, and coarsening process are discussed. This work is intended to provide a general overview of the dendritic growth of polymers, to clarify the classification of polymer dendrites as true dendritic morphologies, and to give insights into sidebranching and coarsening processes.

Chapter 3.2 Experimental

Poly(ethylene oxide) and poly(methyl methacrylate) were obtained from Scientific Polymer Products or Polymer Laboratories and used as received. The molecular weights and polydispersities are reported in Table 3.1. In this study, crystallized blend samples are referred to by the PMMA molecular weight (names shown in Table 3.1).

The PEO and PMMA were dissolved in HPLC-grade 1,2 dichloroethane and stirred overnight. The polymer concentration was approximately 1.25 wt%. Silicon wafers (100) were cleaned with a hot solution containing 70 vol% sulfuric acid and 30 vol% hydrogen peroxide for 2 hours. After cleaning, the wafers were rinsed with deionized water and blown dry with nitrogen.

The wafers were rinsed with 1,2-dichloroethane and spun dry. The polymer solutions were then spin-coated onto the silicon wafer at approximately 1000 RPM. The resulting thickness, evaluated by a JA Wollam ellipsometer, was approximately 120 nm. The samples were then dried under vacuum at 60^{o}C for 2 hours and then heated to 80^{o}C for 1 minute (to melt any crystalline nuclei formed during drying). The samples were then crystallized under nitrogen using a Linkam hotstage.

An Olympus BH-2 microscope with a Scion CCD camera was used to observe the crystal growth morphology. A Digital Instruments Dimension Series atomic force microscope (AFM) was used in tapping mode (in air) for higher resolution observations of the dendrite tip. A Nanosensors silicon cantilever was used with an approximate spring constant of 38 N/m and a setpoint of approximately 1.5 V.

Table 3.1. Weight-Average Molecular Weights and Polydispersities of Polymer Samples Used In This Study.

Material	Mw (g/mol)	Mw/Mn
PEO	101,200	1.04
PMMA7	6,880	1.07
PMMA12	12,000	1.08
PMMA18	17,900	1.10
PMMA53	52,700	1.08
PMMA68	68,200	1.13
PMMA101	101,000	1.09

Chapter 3.3 Results and Discussion

Basic Features of Polymer Dendrites

Figures 3.1 shows an example of a typical dendrite observed during crystallization of a 30/70 blend. At optical length scales, sidebranches form at 90^o to the dendrite trunk, reflecting the symmetry of the PEO unit cell [48]. Atomic-force microscopy (AFM) reveals that these branches initially form at an angle of near 45^o and turn back toward the preferred 90^o direction (see Figure 3.2). This "steering effect" toward the crystallographically preferred directions is well known in studies of dendrites [7].

The sidebranches are not correlated along the length of the dendrite trunk, implying that the formation of these sidebranches is a result of noisy growth rather than a limit-cycle mechanism. We have also observed constant growth rates in our measurements, so such a limit-cycle is not expected. However, Ferreiro and coworkers have previously reported oscillatory growth in this blend above a critical thickness value [30]. Our measurements indicate that we are slightly above this limit. The source of the discrepancy has not been identified but may be related to differences in sample preparation or the influence of the clay particles used in their study.

Figure 3.1 Example of a dendrite in a 30/70 PMMA7 sample crystallized at 37°C.

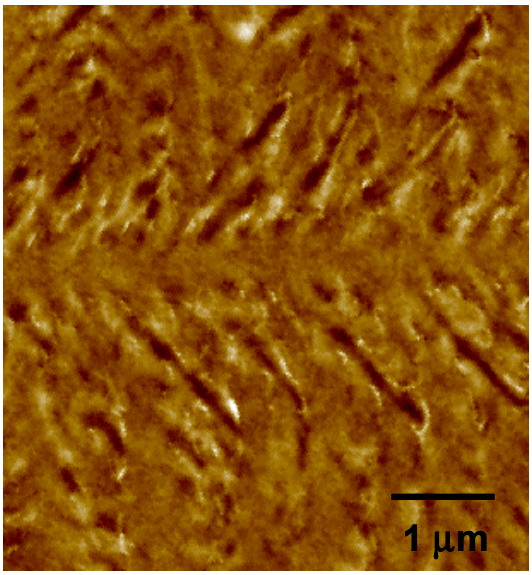

Figure 3.2 Atomic-force height micrograph of the sidebranching near the trunk of a 30/70, PMMA18 dendrite crystallized at 37°C. The z-range is 30nm.

The growth tip of a dendrite is shown in Figure 3.3. The tip of the dendrite is curved and facets are apparent on either side. This type of dendrite has generally been referred to as "faceted dendrites" [49,50,51]. Faceting is also known to occur in small molecule systems such as NH_4Br (under specific growth conditions). The presence of these facets is often indicative of a large anisotropy in the attachment kinetics as is expected in polymeric systems due to their large entropy of fusion.

The curved portion of the growth tip indicates that some mechanism destabilizes these facets. Curved interfaces in facet-forming polymeric materials have been reported in other studies (albeit rarely) [52,53,54]. First, it must be pointed out that the thermal roughening temperature of polymeric systems is believed to be above the melting point in all cases [55]. Second, "kinetic roughening" is not believed to be important here because regime III crystallization (where surface nucleation rates are very large) has not been observed in PEO [56]. The most likely scenario is that the surface becomes rough due to the presence of the non-crystallizable PMMA. Roughening of the crystal interface in this manner has been discussed Geil et al. [26]. Similar mechanisms have also been discussed by Chernov [57] and Yokoyama et al [58], although these cases involve some kinetic roughening process rather than the one described here. In the case of PEO/PMMA, the apex of the crystal is exposed to the largest number of crystallizable chains (largest supersaturation). As a result of this large supersaturation, secondary nucleation (of a new layer) is most likely to occur very close to the apex of the crystal. The PMMA chains must diffuse away from the crystal surface in order for lateral growth to proceed. In the meantime, however, nucleation of new layers can continue at the crystal apex. The result of this competition between diffusion and lateral growth results in a highly serrated (curved) interface. The global shape of the crystal reflects the diffusion limitations, and thus should approach a parabola as seen in metals and small molecules. The formation of sidebranches in this case has not been studied in detail but may be related to the formation of reentrant corners, as suggested by Geil et al. [26].

In normal dendritic growth, secondary branches typically form a few tip radii (1-5 ρ) from the growth tip [59,60,61,62]. Using the method described by Çadirli and coworkers [63], the tip radius was determined to be on the order of 50 nm (from Figure

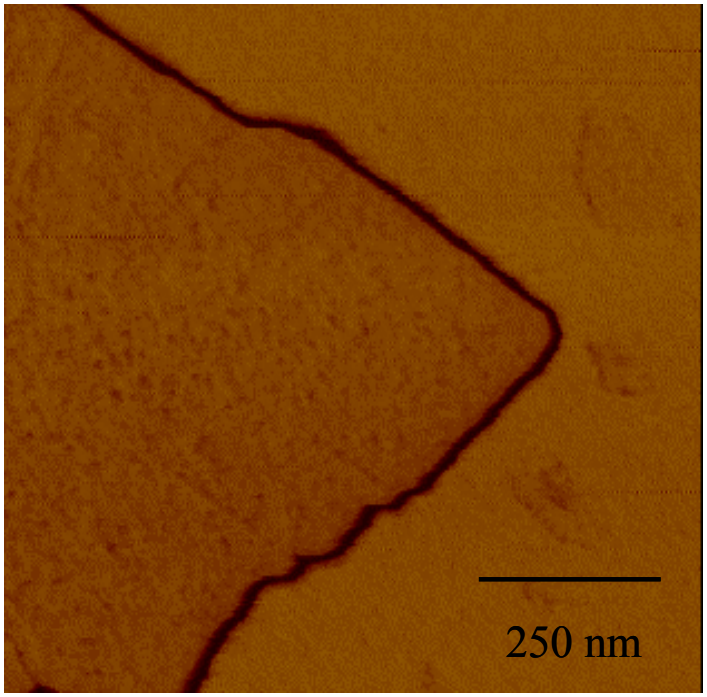

Figure 3.3 Atomic-force phase micrograph of a growth tip of a 30/70 PMMA68 sample growing at 25^{o}C. The phase range is 80 degrees.

3.3). This measurement was only carried out at room temperature but was relatively independent of PMMA molecular weight (obviously there is considerable uncertainty in this measurement given the difficulty in resolving tips of such a small radius during in-situ AFM experiments). In addition, the early stages of growth are difficult to study because of the small length scales involved (well below the optical limit). However, since the tip radius is on the order of 50 nm, sidebranching is expected to occur at distances of 50-250 nm from the dendrite tip. The observed sidebranch spacing in Figure 3.2 verifies that this approximation is indeed justified. Taking the radius of curvature as 50 nm and the growth rate as 10^{-4} microns/sec, we can infer that the diffusion coefficient is approximately 10^{-14} cm^2/sec. This estimate seems reasonable [37], although no such measurements have been reported to date for the PEO/PMMA thin film blends used in this study.

Figures 3.4 and 3.5 show dendritic morphologies for several molecular weights for the 35/65 and 30/70 blends, respectively. Several important features are immediately apparent from these figures. No morphological transitions are observed despite the relatively large change in PMMA molecular weight. In addition, the growth envelope and sidebranch spacing are observed to change significantly over the range of conditions studied. These features are discussed in more detail below.

Tuning of the Diffusion Coefficient (and Diffusion Length)

As discussed above, the diffusion coefficient in homopolymers varies as $M^{-2.2}$ in the entangled regime [43]. In polymer blends, the situation is more complicated. "Fast" [45,46] and "slow" theories [44] have been developed, but experimental results have generally shown the fast theory to be more applicable. Bulk diffusion studies in PEO/PMMA blends have been reported and showed that neither the fast nor the slow theory is directly applicable to this system [64]. A number of experimental and theoretical limitations exist for an exact calculation of the diffusion coefficient, [47,64]

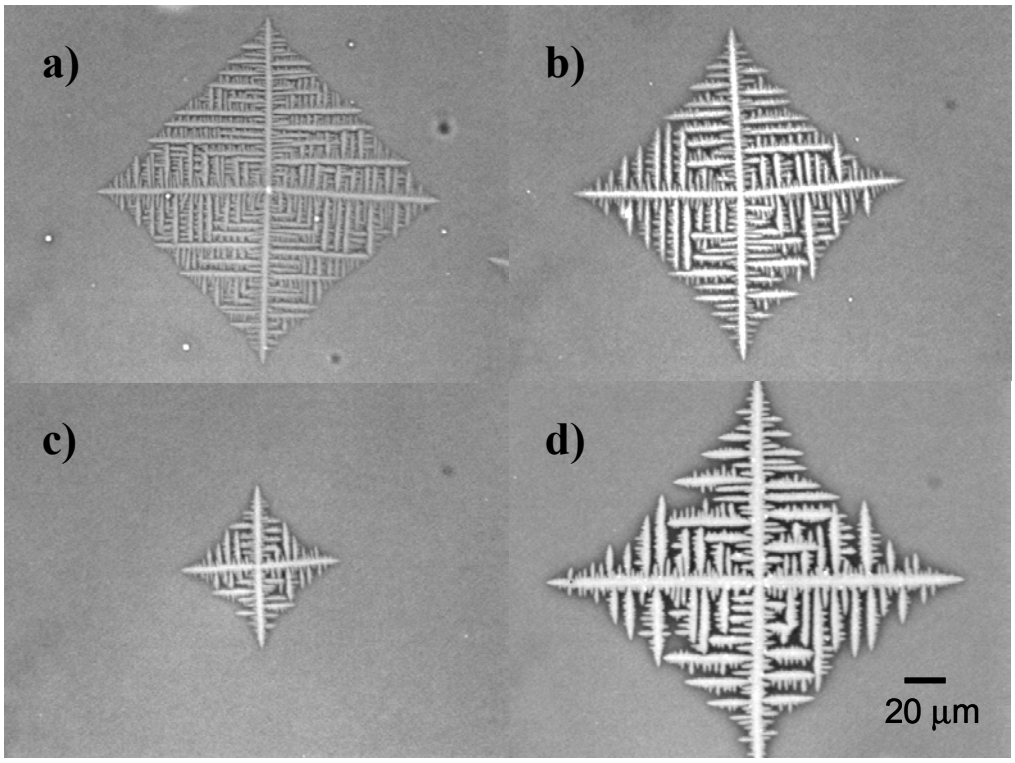

Figure 3.4 Effects of the PMMA molecular weight on the observed morphology for 35/65 blends crystallized at 37°C: a) PMMA18, b) PMMA30, c) PMMA68, and d) PMMA101.

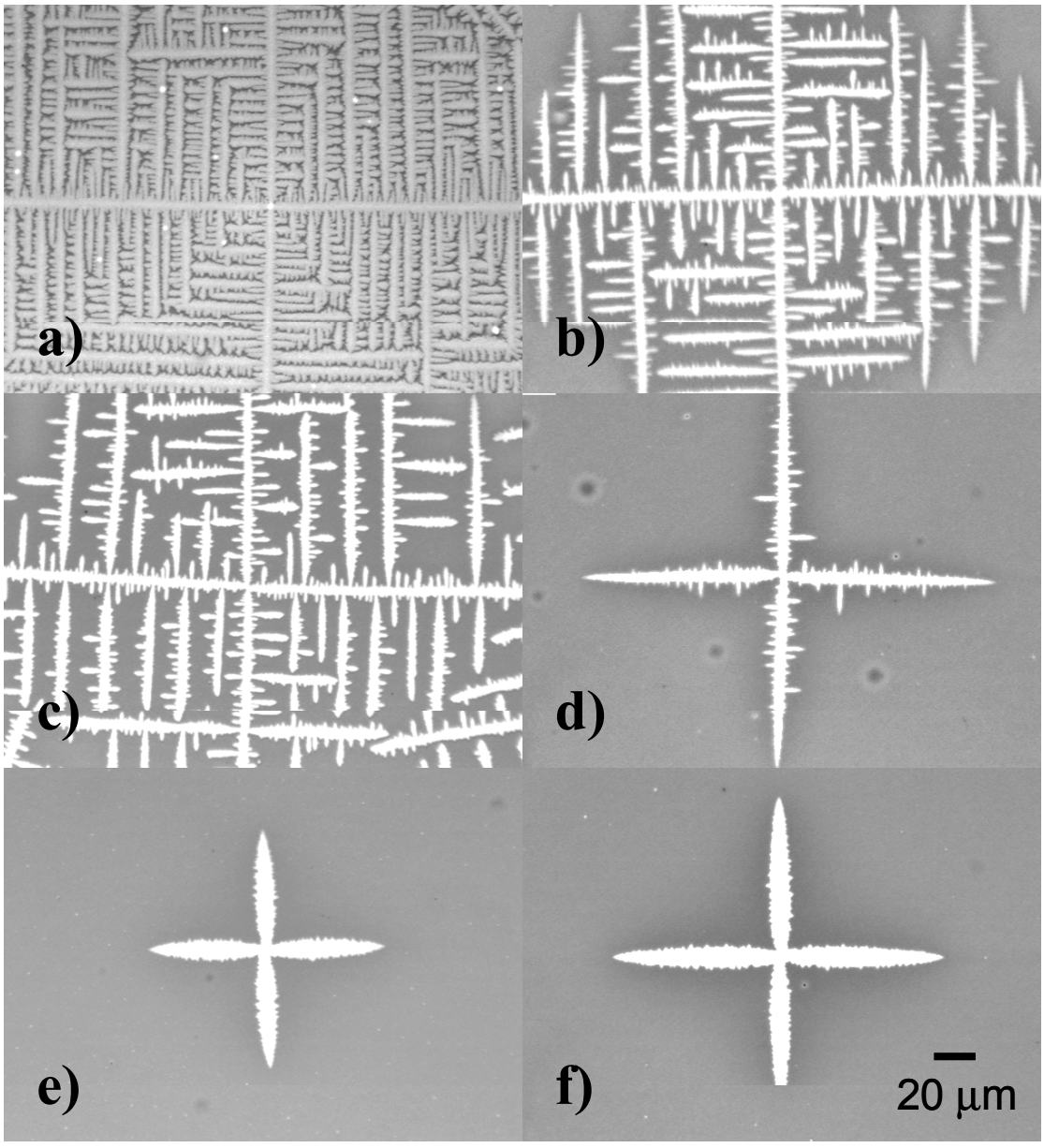

Figure 3.5 Effects of the PMMA molecular weight on the observed morphology for 30/70 blends crystallized at 37°C: a) PMMA7, b) PMMA12, c) PMMA18, d) PMMA53, e) PMMA68, and f) PMMA101.

but the results can be compared on a qualitative basis. In any case, the blend diffusion coefficient is expected to decrease with increasing PMMA content or molar mass [64].

These changes in the diffusion coefficient affect the value of the diffusion length. The crystal growth rate does not vary significantly (less than an order of magnitude for each blend composition) for the various PMMA molecular weights [65]. However, given the variation in chain length and glass transition temperature [66] with PMMA molecular weight, the diffusion coefficient should decrease with increasing molecular weight. Thus, changes in the diffusion coefficient are expected to dominate the value of the diffusion length.

The fact that observed morphologies are very similar (all dendritic) in Figures 3.4 and 3.5 indicates that the diffusion length is not changing markedly over the range of molecular weights studied. However, small changes in the blend composition (35/65 to 30/70) result in significant changes in the morphology (compare Figure 3.4d and Figure 3.5f for PMMA101 blends). Hence, the self-diffusion coefficient of PEO must be the most important factor controlling the mutual diffusion coefficient and the value of the diffusion coefficient for the PMMA chains only slightly alters this value.

Crystallization Envelope

The growth envelope contains important information about the processes involved in pattern formation. For example, Kupferman and coworkers have used the concavity of the growth envelope and shape of the growth unit to distinguish between the dense-branched and the dendrite morphologies [33]. For dendritic growth, the envelope is either polyhedral or polyhedral with concave sides, indicating that information about competition between sidebranches is also contained in the envelope [67]. The development of this growth envelope occurs at a very early stage in the development of a dendrite. If selection of the winning sidebranches takes a long time (during which the growth rate of the sidebranches is slower than that of the trunk) a concave shape is developed. For shorter selection times, the angle between the dendrite trunk and the tangent to the growth envelope rapidly nears 45^{o} (for a cubic material).

There are several methods of categorizing the shape of the crystallization envelope. Given the fact that dendritic growth is inherently a noisy process, the growth envelope is often highly irregular making precise analysis difficult. We have measured the length of these leading sidebranches (L_S) as a function of distance from the dendrite tip (L_T) at a fixed time to characterize the envelope (as to take a snapshot of the dendrite). Isothermal coarsening effects are ignored for reasons discussed later. Initially, there is some incubation time that is related to the time for competition between branches to set in. Following this incubation time, the competitive growth regime begins. In this region, the growth rate is non-linear due to competition between sidebranches and their diffusion fields (defining the envelop as discussed above). Once winning branches are selected, they speed up until they have the same growth rate as the dendrite tip (in the absence of other competing diffusion fields). These regimes are summarized in Figure 3.6.

Experimental data for L_S versus L_T for several PMMA molecular weights and blend compositions are reported in Figure 3.7. For blends with a composition of 35/65, square dendrites are observed at low molecular weight, indicating that the selection time (incubation and coarsening time) for winning sidebranches is very small. Increasing the PMMA content and molecular weight result in increasingly needle-shaped dendrites, as shown in Figures 3.4 and 3.5. These observations suggest that the noise may play an important role [36]. High PMMA content and molecular weight result in slower dynamics (lower noise), meaning that growth must occur for a longer period of time before the system can reach a steady-state and winning sidebranches are selected (as observed in the 30/70 PMMA53 sample).

Sidebranch Spacing and Dynamic Coarsening

The spacing between sidebranches near the dendrite tip (S_{TIP}) is expected to be on the order of a few ρ (where the Mullins-Sekerka instability is active). In the current study, information about the initial sidebranch spacing can not be determined by optical means as is typical in small molecule systems because of the very small length scales involved in this study. As discussed above, using our estimate of the radius of curvature

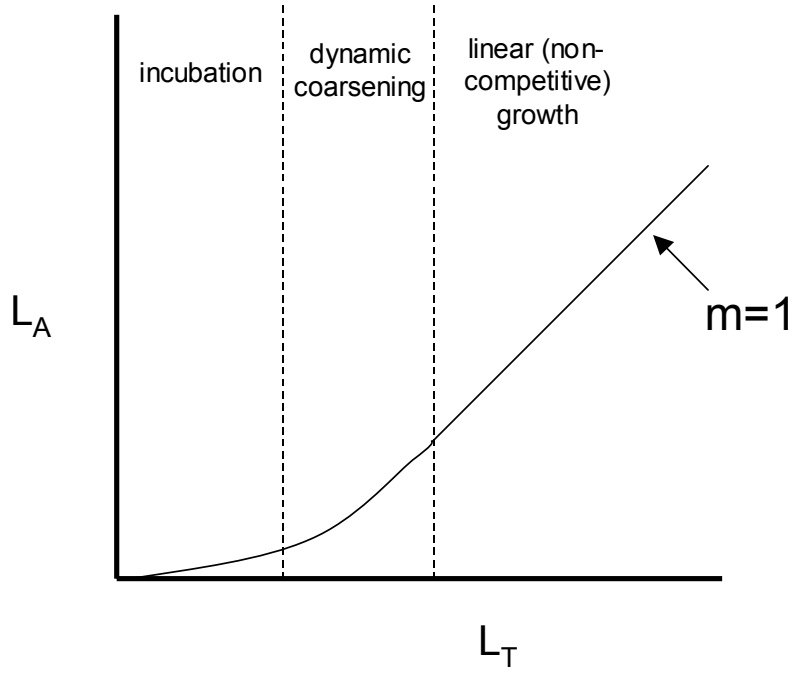

Figure 3.6 Schematic of different growth regions for secondary sidebranches.

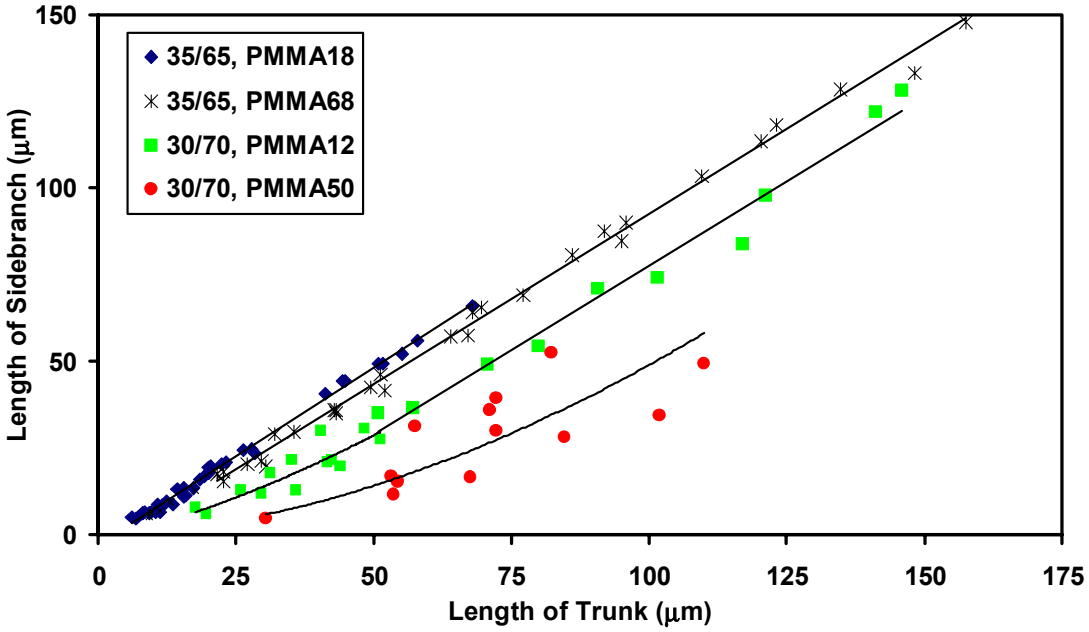

Figure 3.7 Experimental La/Lt values for several blends crystallized at 37°C.

from AFM measurements and by examination of Figure 3.2, the expected initial sidebranch spacing should be on the order of 50-250 nm.

In our studies, we find that the dendrite spacing in the PEO/PMMA system does not change with time at a fixed position from the dendrite trunk. That is, no isothermal coarsening occurs (at any observable length scale). This observation can be qualitatively understood as follows. During crystallization, the PMMA is rejected from the crystal resulting in a large amount of PMMA surrounding the crystal. The increase in PMMA content increases the local glass transition temperature, effectively cutting off the sides of the dendrite from access to any new crystallizable PEO and essentially stops crystallization. Because all of the branches that formed during growth are still present, the sidebranch spacing can easily be analyzed after crystallization is complete. Huang and Glicksman chose to analyze their sidebranch spacing at a fixed time during the crystallization process by using the spacing at a fixed distance behind the dendrite tip [32]. Although there is no real difference in such an analysis, we obtain a much larger number of measurements at each distance, improving the accuracy of the measurement. The sidebranch spacing (S) as a function of the distance from the dendrite trunk is reported in Figure 3.8. As the PMMA molecular weight increases (diffusion length decreases), the distance between sidebranches also increases. This result is consistent with Huang and Glicksman's report that showed that the sidebranch spacing increased with increasing supercooling at a fixed time (decreasing diffusion length). In our system, we also note that changes in composition have a similar effect as changes in the PMMA molecular weight. The 35/65 PMMA30 sample has a similar spacing to that of the 30/70 PMMA7 sample. Indeed these two samples have very similar appearances (Figures 3.4 and 3.5), so the sidebranch spacing may be used as a measure of comparison of the diffusion coefficients.

As discussed above, as the sidebranches grow, they begin to compete with each other. Slowing down of a sidebranch as a result of competition or thermal fluctuation, may allow neighboring branches to take over and readjust their spacing. The result of this coarsening process is that the sidebranch spacing increases with distance from the dendrite trunk (or the tip). Huang and Glicksman have suggested that this competition

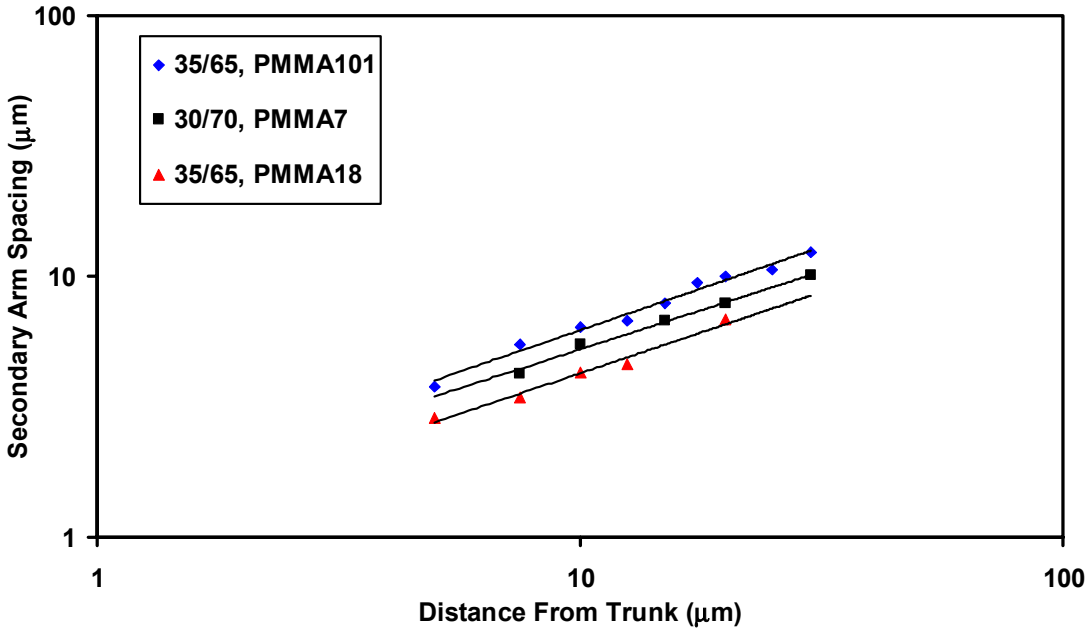

Figure 3.8 Secondary sidebranch spacing as function of distance from dendrite trunk for several blends.

should only occur if the diffusion fields overlap, and thus should cease when the proper spacing has been obtained. However, this suggestion relies on the fact that diffusion field is the only factor that selects the sidebranch spacing. Another mechanism for adjustment of the sidebranch spacing is that higher-order sidebranches that develop on neighboring secondary branches effectively coarsen the structure by cutting off neighboring secondary branches. This process should be continuous and only requires that some of the secondary branches slow (momentarily) long enough that a previous arm can develop a tertiary sidebranch in time to cut off the secondary branch. This mechanism is particularly effective when the sidebranches develop very near the tip and do not compete with neighboring sidebranches for long periods of time (they grow at the same rate as the dendrite tip). In this coarsening mechanism, the secondary sidebranch spacing *always* increases and the growth envelope is made up of increasingly higher order sidebranches.

For a 35/65, PMMA101 sample crystallized at 37^{o}C, the secondary sidebranch spacing is approximately 10 microns at a distance of 20 microns from the dendrite trunk. Obviously this value is well above (orders of magnitude) the effective diffusion length, and so the diffusion field can not be responsible for coarsening in this case. Instead, competition between secondary and tertiary sidebranches is responsible for the observed changes in the secondary sidebranch spacing. In Figure 3.9, an example of this coarsening mechanism is clearly shown. However, at lower PEO content and/or higher PMMA molecular weight (i.e. 30/70 PMMA68), the dynamic coarsening process is still well underway and this type of coarsening is not yet active. We can speculate that given enough time, many systems undergo a similar coarsening process.

In a manner similar to Huang and Glicksman, we can also obtain the solidification time by dividing the distance from the trunk by the growth rate of the tip. Although there is some difference in the actual solidification time and the value obtained in this manner, the difference is too small to matter (due to the relatively small diffusion length involved in this system).

We also attempted to measure the "incubation length", which represents the area around the dendrite tip where dynamic coarsening (in the sense of Huang and Glicksman) does not occur. This can be found at a value of $S/S_{TIP} = 1$, where S_{TIP} is the sidebranch spacing near the dendrite tip. The sidebranch spacing data was normalized by the tip

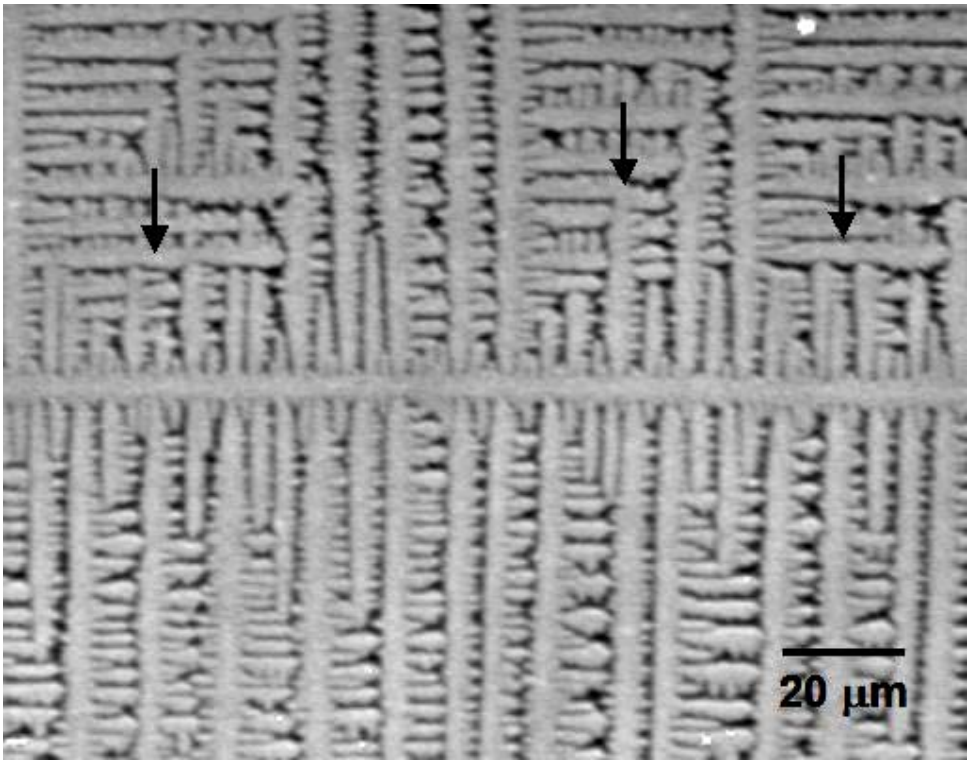

Figure 3.9 Example of coarsening of the secondary sidebranch spacing by higher order arms in a 30/70 PMMA7 blend at 33°C.

radius (despite the fact that we assuming a constant radius of approximately 50 nm) in order to determine the length where $S/S_{TIP} = 1$. The values of the incubation length calculated at $S/S_{TIP} = 1$ are rather inaccurate but give values of approximately 5 nm. These measurements were only carried out for three samples (indicated in Figure 3.10) were a relatively large number of sidebranches were present. The accuracy is greatly affected by the low number of measurements and the extrapolation to very small length scales using optical measurements. Samples still undergoing dynamic coarsening (e.g. 30/70, PMMA68) were not studied here because of the relatively small number of measurable sidebranches (at reasonable time scales).

These results indicate secondary sidebranch spacing is not a good measure of the local microstructure because the secondary sidebranch spacing increases dramatically with time (distance from the trunk) but the local microstructure is relatively the same due to the formation of higher order branches (for example, see Figure 3.1). This result contrasts suggestions that the sidebranch spacing depends on the effective solidification time [8] because the sidebranch spacing is constantly renewing itself as higher order branches are formed.

Chapter 3.4 Conclusions

Dendritic crystallization of PEO/PMMA thin films has been studied. These dendrites appear very similar to those reported for other materials. Some of the basic aspects of these dendrites have been discussed such as sidebranching and rejection of impurities. The tip curvature, growth envelope, and sidebranch spacing have also been reported. The measured tip curvature was approximately 50 nm. The diffusion coefficient was tuned and shown to play an important role in the secondary sidebranch spacing. Isothermal coarsening was not observed to be active in these experiments. In addition, dynamic coarsening was only observed to be important in cases where the diffusion length was very small. Another mechanism for coarsening is believed to be related to the formation of high order sidebranches that "cut off" neighboring branches,

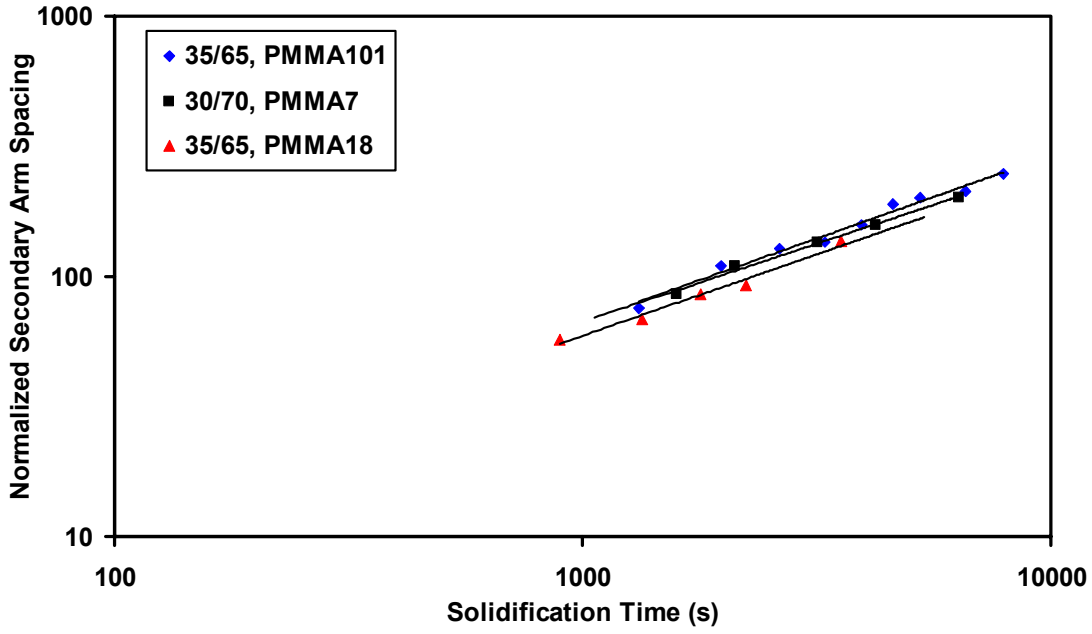

Figure 3.10 The normalized secondary arm spacing as a function of solidification time for several blends.

rather than the interaction of diffusion fields. The results are analyzed in the manner of Huang and Glicksman and are very similar to those reported in other systems (i.e. succinonitrile), indicating that the formation of polymer dendrites occurs by processes similar to those in small molecules.

Chapter 3.5 References

[1] GP Ivanstov. Dokl Akad Nauk SSSR 58, 567 (1947).

[2] DE Temkin. Dokl Akad Nauk SSSR 132, 1307 (1960).

[3] GF Bolling and WA Tiller. Journal of Applied Physics 32(12), 2587 (1961).

[4] JS Langer and H Muller-Krumbhaar. Acta Metallurgica 26, 1681 (1978).

[5] ME Glicksman, RJ Schaefer, and JD Ayers. Metallurgical Transactions A 7A, 1747 (1976).

[6] SC Huang and ME Glicksman. Acta Metallurgica 29, 701 (1981).

[7] SC Huang and ME Glicksman. Acta Metallurgica 29, 717 (1981).

[8] JS Langer. Reviews of Modern Physics 52, 1 (1986).

[9] DA Kessler, J Koplik, and H Levine. Advances in Physics 37(3), 255 (1988).

[10] ME Glicksman and SP Marsh. In *Handbook of Crystal Growth, Fundamentals: Transport and Stability*, Volume 1B, pages 1075-1122, Elsevier Science Publishers B.V.: New York (1993).

[11] B Billia and R Trivedi. In *Handbook of Crystal Growth, Fundamentals: Transport and Stability,* Volume 1B, pages 899-1073, Elsevier Science Publishers B.V.: New York (1993).

[12] O Martin and N Goldenfeld. Physical Review A 35(3), 1382 (1987).

[13] R Pieters and JS Langer. Physical Review Letters 56(18), 1948 (1986).

[14] DA Kessler and H Levine. Europhysics Letters 4(2), 215 (1987).

[15] PH Bouissou, A Chiffaudel, B Perrin, and P Tabeling. Europhysics Letters 13(1), 89 (1990).

[16] LR Morris and WC Winegard. Journal of Crystal Growth 1, 245 (1967).

[17] Y Sawada, B Perrin, P Tabeling, and P Bouissou. Physical Review 43(10), 5537 (1991).

[18] H Honjo, S Ohta, Y Sawada. Physical Review Letters 55(8), 841 (1985).

[19] JC LaCombe, MB Koss, JE Frei, C Giummarra, AO Lupulescu, and ME Glicksman. Physical Review E 64, 031604-1 (2002).

[20] WW Mullins and RF Sekerka. Journal of Applied Physics 34(2), 323 (1963).

[21] KA Jackson. Liquid Metals and Solidification ASM. Cleveland, Ohio, 174 (1958).

[22] DM Sadler. Polymer 24, 1401 (1983).

[23] KA Armistead, G Goldbeck-Wood in "Advances in Polymer Science", Volume 100, pp 219-312, Springer-Verlag: New York (1992).

[24] A Keller. Philosophical Magazine 2, 1171 (1957).

[25] F Khoury and FJ Padden. Journal of Polymer Science XLVII, 455 (1960).

[26] PH Geil and DH Reneker. Journal of Polymer Science 51, 569 (1961).

[27] B Wunderlich and P Sullivan. Journal of Polymer Science 61, 195 (1962).

[28] F Zhang, J Liu, H Huang, B Du, and T He. European Physical Journal E8, 289-297 (2002).

[29] K Taguchi, H Miyaji, K Izumi, A Hoshino, Y Miyamoto, R Kokawa. Polymer 42, 7443 (2001).

[30] V Ferreiro, JF Douglas, JA Warren, and A Karim. Physical Review E 65, 042802-1 (2002).

[31] V Ferreiro, JF Douglas, J Warren, and A Karim. Physical Review E 65, 051606-1 (2002).

[32] ME Glicksman, RJ Schaefer, and JD Ayers. Metallurgical Transactions A 7A, 1747 (1976).

[33] R Kupferman, O Shochet, and E Ben-Jacob. Physical Review E 50(2), 1005 (1994).

[34] E Brener. Physical Review Letters 71(22), 3653 (1993).

[35] A Dougherty and A Gunawardana. Physical Review E 50(2), 1349 (1994).

[36] R Kobayashi. Physica D 63, 410 (1993).

[37] JM Schultz. Polymer 32(18), 3268 (1991).

[38] JL Keddie, RAL Jones, and RA Cory. Faraday Discussions 98, 219 (1994).

[39] JH van Zanten, WE Walace, and W Wu. Physical Review E 53(3), R2053 (1996).

[40] DS Fryer, RD Peters, EJ Kim, JE Tomaszewski, JJ de Pablo, PF Nealey, CC White, and W Wu. Macromolecules 34, 5627 (2001).

[41] TG Fox. Bulletin of the American Physical Society 1, 123 (1956).

[42] S Akamatsu, O Bouloussa, K To, and F Rondelez. Physical Review A 46(8), R4504 (1992).

[43] TP Lodge. Physical Review Letters 83, 3218 (1999).

[44] F Brochard, J Jouffroy, and P Levinson. *Macromolecules* 16, 1638-1640 (1983).

[45] EJ Kramer, P Green, and CJ Palmstrom. Polymer 25, 473 (1984).

[46] H Silescu. Makromolecular Chemistry, Rapid Communications 5, 519 (1984).

[47] TE Shearmur, AS Clough, DW Drew, MGD van der Grinten, RAL Jones, Macromolecules 29(22), 7269 (1996).

[48] AJ Kovacs, B Lotz, and A Keller. Journal of Macromolecular Science – Physics B3(3), 385 (1969).

[49] J Maurer, P Bouissou, B Perrin, and P Tabeling. Europhysics Letters 8(1), 67 (1989).

[50] M Ben Amar and Y Pomeau. Europhysics Letters 6(7), 609 (1988).

[51] M Adda Bedia and M Ben Amar. In *Growth and Form*, p 187, Plenum Press: New York (1991).

[52] A Toda. Polymer 32(5), 771 (1991).

[53] ML Mansfield. Polymer 34(23), 4904 (1993).

[54] F Khoury and JD Barnes. Journal of Research of the National Bureau of Standards A 78A(2), 95 (1974).

[55] JD Hoffman. Private communication.

[56] Z Huang. *PhD Dissertation*. Virginia Polytechnic Institute & State University, 2004.

[57] AA Chernov. Journal of Crystal Growth 24/25, 11 (1974).

[58] E Yokoyama and T Kuroda. Physical Review A 41(4), 2038 (1990).

[59] A Dougherty and JP Gollub. Physical Review A 38(6), 3043 (1988).

[60] JP van der Eerden and H Muller-Krumbhaar. Acta Metallurgica 34, 839 (1986).

[61] Y Saito, G Goldbeck-Wood, and H Muller-Krumhaar. Physical Review Letters 58, 1541 (1987).

[62] CA van Driel, AEDM van der Heijden, and GM van Rosmalen. Journal of Crystal Growth 128, 229 (1993).

[63] E Çadirli, İ Karaca, H Kaya, and N Maraşli. Journal of Crystal Growth 255, 190 (2003).

[64] CH Wang, XQ Zhang, G Fytas, and J Kanetakis. Journal of Chemical Physics 91(5), 3160 (1989).

[65] Alfonso and Russell (G Alfonso and TP Russell. Macromolecules 19(4), 1143 (1986)) showed a large decrease in the compositional dependence of the crystal growth rate with increasing PMMA content. At the blend compositions in this study, the compositional dependence of the growth rate should be very small.

[66] See, for example: K Tanaka, A Takahara, and T Kajiyama. Macromolecules 31(3), 863 (1998).

[67] H Sakaguchi and M Ohtaki. Physica A 272, 300 (1999).

Chapter 4. The Dendrite to Dense-Branched Morphology Transition and Other Morphological Transitions During Crystallization of PEO/PMMA Thin Films

Chapter 4.1 Introduction

Crystallization morphologies have been studied for a number of years in efforts to understand a number fundamental processes involved in solidification, such as crystal growth mechanisms [1]. In addition, crystalline morphologies are of interest because the microstructure is known to play a large role in the resulting material properties [2]. Despite the fact that only a handful of crystal morphologies are normally observed, work in this area has been going on for well over a hundred years [3].

The most commonly encountered morphology in solidification of metals is the dendrite. A dendrite is a tree-like morphology composed of a several primary arms, or trunks, and many generations of sidebranches radiating from these trunks. These dendritic morphologies result from instability of the solid-liquid interface due to rejection of heat or solute from the growing crystal. Ivanstov is credited with the first model of the dendrite [4]. In this model, the dendrite is considered to be a parabolic needle with no sidebranching. Later improvements to this model include the addition of anisotropic surface energy, attachment kinetics, and a description of sidebranching. Langer [5], Levine et al. [6], Woodruff [7], Glicksman et al. [8], and Billia et al. [9] have written detailed reviews of solidification and dendritic growth.

Early studies of crystallization in polymeric materials revealed that polymers normally crystallize in a faceted manner [10]. In dilute solutions, these crystals take the shape of large polyhedrons, reflecting some anisotropy in the molecular attachment kinetics. During bulk crystallization from melt, however, spherulitic morphologies are often observed. These spherulites are comprised of a number of highly elongated faceted crystals that attempt to fill three-dimensional space through splaying and repeated formation of screw dislocations [11,12,13].

Recent theoretical studies of crystal morphologies have focused on the dense-branched morphology (DBM) or seaweed [14,15]. This morphology is characterized by

frequent splitting of the growth tips and lack of pronounced order in the crystal shape [14]. Tip-splitting takes the form of a "doublon" which is a bifurcation of the growth tip [16]. DBM is common in Hele-Shaw studies [17,18] but is less common in crystal growth experiments. In the existing experimental studies, both single-crystal [19,20] and polycrystalline [18] morphologies have been reported. The term "DBM" has been used to describe both, despite that fact that these morphologies may grow by very different growth processes. In our view, the term "DBM" should only be used for these single-crystals because dendrites are also single-crystals and recent efforts to compare these morphologies [21] rely on the fact that they grow by similar mechanisms.

There have been a number of attempts by theorists to develop morphology maps based on the systems control parameters, such as the anisotropy of the surface energy and the undercooling [22,23,24,25]. These maps predict morphological transition upon passing through some critical value of a control parameter. The most interesting of these transitions is that between dendrites and DBM because these are the most commonly encountered morphologies in these theoretical studies and particularly elusive in experimental studies. Theoretical studies have pointed to the importance of noise [21] in this transition, a variable that is not easily accessible in standard laboratory experiments involving metals and small molecules.

Hutter et al. reported a number of morphological transitions in crystallization experiments [26]. In conjunction with these transitions, jumps in the crystal growth velocity were observed and compared to thermodynamic phase-transitions. Chan and coworkers reported similar velocity jumps upon changes in the crystal growth plane in ammonium chloride crystallized from solution [27]. With exception of these latter investigations, in-situ observations of morphological transitions are rarely reported. In many cases, crystal growth rates are reported without supporting micrographs or individual morphologies are reported without a clear demonstration of the transition between them. In particular, in-situ observations of the dendrite/DBM transition in melt systems have not been clearly demonstrated in any previous experimental reports.

Recently, Ferreiro and coworkers reported a number of morphologies in crystallization of poly(ethylene oxide) (PEO) / poly(methyl methacrylate) (PMMA) blends in thin film geometries [28,29]. The crystallization morphology was tuned with

changes in the blend composition. This system is an obvious candidate for studies of morphological transitions because of the ability to vary many of the parameters controlling the crystal growth process (diffusion length, crystal growth velocity, etc).

In Chapter 2, we reported a map demonstrating the location of different morphologies in relation to a number of experimental control parameters (PMMA molecular weight, blend composition, and crystallization temperature). Using this map to locate transition regions, we now report more detailed studies of these transitions. The transitions studied here include the dendrite/DBM, the needle/stacked-needle/DBM, and the transition involving a 45^{o} change in the growth direction. Morphological evidence and crystal growth rates are used to describe these transitions and propose mechanisms for their existence.

Chapter 4.2 Experimental

Poly(ethylene oxide) and poly(methyl methacrylate) were obtained either from Scientific Polymer Products or Polymer Laboratories and used as received. The molecular weights and polydispersities are reported in Table 4.1. In this study, crystallized blend samples are referred to by the PMMA molecular weight, as shown in Table 4.1.

The PEO and PMMA were dissolved in HPLC-grade 1,2-dichloroethane and stirred overnight. The polymer concentration was approximately 1.25 wt% and the composition of the blend was varied from 30 to 40 wt% PEO. Silicon wafers (100) were cleaned with a hot solution of 70 vol% sulfuric acid and 30 vol% hydrogen peroxide for 2 hours to create a hydrophilic surface. After cleaning, the wafers were rinsed with deionized water and blown dry with nitrogen.

The wafers were rinsed with 1,2-dichloroethane and spun dry. The polymer solutions were then spin-coated onto the silicon at approximately 1000 RPM. The resulting film thickness was approximately 120 nm, as determined using a JA Woollam spectroscopic ellipsometer. Spin-coated samples were then dried under vacuum at 60^{o}C for 2 hours and then heated to 80^{o}C for 1 minute (to melt any nuclei formed during

drying). Subsequent to melting, the samples were crystallized under nitrogen in a Linkam hotstage.

An Olympus BH-2 reflected light microscope equipped with a Cohu CCD camera was used to observe the crystal growth morphology. The image contrast was digitally enhanced to show the morphologies more clearly.

In this report, single samples are used for growth rate measurements over a range of temperature values. Single samples were used to minimize the unavoidable scatter associated with sample preparation. Experiments were repeated with different samples to ensure the existence of the transitions and confirm the relative temperature dependence of the crystal growth rate.

Table 4.1 Weight-Average Molecular Weights and Polydispersities of Polymers Used in this Study

Material	Mw (g/mol)	Mw/Mn
PEO	101,200	1.04
PMMA17	16,700	1.06
PMMA18	17,900	1.10
PMMA68	68,200	1.13
PMMA101	101,000	1.09

Chapter 4.3 Results and Discussion

The Dendrite / Dense-Branched Morphology (DBM) Transition

Figure 4.1a shows a dendrite grown in a 50/50 (PEO/PMMA) blend at small undercooling. As discussed in Chapter 2, the dendrite arms grow at 90^{o} to the dendrite trunk. At larger undercooling, a transition to the dense-branch morphology is observed. An example of DBM is shown in Figure 4.1b. A number of bifurcations of the growth front are observed, resulting in a circular space-filling envelope.

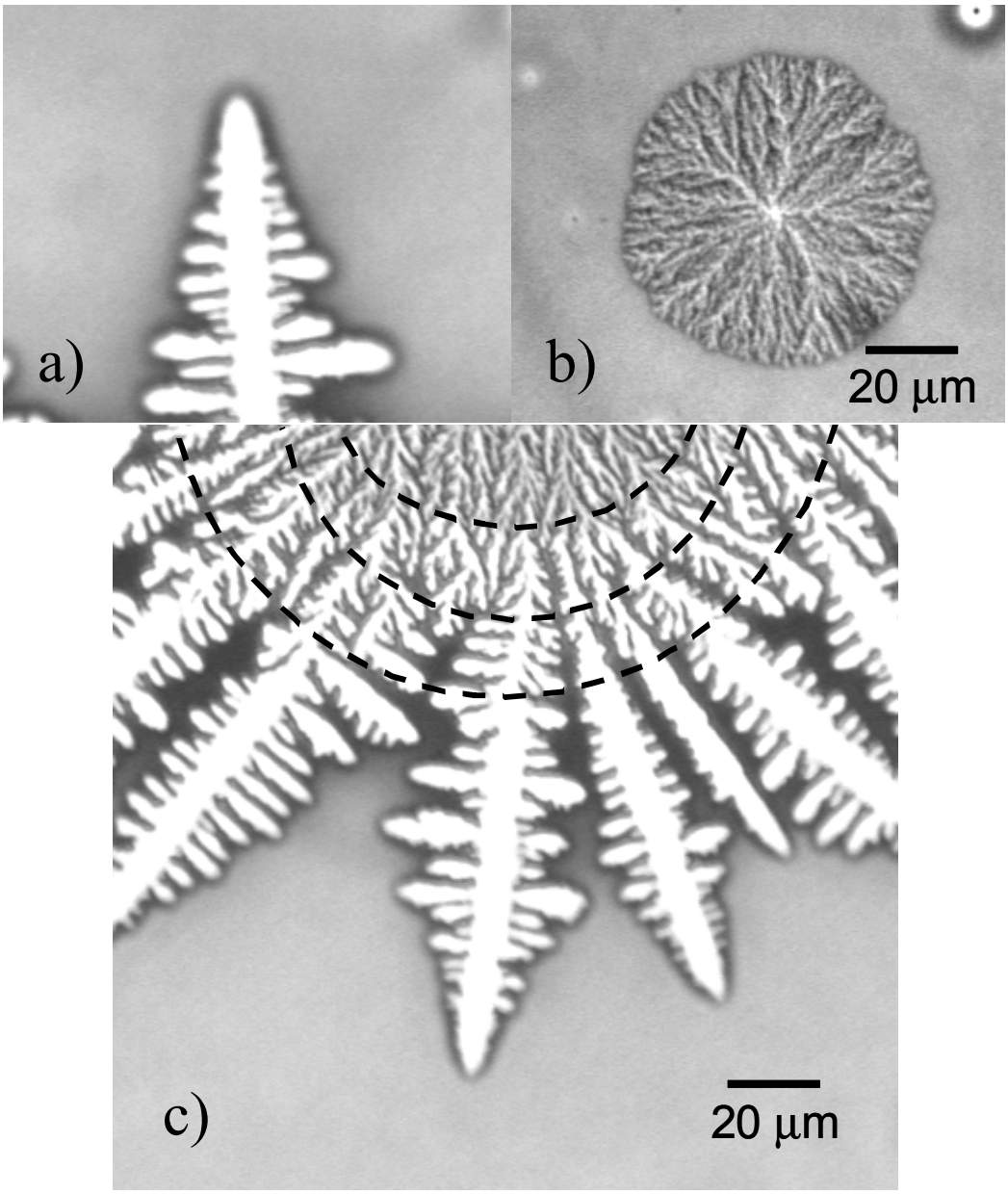

Figure 4.1 (a) Dendritic (Tx=58°C) and (b) dense-branched morphology (Tx=37°C) in a 50/50 PMMA17 blend. (c) In-situ observations of the dendrite/DBM transition as the undercooling is varied (from top to bottom) Tx = 41, 51, 55, and 58°C.

Figure 4.1c shows the transition between a dense-branched morphology and the dendrite upon variation in the undercooling. This transition occurs over a range of undercooling with a gradual change in the shape and size of the morphological features (trunk width, branch density, etc.). The fact that this transition occurs slowly (over a range of undercooling) indicates that the transition is not "sharp" and a small activation barrier exists between morphologies. The width of the branches clearly increases with decreasing undercooling, indicating an increase in the diffusion length. This increase in diffusion length is also associated with a decrease in the number of bifurcations per unit length. Since the transition occurs continuously, this transition is likely associated with a change in the effective anisotropy due to changes in the undercooling. A similar suggestion is made by Xu et al. in simulations of crystallization of thin polystyrene films [30].

Figure 4.2 shows the crystal growth velocity as a function of temperature. The onset of the glass transition temperature results in a growth rate maximum at low temperature. There is no clear break in the curve over the temperature range where this transition occurs, further demonstrating that the DBM/dendrite transition is not a sharp transition. Longer crystallization times may allow the "correct" (more stable) morphology to win out; however, clearly if the transition was sharp, such a diffuse change in morphology would not be observed over such a large range of conditions. We believe this is the first clear *in-situ* experimental demonstration of a transition between DBM and dendrites in a melt system (we are aware of only one such example in solution growth [31]).

Figure 4.3 shows an example of a "doublon" that makes up the dense-branched morphology. Our studies indicate that the formation of the doublon results in slightly slower growth than a dendrite under the same conditions, in contrast to theoretical studies of these morphologies that show that the doublon grows faster than the dendrite [15,16]. However, measurements of the growth rates were only carried out very close to the initial formation of the doublon and may not reflect the growth rate of the doublon at longer times (when the doublon can adjust the spacing between growth tips). The bifurcation of the growth tip likely results in an initial slow growth period where the diffusion fields overlap significantly.

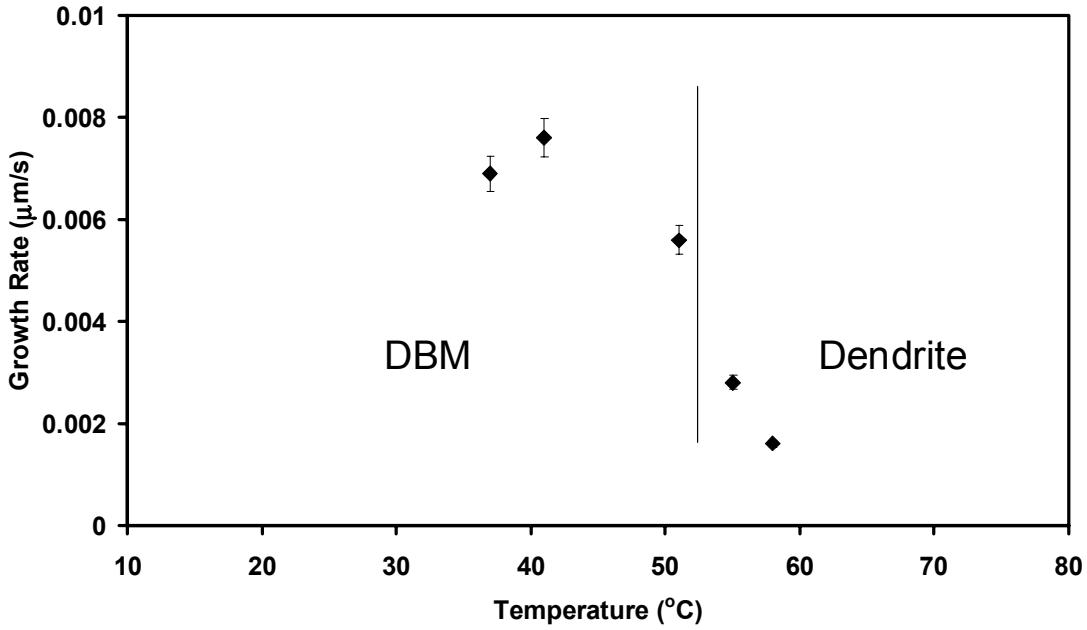

Figure 4.2 Growth rate data for the 50/50 PMMA17 blend. The line represents an approximate transition temperature.

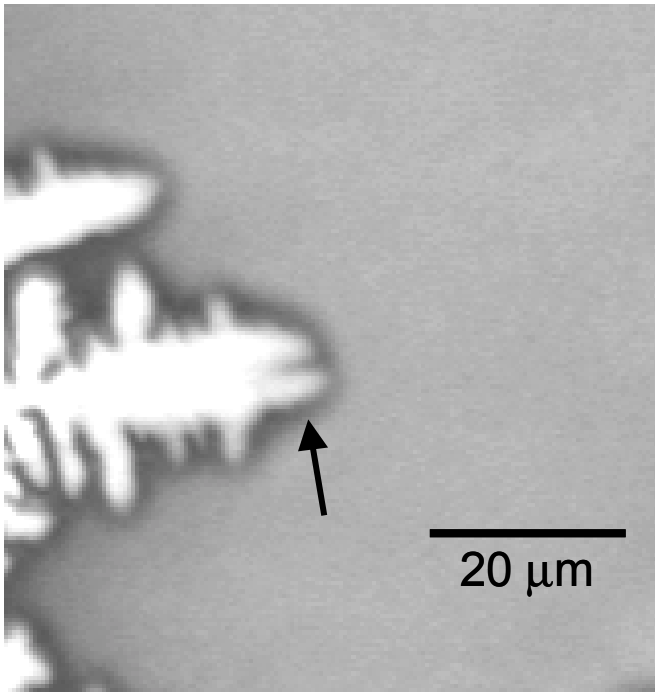

Figure 4.3 The arrow indicates a "doublon" in the 50/50 PMMA17 blend at 58^{o}C.

DBM/Stacked-Needle/Needle Transition

In Chapter 2, we reported a morphological map of the PEO/PMMA system with a blend composition of 50/50 showing the regions of stability of DBM, needle, and stacked-needle morphologies. Figures 4.4a-4.4c show examples of the DBM, stacked-needle, and needle morphologies, respectively.

To the best of our knowledge, needle crystals (with little to no sidebranching) have not been reported for PEO or its blends. However, studies of crystalline morphologies in other systems (such as undercooled water [32]) revealed similar needle morphologies. The growth of needle crystals is not well understood but may be common to systems with large anisotropies of kinetic attachment (as discussed in Chapter 2).

A transition from DBM to stacked-needles is observed with increasing undercooling (from 45^{o}C to 42^{o}C), as shown in Figure 4.5a. Figure 4.5a also shows the coexistence of the stacked-needle and DBM morphologies at higher temperature (regions I and II, crystallized previously at 45^{o}C). Such coexistence may be associated with a relatively large activation barrier and relatively low noise level. Changing the undercooling during growth of the stacked-needle morphology (region II to region III) results in a disruption of the stack (arrow in Figure 4.5c). Examination of this transition region reveals that these stacks are, in fact, composed of arrays of needle crystals. Growth rate data near the DBM/stacked-needle transition are reported in Figure 4.6. In this case, a clear jump in growth rates is noted between the DBM and stacked-needle morphologies. In both regions, the growth rate increases as the undercooling increases. The jump in crystal growth rates may be simply a matter of a change in the growth direction rather than a change in the growth mechanism. The stacked appearance of this morphology indicates that the crystals are oriented with some inclination to the substrate. We hope to carry out X-ray diffractions studies to at a later date to confirm this speculation.

The stacked-needle to needle transition is shown in Figure 4.5b. While, the stacked needle morphology likely grow as some inclination to the substrate, these needles

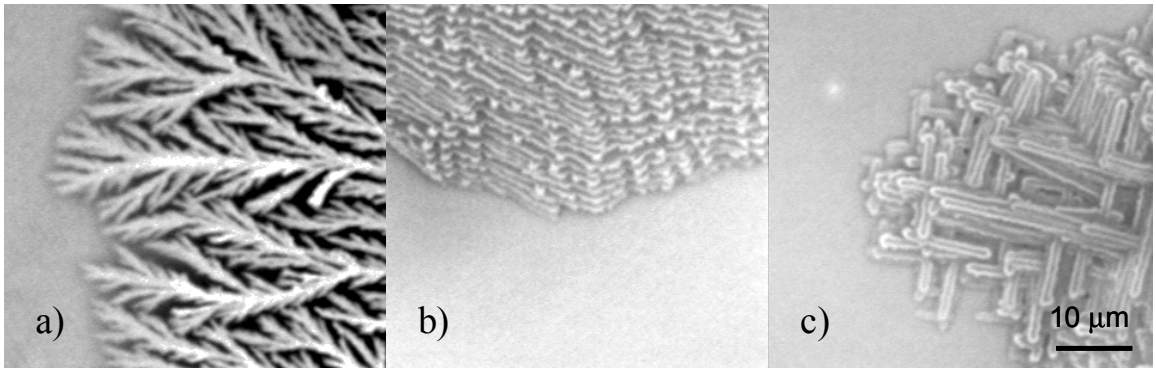

Figure 4.4 Needle and stacked-needle morphologies in a 50/50 PMMA101 blend. a) DBM (Tx = 50°C), b) Stacked-needle morphology (Tx = 42°C), c) Needle morphology (Tx = 40°C).

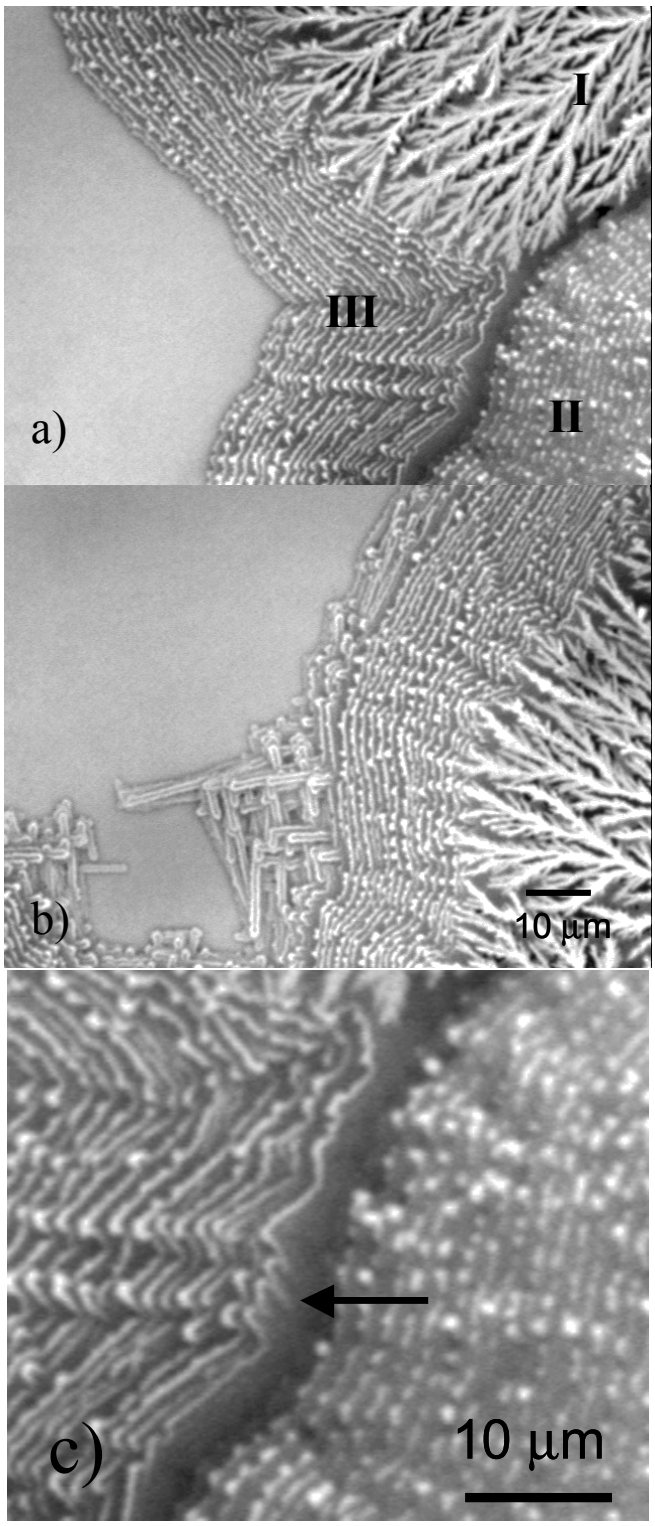

Figure 4.5 Morphologies in a 50/50 PMMA101 blend: a) DBM/stacked-needle transition. Regions I and II correspond to Tx = 45°C, while region III corresponds to 42°C) b) Stacked-needle/needle transition (Tx = 42°C to 40°C) c) Needles make up the stacked morphology (Tx = 44°C to 42°C).

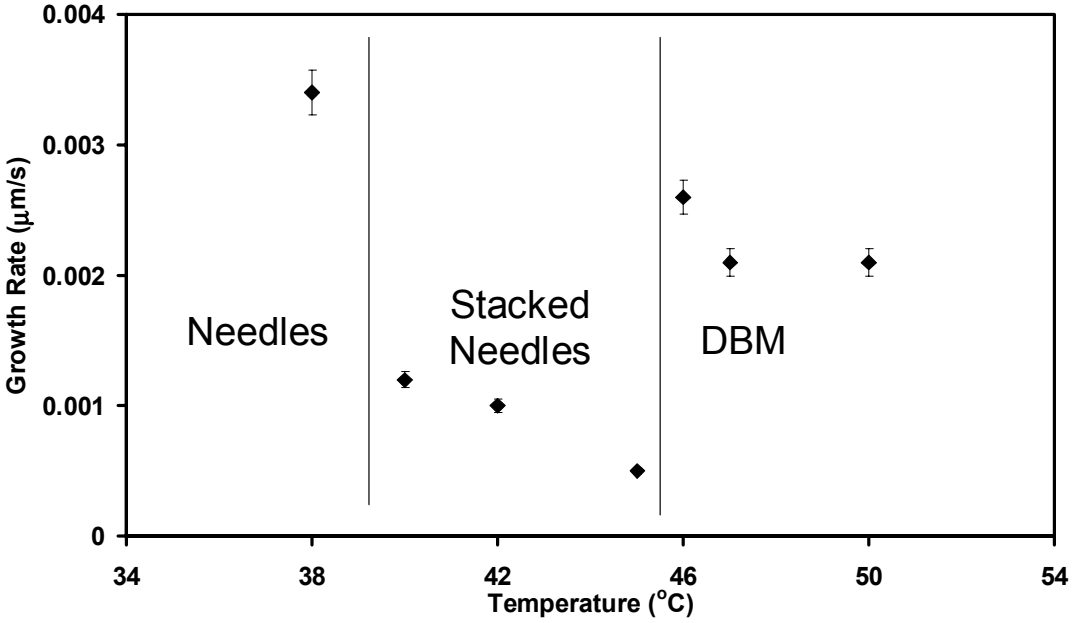

Figure 4.6 Crystal growth rate data for the 50/50 PMMA101 blend. The lines represent the transition temperatures.

appear to grow in a parallel direction. Growth rate data for the needle morphology is reported in Figure 4.6 shows a jump in the growth rate of the needles over the stacked needles, indicating that this situation is likely. Growth rate data for the needle morphology is not reported over a larger range of temperatures because their growth rate increases dramatically over a few degrees and the growth tips of the needles often stop growing and branch at 90^{o}.

A Growth Direction Transition

In Chapter 2, we also reported a transition in the direction of dendritic sidebranching from 90^{o} to 45^{o} with decreasing undercooling in 30/70 and 35/65 samples. In 30/70 samples, the branches clearly form at 45^{o} to the dendrite trunk, as shown in Figure 4.7a. However, by increasing the level of noise (increasing the PEO content and/or decreasing the PMMA molecular weight), a dense-branched morphology is observed to grow in the 45^{o} direction rather than dendrites. This transition is shown Figure 4.7b.

In low PEO content systems (30/70), the transition involves two dendritic growth morphologies with different orientations. The transition between these orientations does not happen quickly, as demonstrated by the fact that some 45^{o} sidebranches are also observed at 39^{o}C (indicated by the arrows in Figure 4.7a). The fact that this transition does not occur quickly, but is very stable after the transition indicates a relatively large activation energy and is consistent with a low level of noise. The 45^{o} transition in growth direction may be related to the (210)/(010) transition noted by Marentette [33] at higher temperature. The reason that the transition temperature would be depressed is not evident in our case. Chan and coworkers have observed similar transitions during crystallization of ammonium chloride resulting from different degrees of supersaturation [27]. Other workers have reported similar transitions due to changes in the surface tension anisotropy and kinetic anisotropy [34]. However, these issues have not been raised in polymeric materials and any suggestion is purely speculative at this point.

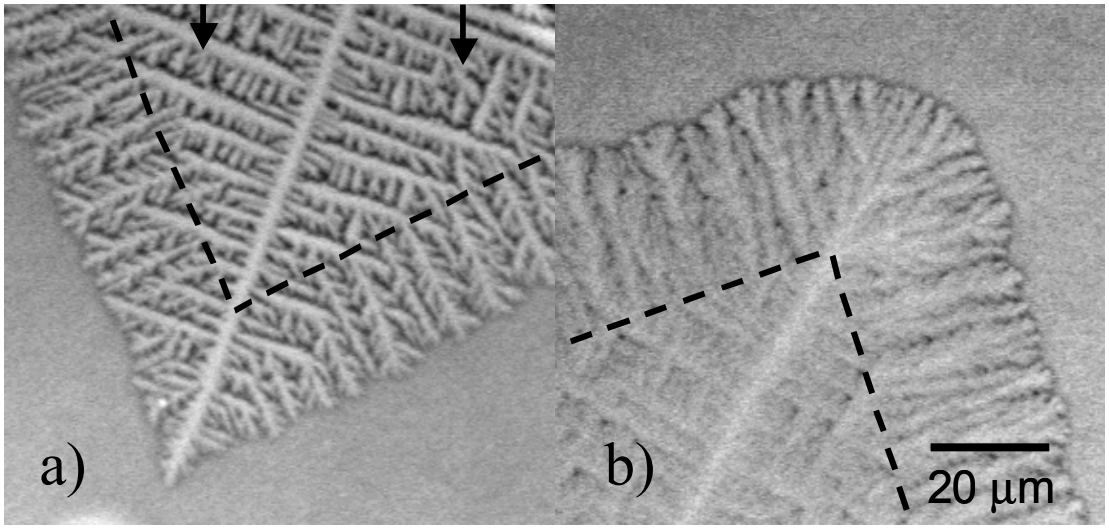

Figure 4.7 a) Dendrite in a 35/65 PMMA18 blend crystallized at 41°C then 43°C. The arrows indicate 45° sidebranches growing at 39°C. b) Dendrite in a 40/60 PMMA68 blend crystallized at 39°C then 41°C.

The noise level (destabilizing influences) is expected to increase with the PEO content, causing the second dendrite morphology to become unstable (resulting in DBM). The observed DBM may involve totally random directions, or a combination of growth of 45^{o} and 90^{o} branches at very small length scales. The macroscopic appearance of the latter branching process is that the morphology is highly disordered with no preferred growth directions. Examination of this morphology by optical microscopy does not allow for the active branching mechanism to be determined because of the small length scales (diffusion length) involved. However, studies of DBM in 60/40 blends (Figure 4.8), which exhibit much larger diffusion lengths, indicate that this is not likely to be the active mechanism. This observation does not rule out the possibility of the crystallographic branching mechanism in other systems. Utter and coworkers noted branching angles in DBM that appeared to be of a crystallographic nature in directionally solidified succinonitrile, indicating that there may actually be some preferred growth direction (anisotropy) in these systems [35]. In this case, the presence of noise must be important for the development of the DBM morphology since dendrites are expected for even small anisotropies. Our results also indicate that noise is indeed important for the formation of the dense-branched morphology.

Figures 4.9 and 4.10 show growth rate data near the transition point for the D90/D45 and D90/DBM samples, respectively. As in the DBM/dendrite transition, the change in growth rate through the transition is relatively smooth for both the 45^{o} dendrites and the DBM cases, further demonstrating that the origin these morphologies only differ in terms of the effective noise.

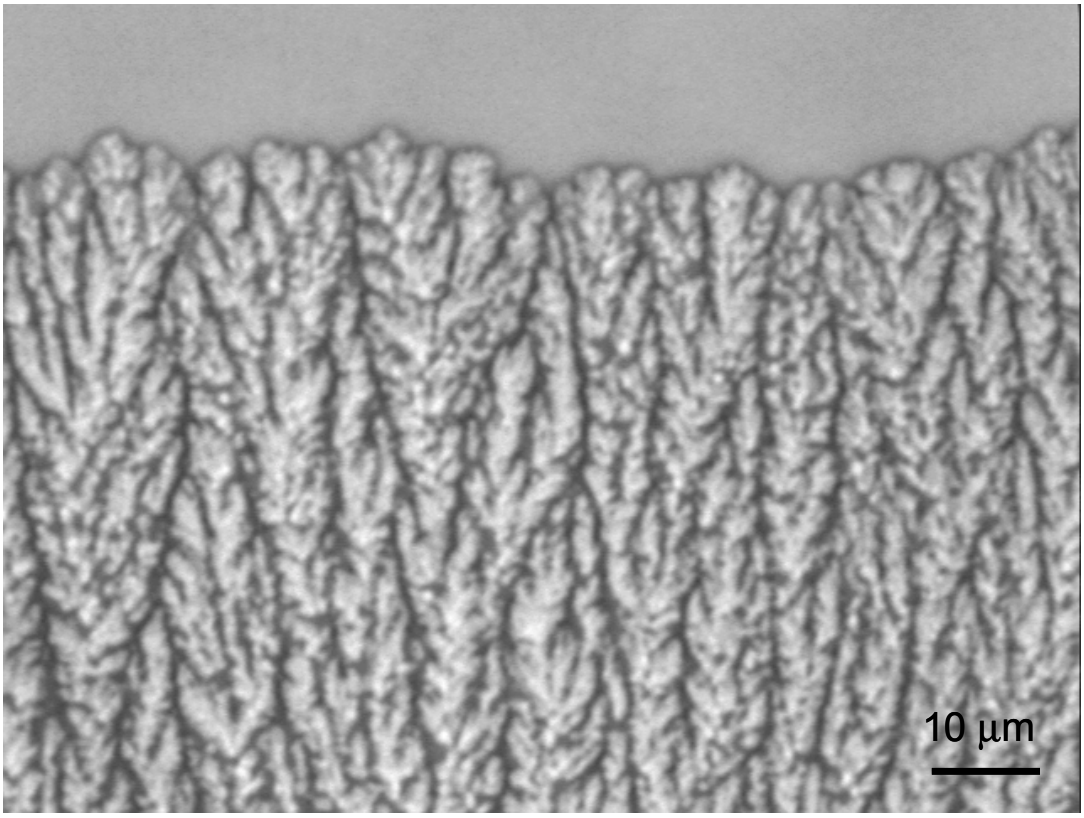

Figure 4.8 DBM in a 60/40 PMMA68 blend crystallized at 56^{o}C.

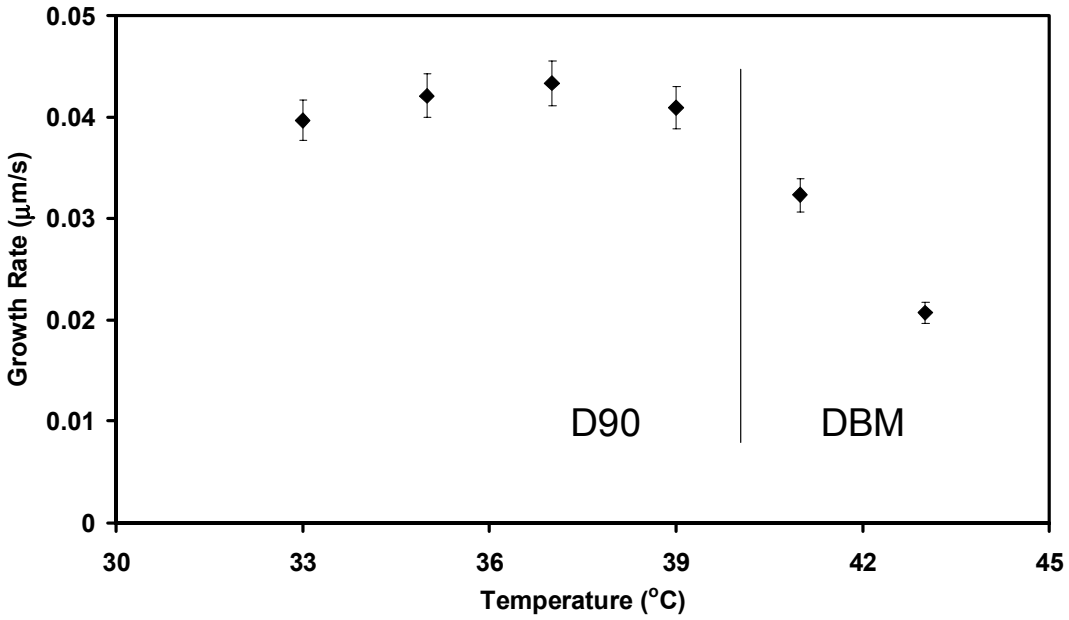

Figure 4.9 Crystal growth rate data near the transition for a 35/65 PMMA18 blend.

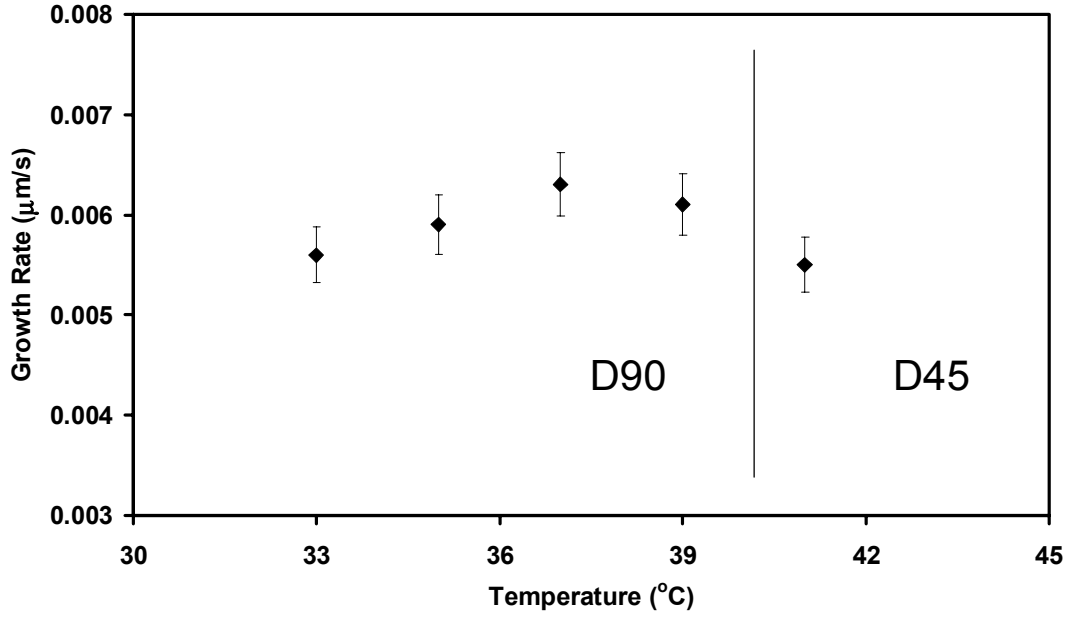

Figure 4.10 Crystal growth rate data near the transition for a 40/60 PMMA68 blend.

Chapter 4.4 Conclusions

We have reported in-situ studies of several morphological transitions during crystallization of thin films of PEO/PMMA blends. Optical micrographs and crystal growth velocity data have been reported for each of these transitions over a range of undercooling. The DBM/dendrite transition occurred over a range of undercooling and the growth rate data showed no clear jump during this transition, indicating the importance of the anisotropy. Tip-splitting (doublon) of the dendrite was clearly shown. DBM/stacked-needle/needle transitions were also demonstrated. The stacked-needle morphology appears to be composed of needles with some inclination to the substrate. In this case, a clear jump in growth rates was observed, and is likely related to this change orientation. A transition from dendrites with sidebranching at 90^{o} to dendrites with 45^{o} sidebranching or the dense-branched morphology with decreasing undercooling was also reported. In systems with high noise levels, transitions between dendrites and DBM are observed instead transitions between dendritic growth directions observed in systems with lower noise. These results indicate the importance of noise in the formation of the dense-branched morphology.

Chapter 4.5 References

[1] KA Jackson, DR Uhlmann, and JD Hunt. Journal of Crystal Growth 1, 1 (1967).

[2] W Kurz and DJ Fisher. *Fundamentals of Solidification*. Trans Tech Publications, Switzerland (1998).

[3] See KA Jackson, Journal of Crystal Growth 264, 519 (2004) and references therein.

[4] GP Ivanstov. Dokl Akad Nauk SSSR 58, 567 (1947).

[5] JS Langer. Reviews of Modern Physics 52(1), 1 (1980).

[6] DA Kessler, J Koplik, and H Levine. Advances in Physics 37(3), 255 (1988).

[7] DP Woodruff. *The Solid-Liquid Interface*. Cambridge University Press, New York (1973).

[8] ME Glicksman and SP Marsh. In *Handbook of Crystal Growth, Fundamentals: Transport and Stability*, Volume 1B, pages 1075-1122, Elsevier Science Publishers B.V., New York (1993).

[9] B Billia and R Trivedi. *In Handbook of Crystal Growth, Fundamentals: Transport and Stability*, Volume 1B, pages 899-1073, Elsevier Science Publishers B.V., New York (1993).

[10] See DC Bassett *Principles of Polymer Morphology*, Cambridge University Press, New York (1981) and PH Geil. *Polymer Single Crystals*, New York: Interscience Publishers (1963) and references therein.

[11] HD Keith and FJ Padden Jr. Journal of Applied Physics 34(8), 2409 (1963).

[12] HD Keith and FJ Padden Jr. Polymer 27, 1463 (1986).

[13] MI Abo el Maaty, IL Hosier, and DC Bassett. Macromolecules 31(1), 153 (1998).

[14] H Müller-Krumbhaar, M Zimmer, T Ihle, and Y Saito. Physica A 224, 322 (1996).

[15] E Brener, H Müller-Krumbhaar, and D Temkin. Physical Review E 54(3), 2714 (1996).

[16] T Ihle and H Müller-Krumbhaar. Physical Review E 49(4), 2972 (1994).

[17] E Ben-Jacob, R Godbey, ND Goldenfeld, J Koplik, H Levine, T Mueller, and LM Sander. Physical Review Letters 55(12), 1315 (1985).

[18] E Ben-Jacob, G Deutscher, P Garik, ND Goldenfeld, and Y Lareah. Physical Review Letters 57(15), 1903 (1986).

[19] K Taguchi, H Miyaji, K Izumi, A Hoshino, Y Miyamoto, and R Kokawa. Polymer 42, 7443 (2001).

[20] AJ Lovinger and RE Cais. Macromolecules 17(10), 1939 (1984).

[21] T Ihle and H Müller-Krumbhaar. Physical Review Letters 70(20), 3083 (1993).

[22] E Brener, H Müller-Krumbhaar, D Temkin, and T Abel. Physica A 249, 73 (1998).

[23] E Brener, H Müller-Krumbhaar, and D Temkin. Europhysics Letters 17(6), 535 (1992).

[24] O Shochet, K Kassner, E Ben-Jacob, SG Lipson, and H Müller-Krumbhaar. Physica A 187, 87 (1992).

[25] VA Bogoyavlenksiy and NA Chernova. Physical Review E 61(2), 1629 (2000).

[26] JL Hutter and J Bechhoefer. Physcial Review E 59(4), 4342 (1999).

[27] SK Chan, HH Reimer, and M Kahlwett. Journal of Crystal Growth 32, 303-315 (1976).

[28] V Ferreiro, JF Douglas, JA Warren, and A Karim. Physical Review E 65, 042802-1 (2002).

[29] V Ferreiro, JF Douglas, J Warren, and A Karim. Physical Review E 65, 051606-1 (2002).

[30] H Xu, R Matkar, and T Kyu. Physical Review E 72, 011804-1 (2005).

[31] B Utter and E Bodenschatz. Physical Review E 66, 051604 (2002).

[32] AA Shibkov, YI Golovin, MA Zheltov, AA Korolev, and AA Leonov. Physica A 319, 65 (2003).

[33] JM Marentette and GR Brown. Polymer 39(6-7), 1405 (1998).

[34] M Ohtaki, H Honjo, and H Sakaguchi. International Journal of Modern Physics 17, 4295 (2003).

[35] B Utter, R Ragnarsson, and E Bodenschatz. Physical Review Letters 86(20), 4604 (2001).

Chapter 5. Future Work

This work has resulted in a number of new avenues for future study. Some of these directions will be discussed here, along with some preliminary results.

Chapter 5.1 Recrystallization

The PEO/PMMA samples used in this work provide some interesting and unique possibilities for studies of recrystallization. Following morphological development during crystallization, a large amount of PEO is concentrated in the crystalline regions. These crystalline regions have very unusual geometries (thin straight lines for dendrites and curvy, highly branched geometries for DBM). Since the PEO content is very high in these regions, the recrystallization morphology may be very different than the original crystallization morphology. The growth rates of these regions should be much larger due to the locally lower glass transition temperature. However, these regions are confined in multiple dimensions due to the glassy PMMA surrounding the crystals and the crystal growth is likely to proceed in the same general direction. There is evidence of misoriented dendrites growing in these channels, shown in Figure 5.1. The sample was crystallized at 25^{o}C, melted for 1 minute at 80^{o}C, and then recrystallized. The light regions around the crystal show the location of the previous crystal (large PEO content). The crystal grows with some misorientation to the original nucleus, resulting in some competition between the anisotropic composition field and the desire of the crystal to grow in its nucleation orientation (related to the surface energy). This 'crystallization in anisotropic concentration fields' has not been reported experimentally.

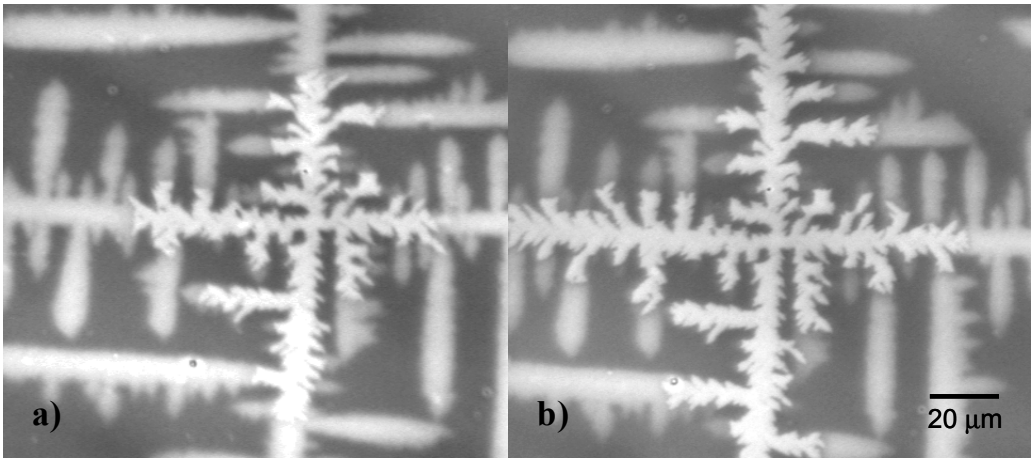

Figure 5.1 Recrystallization of a 30/70 PMMA68 blend.
a) Tx = 25°C followed by b) Tx = 43°.

Chapter 5.2 X-ray Diffraction Analysis

X-ray diffraction studies of the orientation of the crystals may be important for explaining the needle and stacked-needle crystals. We are currently unable to propose a mechanism for the formation of these stacked-needle morphologies. X-ray diffraction studies will require the use of high-energy x-rays below the absorption edge of silicon (for transmission studies). Similar studies may also be useful in more accurately describing the dense-branched and spherulitic morphologies (single crystals versus polycrystalline).

Chapter 5.3 Extension of the Morphological Map

Obviously, there is significant opportunity for expanding the map. Dendritic morphologies have also been observed at very large PEO contents (> 50wt%) at high temperature. These regions have been briefly investigated. Some of the observed morphologies for different blend compositions are shown in Figures 5.2, 5.3 and 5.5. Since the diffusion lengths are much larger in these cases, such samples may be extremely useful for quantifying the sidebranch spacing near the dendrite tip. In addition, screw dislocations are readily apparent in the low PMMA content samples (shown in Figure 5.4), but are less apparent for higher PMMA content. These observations may suggest that spherulitic growth forms do not exist at large PMMA content in thin film geometries because of the inability of the crystal to form dislocations (believed to be necessary for the formation of spherulites) in confined geometries.

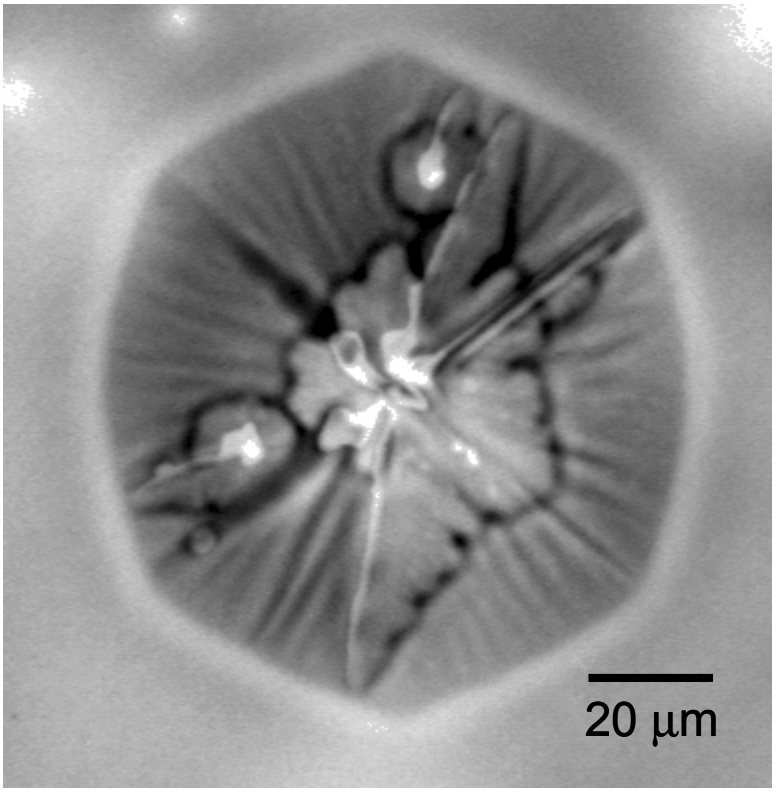

Figure 5.2 Crystal morphology in 90/10 PMMA68 blend at 60°C.

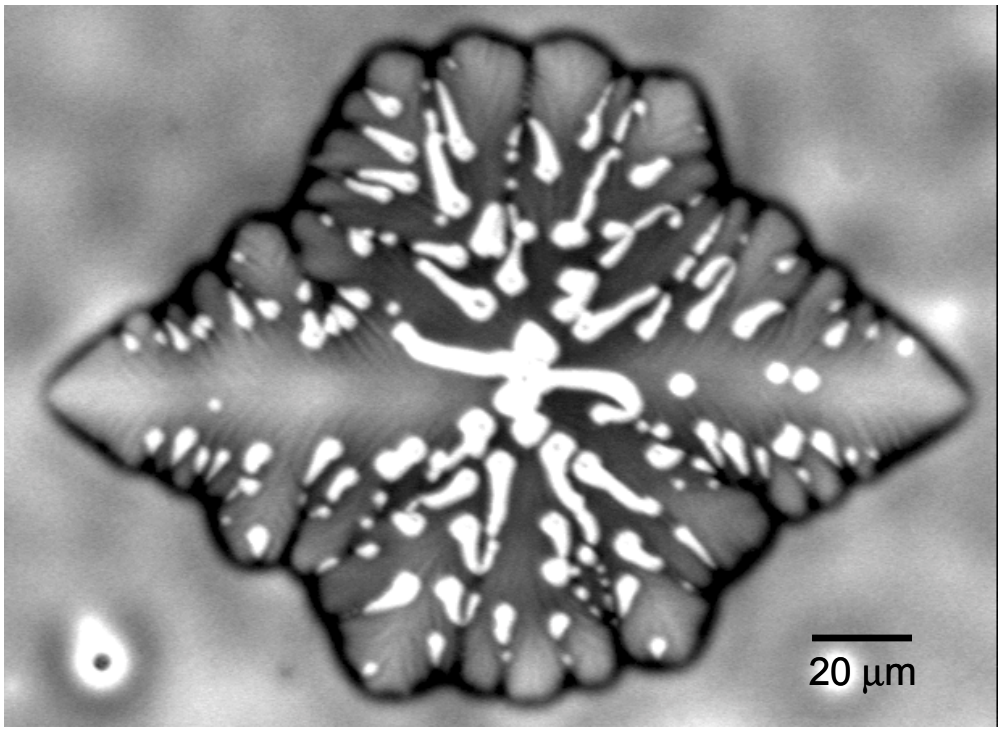

Figure 5.3 Crystal morphology in a 70/30 PMMA68 blend at 60°C.

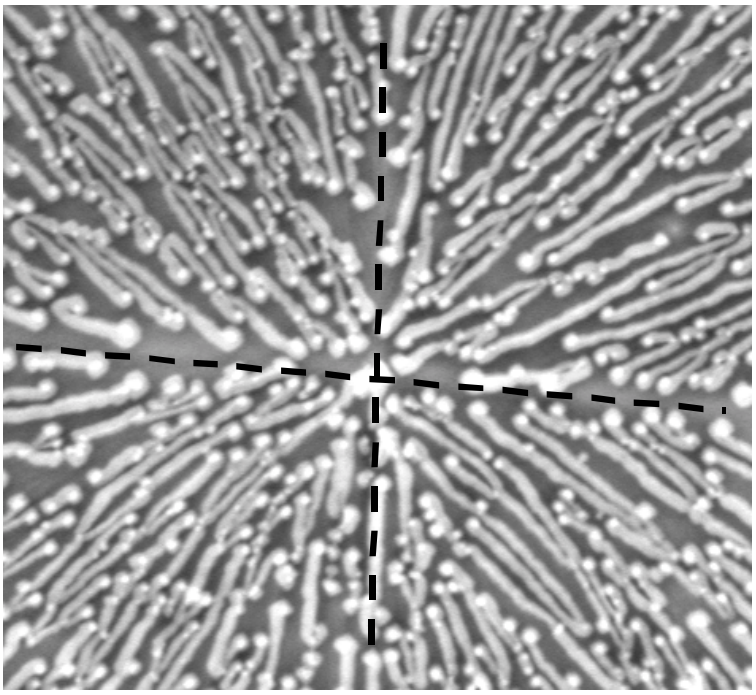

Figure 5.4 Another crystal in a 70/30 PMMA68 blend at 60°C at longer time, showing a number of screw dislocations. The dashed lines show different sectors of the PEO crystal.

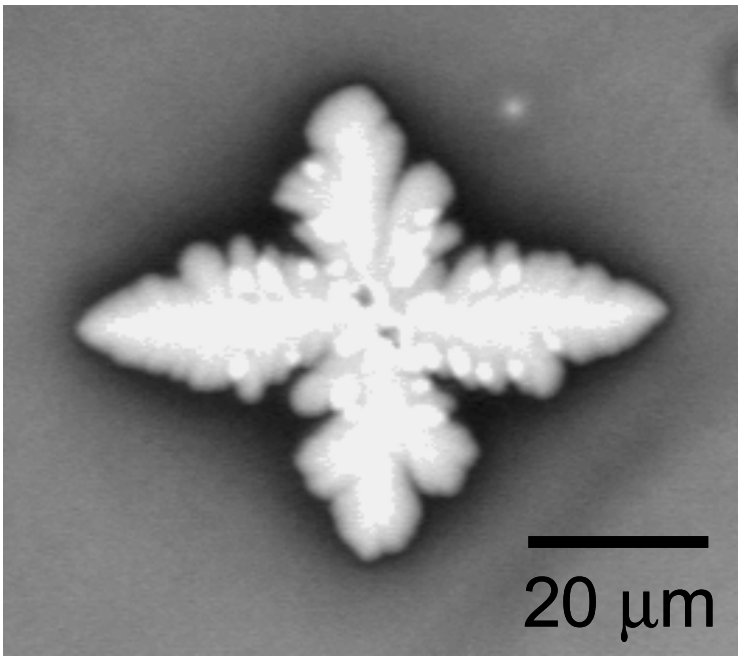

Figure 5.5 Crystal morphology in a 60/40 PMMA68 blend at 60^{o}C.

Low PEO content (< 20wt%) studies would also be interesting because Ferreiro and coworkers reported "fractal" morphologies in that region [1,2]. The existence of such fractal morphologies indicates that growth is highly limited by diffusion (i.e. diffusion-limited aggregation). These fractal morphologies appear very similar to DBM but are likely the result of different growth mechanisms. Further experiments are needed to resolve this issue.

Chapter 5.4 The Glass Transition Temperature, Diffusion Coefficients, and Chain Dynamics

The glass-transition, diffusion, and chain dynamics are areas of intense study in the polymer field. Until more is known about these topics, a complete understanding of the observed crystallization morphologies is not possible. Current measurement techniques are often not suitable for measurements in thin film geometries, despite the obvious need for these measurements. Studies of dendritic morphologies may provide insight into these processes, particularly in determination of the diffusion coefficient. Dendrite theory predicts a relationship between the radius of curvature of the dendrite tip and the growth velocity [3]. The radius of curvature can also be related to the diffusion length. Variation of the crystallization temperature over very small ranges may yield very different curvatures. Our current experimental setup is not sufficient for such measurements (our setup allows temperature control of $1^{o}C$ with an accuracy of $\pm 0.1^{o}C$, and temperature control of $\pm 0.1 - 0.01^{o}C$ would be helpful because large changes in the dendrite radius are observed over very narrow temperature ranges at low undercooling). These studies would need to be carried out in high PEO content samples near the melting point where the diffusion length is very large (so the curvature can be monitored by optical microscopy).

Chapter 5.5 Variation of the PEO Molecular Weight

Variation of the PEO molecular weight may provide some insight into the mutual diffusion coefficient of PEO/PMMA blends. In our studies, the observed morphologies do not vary significantly with PMMA molecular weight, indicating that the PMMA is not highly responsible for the value of the mutual diffusion coeffcient. Such a result is expected for the "fast" theory of mutual diffusion [4,5]. By varying the PEO molecular weight, much larger changes in the diffusion coefficient are expected. Such studies would be limited to high molecular weight PEO because the melting point of PEO varies with molecular weight at small chain lengths and such variation may affect the anisotropy of the system (the undercooling would vary at the same temperature).

Chapter 5.6 References

[1] V Ferreiro, JF Douglas, J Warren, and A Karim. Physical Review E 65(4), 042802-1 (2002).

[2] V Ferreiro, JF Douglas, J Warren, and A Karim. Physical Review E 65(5), 051606-1 (2002).

[3] See, for example: B Billia and R Trivedi. *In Handbook of Crystal Growth, Fundamentals: Transport and Stability*, Volume 1B, pages 899-1073, Elsevier Science Publishers B.V., New York (1993).

[4] Kramer EJ Kramer, P Green, and CJ Palmstrom. Polymer 25, 473 (1984).

[5] H Silescu. Makromolecular Chemistry, Rapid Communications 5, 519 (1984).

Appendix 1. Ellipsometry

Appendix 1.1 Introduction

In this section, only the basic aspects and assumption used in ellipsometry will be discussed (as the measurements in this dissertation only involve characterization of the film thickness). Detailed discussions of the underlying physics are well beyond the scope of this Appendix; however, more detailed discussions can be found in a review by Woollam [1]. The focus in this section will be on techniques used in data collection for this dissertation, and thus only data collection and analysis for thin film samples on a flat substrate (silicon) in reflectance mode will be discussed.

Ellipsometry is a measurement technique often used to characterize the thickness and optical properties of thin films. A monochromatic polarized light beam is reflected off a sample surface and into a detector. The change in polarization of the light is measured and used to determine the optical properties of the material. The important measured values are expressed as psi (Ψ) and delta (Δ). Psi and delta are related to the Fresnel reflection coefficients (R_p and R_s), for p- (plane of incidence) and s- (perpendicular to p in a direction to make a right-handed Cartesian coordinate system with p- and the direction of propagation) polarized light, respectively:

$$\rho = R_p / R_s = \tan(\Psi)\, e^{i\Delta} \qquad \text{Eq (A1.1)}$$

where ρ is the resulting change in polarization.

Spectroscopic ellipsometry allows for the determination of the dispersion of the optical constants, which helpful if parts of the spectrum are inaccessible due to sample limitations.

Several sample limitations exist for the use of ellipsometry. First, the film thickness must not be too much larger or smaller than the wavelength of light used for the measurement. Second, the roughness of the surface should be less than ~10% of the beam wavelength. Higher amounts of roughness may cause non-specular scattering. The third limitation is that the uniformity of the film thickness should not vary by more than about ~10%.

Appendix 1.2 Basic Procedure

There are four stages to ellipsometry experiments: measurement, modeling, fitting, and the results. The parameters of interest are not measured directly, and thus must be modeled to estimate the parameters from the data predicted by the model. The measurements include quantities such as the reflected beam and transmitted beam intensities and polarization states (i.e. R,T,Ψ,Δ). Following data collection, the model must be constructed. The model contains known parameters such as the wavelength of incident light, the incident beam polarization state, and the angle of incidence. The model also must contain unknown information such as the layer thickness and optical constants. Fitting the model involves generating sets of data until a set of optimized parameters that closely matches the optical data is found. This fit must involve data that is unique, reasonable (physically), and not strongly correlated. Statistical quantities are also used to evaluate the accuracy and precision of the fit results. Once the model has been developed, the calculated parameters are compared with the measured values. Providing the fit is good, the film thickness and optical constants can be assumed accurate.

Several assumptions are implicit to ellipsometry. First, the light beam entering the detector is considered to be completely polarized (back-surface reflection or significant roughness may be problematic). Second, all interfaces between layers are sharp and perfectly flat. Third, all films (and the substrate) are considered uniform in a direction normal to the substrate, unless otherwise specified. Fourth, the sample is considered to be isotropic, unless otherwise specified. Finally, optical constants fixed for any layer are described exactly.

Appendix 1.3 Ellipsometry Experiments in this Dissertation

Experimental data was obtained using a spectral range of 250-1000 nm with angles of incidence of 70^{o}, 73^{o}, and 76^{o} using a JA Woollam spectroscopic ellipsometer. The silicon wafer substrate used in this study was modeled first. Using well known

optical constants and dispersion data for silicon, the oxide layer was determined to be approximately 3 nm. The information is used as the first "layer" of the sample because it has some influence on the fitting of the model. The polymer film is considered to be the second "layer."

A Lorentz model was developed to analyze the data. The Lorentz model is comprised of a Lorentz oscillator (related to the Drude model for free electron absoption), generally formulated as:

$$\varepsilon(E) = \varepsilon_1(\infty) + \sum (A_1 / (E_k^2 - E^2 - \Gamma_1 E) + (A_2 / (E_k^2 - E^2 - 2\Gamma_2 E) + \ldots \qquad \text{Eq (A1.2)}$$

where $\varepsilon(E)$ is the dimensionless complex dielectric function as a function of photon energy and $\varepsilon_1(\infty)$ is the value of the real part of the dielectric function at very large photon energies. The summation occurs for the number of oscillators defined. Each oscillator is described by three parameters: A_i is the amplitude of the i^{th} oscillator, B_i is the broadening of the i^{th} oscillator, and E_i is the center energy of the i^{th} oscillator. In our case, a single Lorentz oscillator was used.

Thickness non-uniformity effects were included in the model because some sample roughness was observed by optical microscopy (variation in the film color resulting form different optical path lengths).

Thickness data for several blend compositions and PMMA molecular weights are reported below (Figure A1.1). Since the goal was only to verify that the thickness was relatively constant over the range of conditions, measurements were often made only one time.

An atomic-force microscopy scratch measurement, shown in Figure A1.2, indicates that the model is approximately correct in predicting the film thickness.

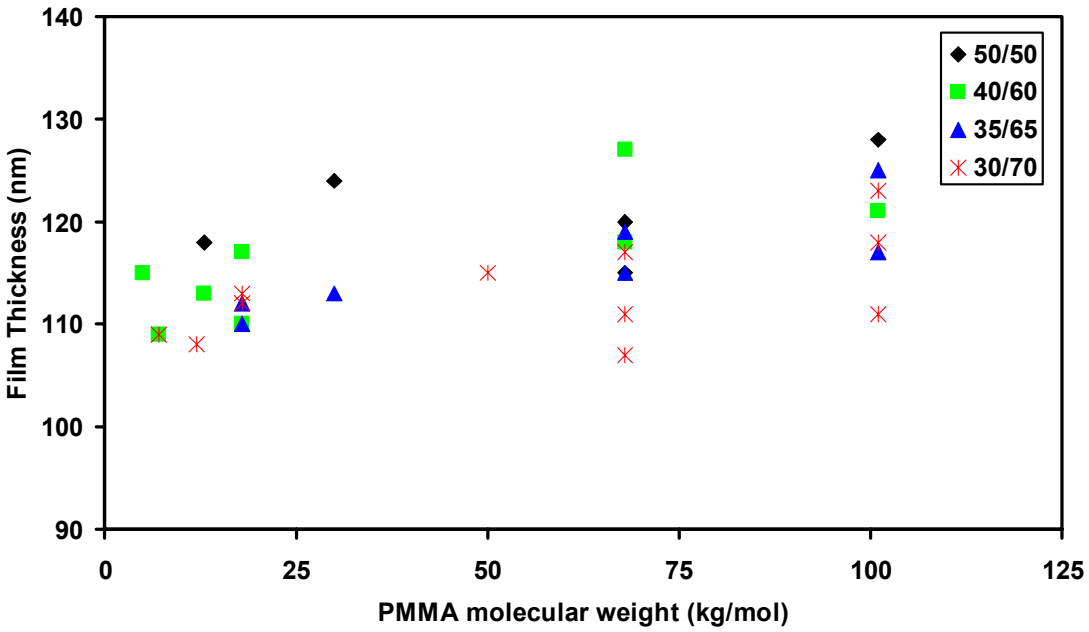

Figure A1.1 Film thickness versus molecular weight for blends with a polymer concentration of 1.25wt%.

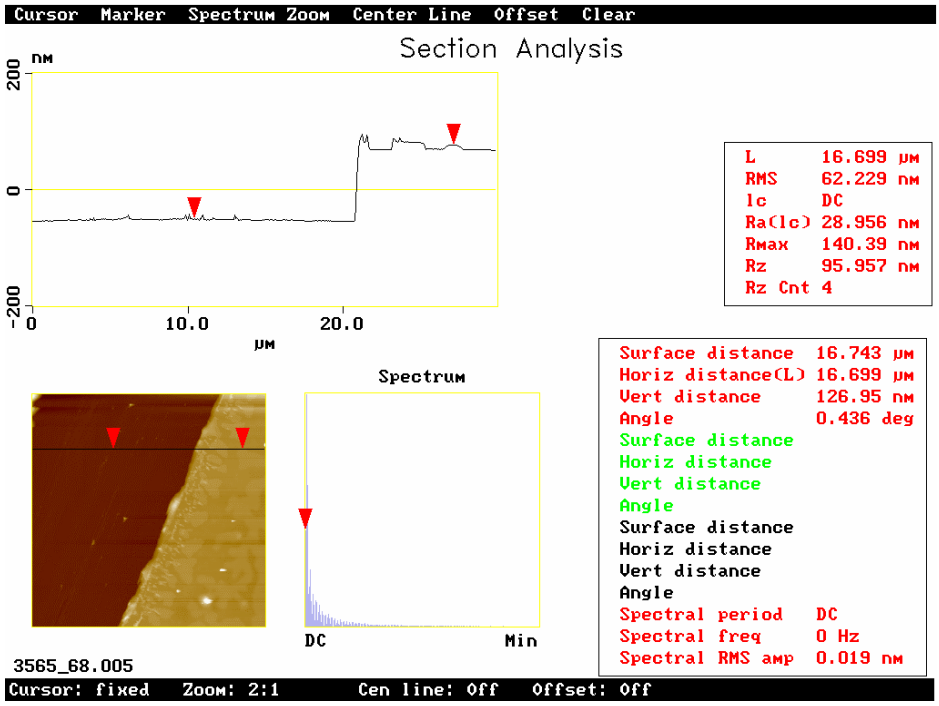

Figure A1.2 AFM section analysis for a 35/65 PMMA68 sample, showing a step height of 127 nm.

Appendix 1.4 References

[1] JA Woollam. In *Wiley Encyclopedia of Electrical and Electronics Engineering: Supplement 1*, JG Webster, ed. p 109-117, John Wiley & Sons, Inc: New York (2000).

Appendix 2. Glass-Transition Temperatures

Appendix 2.1 Glass-transition temperature measurement

Glass transition temperatures (Tg) of several of the PMMA samples used in this dissertation were measured by DSC (scan rate ~ 10^{o}C/min) and are reported below. The Tg of the PEO was not measured, but the value of -67^{o}C is obtained from literature [1].

Using the measured values of Tg for the individual components, the bulk Tg values predicted by the Fox equation [2] for several blends (different compositions and PMMA molecular weights) are reported in the in Figure A2.2. Experimental results reported by Alfonso and Russell support this approach [3]. As discussed in the Introduction, these values may have no relevance in thin film studies where the Tg can vary significantly with film thickness and position in the film. In particular, the Tg near the surface of thin film samples of PEO/PMMA may be much lower than the predicted value, while the Tg near the substrate may be much higher due to attractive interactions between the PEO/PMMA and the silicon.

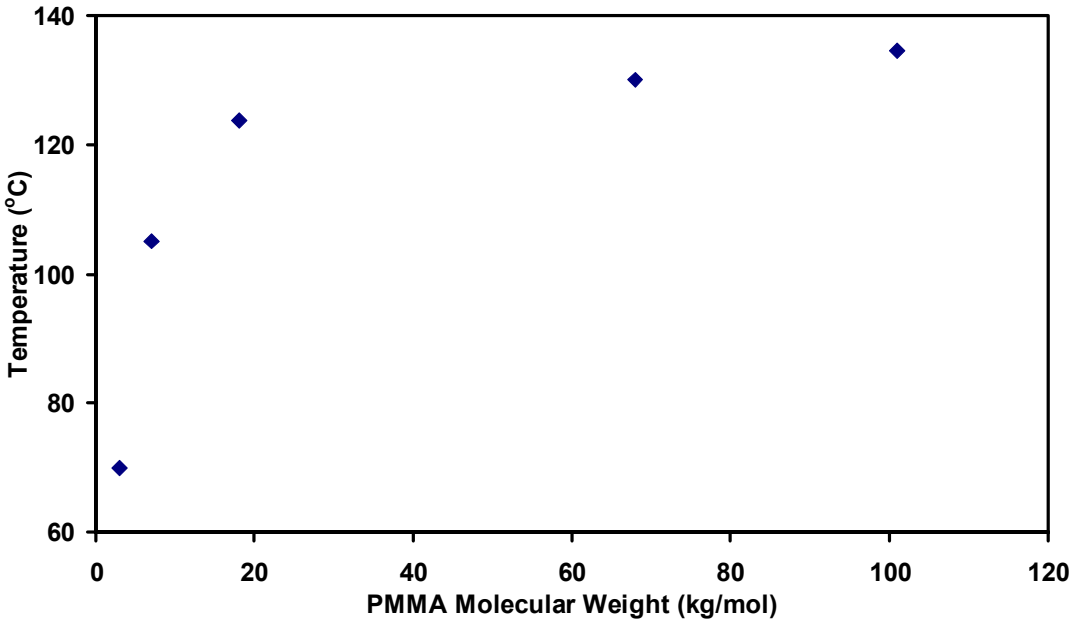

Figure A2.1 Glass-transition temperature of several of the PMMA samples.

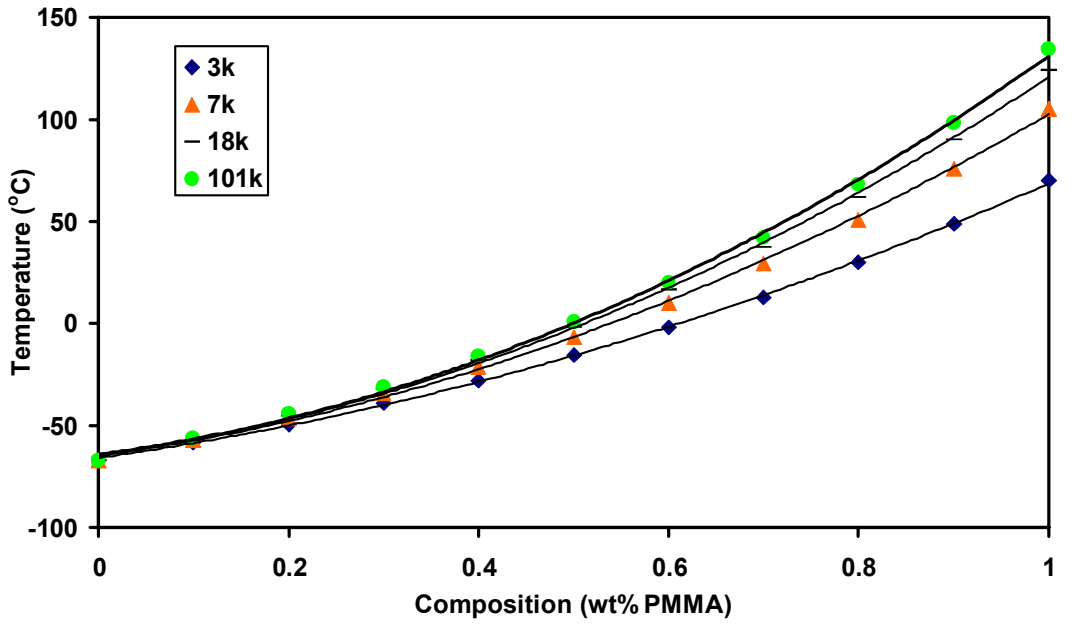

Figure A2.2 Glass-transition temperature for PEO/PMMA blends calculated from the Fox equation (using data in Figure A2.1)

Appendix 2.2 References

[1] S Balijepalli, JM Schultz, and JS Lin. Macromolecules 29(20), 6601 (1996).

[2] TG Fox. Bulletin of the American Physical Society 1, 123 (1956).

[3] GC Alfonso and TP Russell. Macromolecules 19, 1143 (1986).